Title

Characterizing the Effects of PKC Modulator HIV Latency Reversing Agents on Kick and Kill Strategies

Author

Dimapasoc, Melanie Aguirre

Publication Date

2024

Peer reviewed|Thesis/dissertation

UNIVERSITY OF CALIFORNIA

Los Angeles

Characterizing the Effects of Protein Kinase C Modulator Human Immunodeficiency Virus Latency Reversing Agents on Kick and Kill Strategies

A dissertation submitted in partial satisfaction of the

requirements for the degree Doctor of Philosophy

in Molecular Biology

by

Melanie Aguirre Dimapasoc

2024

ABSTRACT OF THE DISSERTATION

Characterizing the Effects of Protein Kinase C Modulator Human Immunodeficiency Virus Latency Reversing Agents on Kick and Kill Strategies

by

Melanie Aguirre Dimapasoc

Doctor of Philosophy in Molecular Biology

University of California, Los Angeles

Professor Jerome A. Zack, Chair

Human immunodeficiency virus (HIV) remains a significant global health challenge, despite advancements in treatment. Antiretroviral therapy (ART) suppresses viral replication, but is not a cure. HIV persists in reservoirs of long-lived, memory $CD4^+$ T cells harboring integrated, replication-competent provirus in a latent state. Viral persistence not only jeopardizes long-term health outcomes, but also complicates efforts to eradicate the virus, underscoring the need for innovative therapeutic approaches to achieve a cure.

One strategy known as the “kick and kill” approach aims to eliminate latently infected cells via pharmacological latency reversing agents (LRAs), which activate viral transcription, protein expression and virion production, thereby triggering these cells to be eliminated by viral-mediated cytolysis, immune detection or HIV-specific antiviral therapies. Despite some success in viral reactivation, existing LRAs failed to clear reactivated cells *in vivo*, emphasizing the urgent need for more effective treatments to promote the turnover of latently-infected cells.

In collaboration with Paul Wender's group at Stanford, our lab previously demonstrated that the latency-reversing capabilities and tolerability of naturally occurring protein kinase C (PKC) modulators, including bryostatin-1 and prostratin, can be improved by designing synthetic analogs of these compounds. SUW133, a potent bryostatin-1 analog, triggered latent HIV expression and led to the death of reactivated cells in humanized mice. However, whether this translates into clinically relevant outcomes remains unknown.

In this dissertation, I present a study evaluating the efficacy of PKC modulating HIV latency reversing agents, particularly SUW133, in the context of a "kick and kill" approach, as a novel therapeutic strategy against HIV persistence. Using a genetically barcoded HIV library in the context of a humanized mouse model, we quantified changes in the viral reservoir and found that SUW133 delayed viral rebound and reduced the number of unique barcoded viruses rebounding from the reservoir. Additionally, the combination of SUW133 plus NK cells further delayed rebound and reduced rebounding viral clones, even seemingly eliminating the viral reservoir in a subset of mice.

Next, we characterized the effects of SUW133 on NK cells to evaluate whether it modulates effector functions to enhance clearance of reactivated cells. While SUW133 induced changes in the activation profile of NK cells, it did not result in enhanced killing. Transcriptomic analysis revealed that $CD4^+$ T cells had stronger responses to LRA than did NK cells, suggesting its effect on reservoir reduction is primarily due to augmenting the "kick" rather than "kill" arm of this therapeutic approach.

Lastly, I conclude with potential future directions, including some preliminary work evaluating synergistic combinations of SUW133 and histone deacetylase inhibitors (HDACi) as another novel

therapeutic strategy towards latency reversal. Together, the work presented in this dissertation represents a multifaceted examination of the effects of SUW133 on latency reversal, highlighting new and exciting opportunities for its use towards an HIV cure.

This dissertation of Melanie Aguirre Dimapasoc is approved.

Oliver I. Fregoso

Man Hing Li

Matthew D. Marsden

Otto Orlean Yang

Jerome A. Zack, Committee Chair

University of California, Los Angeles

2024

DEDICATION

This dissertation is dedicated to my family, who are the heart and soul of everything I do.

TABLE OF CONTENTS

LIST OF FIGURES AND TABLES

CHAPTER 1

CHAPTER 2

CHAPTER 4

ACKNOWLEDGEMENTS

I would like to begin by thanking my mentor, Dr. Jerome Zack. Prior to graduate school, I had developed an early interest in HIV research and was fortunate enough to interview with him during the admissions process. Needless to say, I was already familiar with his innovative work in the field, but the thing that impressed me the most upon our initial meeting was how personable and caring he was. I am grateful to have been accepted as a graduate student in the lab, despite him not actively recruiting. His general hands-off approach to mentorship challenged me to be more independent, which I believe has made me a better scientist (though I know if I ever needed him, he was never more than an e-mail away). He provided unwavering support and patience throughout all of the challenges I faced, whether they were project-related or personal. It has truly been an honor to learn under his tutelage.

Thank you to the members of my thesis committee: Drs. Oliver Fregoso, Melody Li, Matthew Marsden and Otto Yang for all of their invaluable wisdom and guidance throughout my doctoral studies. Drs. Fregoso and Li were two of my rotation mentors who provided me with my first foray into graduate-level research, teaching me many valuable technical and critical thinking skills. Dr. Marsden nurtured me during my early stages in the Zack lab, as I began working on many of his projects. He also played an integral role in the writing and editing of my first-authored manuscript. Dr. Yang posed many thought-provoking questions and insightful critiques that challenged me to think deeper.

A heartfelt thanks to all who have supported me along my scientific journey and contributed to my project. Thank you to all of the members of the Zack lab, both past and present, for their camaraderie and encouragement. Special thanks to Xiaomeng Wu and Hongying Chen, who

played an integral role in my initial training, and to Dr. Jocelyn Kim for all of her help and advice with my NK experiments. Thank you to Tian-Hao Zhang for all of his assistance and expertise with the viral barcode. Thank you to Jose Moran for performing the experiments to test the conditioned media on latency cell lines. Thank you to Steve Cole for all of his help with transcriptomic analysis. Thank you to all of our collaborators in Paul Wender's lab at Stanford, the CFAR Humanized Mouse Core, the UCLA Immune Assessment Core and the UCLA Technology Center for Genomics and Bioinformatics for their support.

Lastly, I would like to thank the members of the UCLA community and MBIDP, especially Dr. Peter Bradley, Ashley Terhorst, Dr. Elissa Hallem, Dr. Zoran Galic and my fellow IMMP cohort for fostering a sense of community and friendship throughout my graduate experience.

Notes about chapters in this thesis:

Chapter 2 is an adaptation of the manuscripts: Marsden, M. D., Zhang, T. H., Du, Y., **Dimapasoc, M.**, Soliman, M. S. A, Wu, X., Kim, J. T., Shimizu, A., Schrier, A., Wender, P. A., Sun, R., Zack, J. A. (2020). Tracking HIV Rebound following Latency Reversal Using Barcoded HIV. *Cell Rep Med, 1*(9), 100162 & Kim, J. T., Zhang, T. H., Carmona, C., Lee, B., Seet, C. S., Kostelny, M., Shah, N., Chen, H., Farrell, K., Soliman, M. S. A., **Dimapasoc, M.**, Sinani, M., Blanco, K. Y. R., Bojorquez, D., Jiang, H., Shi, Y., Du, Y., Komarova, N. L., Wodarz, D., Wender, P. A., Marsden, M. D., Sun, R., Zack, J. A. (2022). Latency reversal plus natural killer cells diminish HIV reservoir *in vivo*. *Nat Commun, 13*(1), 121.

For the Marsden, *et al.* paper, M.D.M., T.-h.Z., Y.D., M.D., X.W., M.S.A.S., J.T.K., A. Shimizu, and A. Schrier conducted the experiments and acquired the data. M.D.M., T.-h.Z., Y.D., M.D., X.W., M.S.A.S., J.T.K., R.S., P.A.W., and J.A.Z. participated in LRA analog selection and supply

and data interpretation and analysis. All of the authors contributed text, edited the manuscript, and approved the final version. This was supported by the National Institutes of Health (P01 AI131294 to J.A.Z., CA31845 to P.A.W., AI124763 to M.D.M., AI124743 to J.A.Z. and P.A.W.), the National Center for Advancing Translational Sciences UCLA CTSI Grant (UL1TR001881 and UL1TR000124), and the UCLA Center for AIDS Research (AI28697). The UCLA AIDS Institute and Charity Treks also provided support. ART drugs for humanized mouse studies were kindly provided by Merck (RAL) and Gilead Sciences (TDF and FTC). For the Kim, *et al.* paper, J.T.K., M.D.M., J.A.Z. and P.A.W. designed the study and developed SUW133. J.T.K., C.C., B.L., C.S., K.F., H.C., M.K., M.D., M.S.A.S. and M.S. performed the immunological and virologic assays. J.T.K., C.S., M.D.M. and J.A.Z. analyzed/interpreted the data from immunological and virologic assays. R.S. conceived and supervised the barcode experiments. J.T.K, T.-H.Z., N.S., D.B., K.Y.R.B., Y.S., H.J., Y.D. and R.S. performed the barcode analysis. D.W. and N.L.K. led the mathematical modeling. J.T.K. and J.A.Z. wrote the manuscript with input of all co-authors. This work was supported by the National Institutes of Health (AI155232 to J.T.K., K08CA235525 to C.S.S., AI131294 to J.A.Z. and M.D.M., AI124743 to J.A.Z. and P.A.W., and AI145038 to R.S.), the American Foundation for AIDS Research (110057-69-RGRL to J.A.Z.), the National Science Foundation (DMS1662146/1662096 to N.L.K. and D.W.), the National Center for Advancing Translational Sciences UCLA CTSI Grant (UL1TR001881 to J.T.K.), and the UCLA Center for AIDS Research (AI28697). The UCLA AIDS Institute and the McCarthy Family Foundation and UCLA Department of Medicine also provided support. ART for humanized mouse studies were kindly provided by Merck (RAL) and Gilead Sciences (TDF and FTC).

Chapter 3 is a modified version of the manuscript: **Dimapasoc, M.**, Moran, J. A., Cole, S. W., Ranjan, A., Hourani, R., Kim, J. T., Wender, P. A., Marsden, M. D., Zack, J. A. Defining the effects of PKC modulator HIV latency reversing agents on natural killer cells. *Pathog Immun*. 2024;9(1):108-137.

M.D., J.T.K., M.D.M. and J.A.Z. designed the study. A.R., R.H. and P.A.W. developed SUW133. M.D. and J.A.M. conducted the immunological and virologic assays, including data acquisition and analysis. M.D. and S.W.C. performed the RNA seq data interpretation and analysis. M.D. wrote the manuscript and all of the authors provided input, edited and approved the final manuscript. This work was supported by the National Institutes of Health [AI172727 to M.D.M., AI172410 to P.A.W. and J.A.Z., AI161803 to J.A.Z., AI55232 to J.T.K and CA031845 to P.A.W.] and the UCLA-CDU CFAR [AI152501 to J.TK.]. J.A.M. is a predoctoral trainee supported by U.S. Public Health Service training grant T32 AI007319 from the NIH.

Chapter 4 contains unpublished, preliminary data. I would like to thank everyone who contributed, including Tian-Hao Zhang, Steve W. Cole, Alok Ranjan, Rami Hourani, Paul A. Wender, Matthew D. Marsden and Jerome A. Zack. This work was supported in part by the National Institutes of Health [AI172727 to M.D.M., AI172410 to P.A.W. and J.A.Z., AI161803 to J.A.Z., CA031845 to P.A.W. and T32 training grant (GM007185) to M.D.].

VITA

EDUCATION

2003 - 2006 Bachelor of Science (B.S.)
Biology (Physiology), San Francisco State University

PROFESSIONAL EXPERIENCE

2018 - present Graduate Student Researcher, Zack Lab
Department of Microbiology, Immunology, and Molecular Genetics, UCLA

2015 - 2017 Research Associate II / RAVEN Laboratory and Project Coordinator
Viral Reference Laboratory & Repository Core, Blood Systems Research Institute

2012 - 2015 Research Associate I
Viral Reference Laboratory & Repository Core, Blood Systems Research Institute

2008 - 2011 Assistant Research Scientist I
Compound Repository/New Lead Discovery, Exelixis, Inc.

AWARDS & HONORS

2018 - 2020 Ruth L. Kirschstein National Research Service Award

PUBLICATIONS

Zhang, T. H., Shi, Y., Komarova, N. L., Wordaz, D., Kostelny, M., **Dimapasoc, M.**, Gonzales, A., Bresson-Tan, G., Chen, H., Carmona, C., Oh, C., Harvey, W., Seet, C., Du, Y., Sun, R., Zack, J. A., Kim, J. T. Barcoded HIV-1 reveals proviruses associated with cell clonal proliferation or viremia have distinct chromatin patterns (manuscript in review)

Dimapasoc, M., Moran, J. A., Cole, S. W., Ranjan, A., Hourani, R., Kim, J. T., Wender, P. A., Marsden, M. D., Zack, J. A. Defining the effects of PKC modulator HIV latency reversing agents on natural killer cells. *Pathog Immun.* 2024;*9*(1):108-137.

Kim, J. T., Zhang, T. H., Carmona, C., Lee, B., Seet, C. S., Kostelny, M., Shah, N., Chen, H., Farrell, K., Soliman, M. S. A., **Dimapasoc, M.**, Sinani, M., Blanco, K. Y. R., Bojorquez, D., Jiang, H., Shi, Y., Du, Y., Komarova, N. L., Wodarz, D., Wender, P. A., Marsden, M. D., Sun, R., Zack, J. A. (2022). Latency reversal plus natural killer cells diminish HIV reservoir *in vivo*. *Nat Commun, 13*(1), 121.

Stone, M., Rosenbloom, D. I. S., Bacchetti, P., Deng, X., **Dimapasoc, M.**, Keating, S., Bakkour, S., Richman, D. D., Mellors, J. W., Deeks, S. G., Lai, J., Beg, S., Siliciano, J. D., Pagliuzza, A., Chomont, N., Lackman-Smith, C., Ptak, R. G., Busch, M. P. (2021). Assessing the Suitability of Next-Generation Viral Outgrowth Assays to Measure Human Immunodeficiency Virus 1 Latent Reservoir Size. *J Infect Dis, 224*(7), 1209-1218.

Marsden, M. D., Zhang, T. H., Du, Y., **Dimapasoc, M.**, Soliman, M. S. A, Wu, X., Kim, J. T., Shimizu, A., Schrier, A., Wender, P. A., Sun, R., Zack, J. A. (2020). Tracking HIV Rebound following Latency Reversal Using Barcoded HIV. *Cell Rep Med, 1*(9), 100162.

Pache, L., Marsden, M. D., Teriete, P., Portillo, A. J., Heimann, D., Kim, J. T., Soliman, M. S. A., **Dimapasoc, M.**, Carmona, C., Celeridad, M., Spivak, A. M., Planelles, V., Cosford, N. D. P., Zack, J. A., Chanda, S. K. (2020). Pharmacological Activation of Non-canonical NF-κB Signaling Activates Latent HIV-1 Reservoirs *In Vivo*. *Cell Rep Med, 1*(3), 100037.

Sloane, J. L., Benner, N., Keenan, K., Zang, X., Soliman, M., Wu, X., **Dimapasoc, M.**, Marsden, M.D., Zack, J. A., Wender, P. A. (2020). Prodrugs of PKC Modulators Show Enhanced HIV Latency Reversal and an Expanded Therapeutic Window. *Proc Natl Acad Sci USA, 117*(20), 10688–10698.

Kelly, S., Jacobs, E., Stone, M., Keating, S. M., Lee, T. H., Chafets, D., **Dimapasoc, M.**, Heitman, J., Operskalski, E. A., Hagar, W., Vichinsky, E., Busch, M. P., Norris, P. J., Custer, B. (2020). Influence of Sickle Cell Disease on Susceptibility to HIV Infection. *PLoS One, 15*(4), e0218880.

Rosenbloom, D. S. I., Bacchetti, P., Stone, M., Deng, X., Bosch, R. J., Richman, D. D., Siliciano, J. D., Mellors, J. W., Deeks, S. G., Ptak, R., Hoh, R., Keating, S., **Dimapasoc, M.**, Massanella, M., Lai, J., Sobelewski, M. D., Kulpa, D. A., Busch, M. P. (2019). Assessing Intra-Lab Precision and Inter-Lab Repeatability of Outgrowth Assays of HIV-1 Latent Reservoir Size. *PLoS Comput Biol*, *15*(4), e1006849.

Mirzazadeh, A., Evans, J. L., Hahn, J. A., Jain, J., Briceno, A., Shiboski, S., Lum, P. J., Bentsen, C., Davis, G., Shriver, K., **Dimapasoc, M.**, Stone, M., Busch, M. P., Page, K. (2017). Continued Transmission of HIV Among Young Adults Who Inject Drugs in San Francisco: Still Room for Improvement. *AIDS Behav, 22*(4), 1383–1394.

Stone, M., Brambilla, D., Murcia, K., **Dimapasoc, M.**, Cyrus, S., Cable, R. G., Kiss, J. E., Busch, M. P. (2016). Feasibility of Routine Ferritin Testing for Donor Management: Validation of Delayed Processing and Demonstration of Within Donor Reproducibility Over Time. *Transfusion, 56*(10), 2422–2425.

Stone, M., Murcia, K., **Dimapasoc, M.**, Yip, B., Thompson, M., Kunkel, E. J., Schryver, B., Ehrhard, R. O. (2015). Maximizing PBMC Recovery and Viability: A Method to Optimize and Streamline Peripheral Blood Mononuclear Cell Isolation, Cryopreservation, and Thawing. *Bioprocess International*, *13*, 28-33.

PRESENTATIONS

March 2024 "Defining the effects of PKC modulator HIV latency reversing agents on natural killer cells." Poster presentation. *2024 Palm Springs Symposium on HIV/AIDS,* Palm Springs, CA.

October 2023 "Targeting the HIV reservoir." Oral presentation. *UCLA AIDS Institute Virology Seminar*, Los Angeles, CA.

February 2020 "Optimizing HIV latency reactivation *in vivo* through co-administration of novel PKC modulators and HDAC inhibitors." Oral presentation. *UCLA MBIDP Student Seminar*, Los Angeles, CA.

September 2014 "The contribution of T-cell tolerance to latent HIV infection." Poster presentation. *2014 Blood Systems Research Institute Retreat*, San Francisco, CA.

CHAPTER 1

Introduction

HIV

Human immunodeficiency virus (HIV) is a virus that attacks the body's immune system, causing infected individuals to be more susceptible to opportunistic infection and diseases like tuberculosis and some cancers (WHO, 2023a). Acquired immunodeficiency syndrome (AIDS) is the most advanced stage of the disease, wherein $CD4^+$ T cell counts drop below 200 cells per milliliter of blood (CDC, 2020). In 2022, it was estimated that there were approximately 39 million infected individuals worldwide, with 1.3 million being newly acquired infections (WHO, 2023b). Today, HIV remains one of the top causes of morbidity and mortality worldwide.

ANTIRETROVIRAL THERAPY

With the advent of antiretroviral therapy (ART), the prognosis of HIV infection has drastically changed from a death sentence to a manageable disease. ART prevents viral replication, thus impeding disease progression. Different classes of ART drugs target various stages of the HIV life cycle (Fatkenheuer et al., 2005; Grinsztejn et al., 2007; Pomerantz & Horn, 2003)(Figure 1-1). Entry inhibitors, also known as post-attachment inhibitors, bind to the CD4 receptor on host cells, which prevents binding to the CCR5 and CXCR4 coreceptors, thus blocking viral entry into the cell. Fusion inhibitors block the HIV envelope from merging with the host cell membrane. CCR5 antagonists block the CCR5 coreceptor on the surface of target cells, preventing viral entry. Capsid inhibitors interfere with multiple early and late stages of the viral replication cycle where the HIV capsid plays a critical role. This includes reverse transcription, nuclear transport, virus assembly and release. Nucleoside reverse transcriptase inhibitors (NRTIs) and non-nucleoside reverse transcriptase inhibitors (NNRTIs) block reverse transcription of the viral genome. Integrase inhibitors prevent insertion of the viral DNA into the host genome. Protease inhibitors prevent

viral maturation. Combination therapies including three or more of these drugs are typically administered, in order to effectively suppress viral loads to below the limit of detection of standard clinical assays (Gulick et al., 1997; Hammer et al., 1997; Hirsch et al., 1998; Hull & Montaner, 2011; Perelson et al., 1997). People living with HIV (PLWH) must adhere to a lifelong regimen of ART to manage chronic infection. Although ART greatly improves disease outcomes, there are many challenges associated with the necessity of lifelong therapy, including daily burden (which

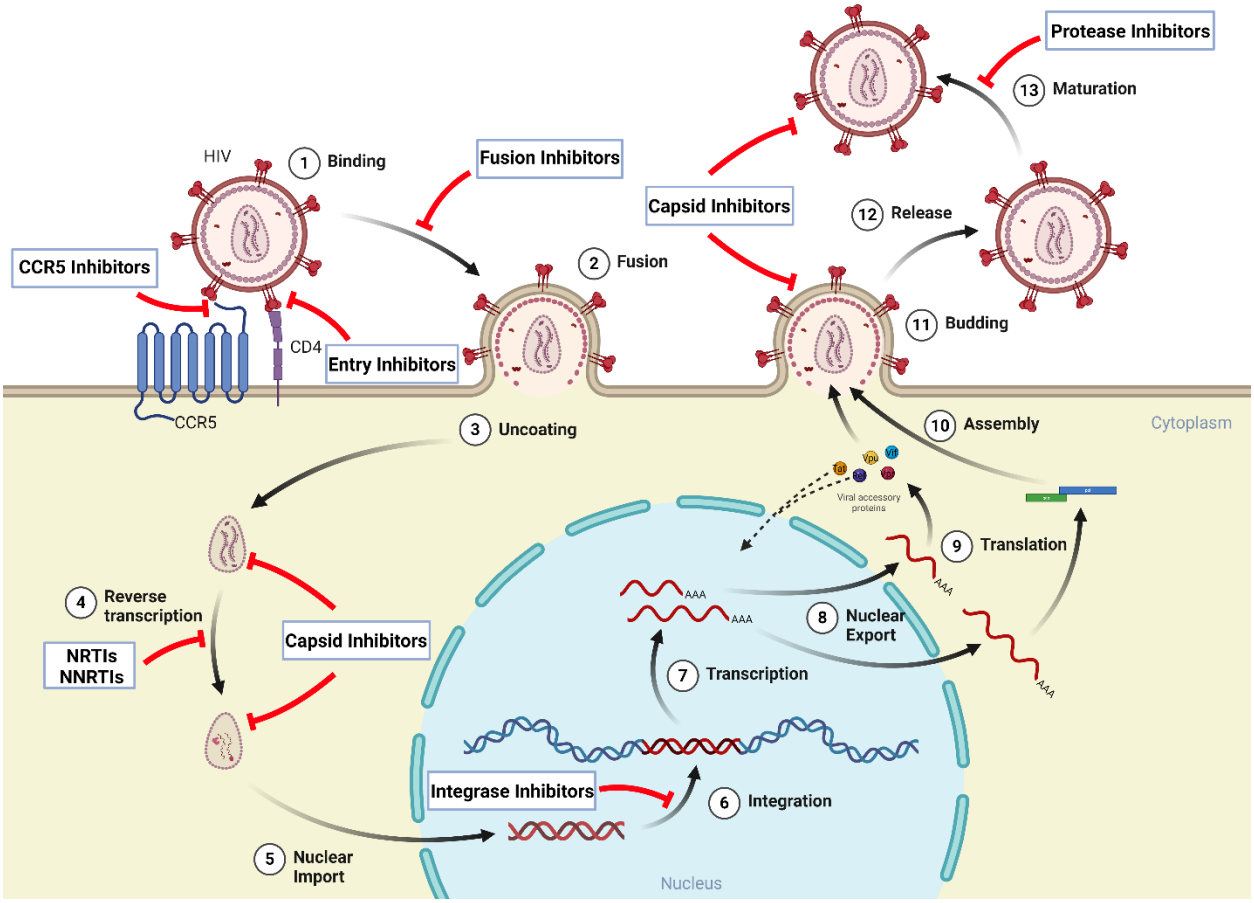

Figure 1-1. Antiretroviral therapy and the HIV life cycle. Different classes of antiretroviral drugs block specific stages of the HIV life cycle, thereby preventing viral replication. Entry inhibitors bind to the CD4 receptor, blocking viral entry. Similarly, CCR5 antagonists block the CCR5 coreceptor to block entry. Capsid inhibitors disrupt the function of the HIV capsid protein during multiple steps of the HIV life cycle, including reverse transcription, nuclear transport, virus assembly and release. Nucleoside reverse transcriptase inhibitors (NRTIs) and non-nucleoside reverse transcriptase inhibitors (NNRTIs) block the reverse transcription of viral RNA to DNA. Integrase inhibitors prevent insertion of proviral RNA into the host genome. Protease inhibitors block viral maturation. Adapted from "Retrovirus Life Cycle", by BioRender.com (2024). Retrieved from https://app.biorender.com/biorender-templates.

may lead to poor treatment compliance), long-term drug toxicity, potential interactions with other drugs, development of drug resistance and limited access (especially in developing countries) (Desai et al., 2012). Most importantly, ART does not cure HIV, as the virus persists in latently infected cells in ART-treated PLWH. When ART is stopped, latent virus leads to the rapid rebound of viral replication (Chun et al., 1999). Therefore, understanding the mechanisms of viral persistence and how to eliminate cellular sources of latent virus remain a global priority in the search for a cure.

HIV LATENCY AND VIRAL PERSISTENCE

The exact mechanisms responsible for establishment of HIV latency *in vivo* are unknown. However, based on characteristics of latently infected cells from PLWH and various experimental models, it is proposed that latency is tied to the transition of $CD4^+$ T cells into a quiescent memory

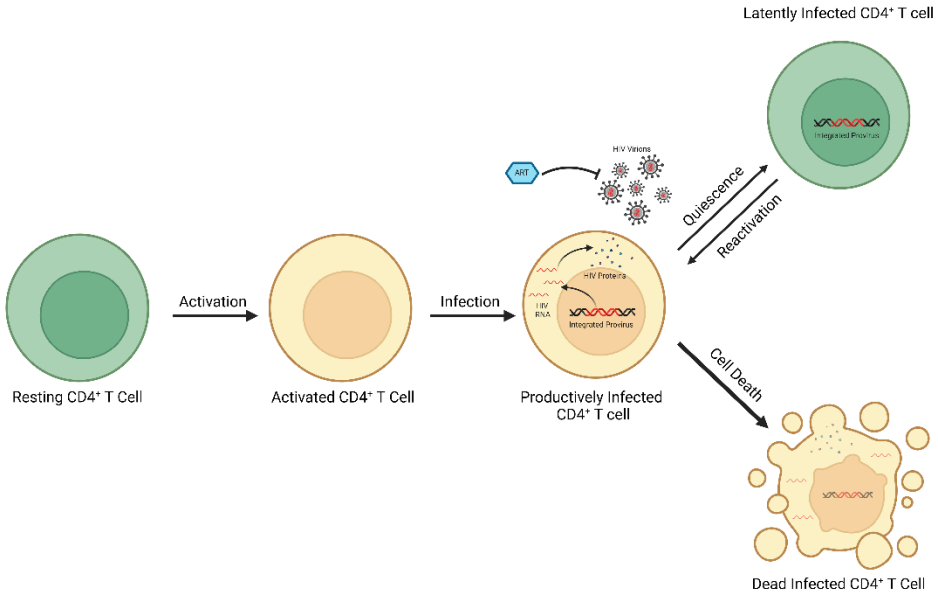

Figure 1-2. Proposed model for the establishment of HIV latency. Resting $CD4^+$ T cells are refractive to HIV infection. However, once activated, they can be readily infected with HIV. A small subset of HIV-infected, activated $CD4^+$ T cells revert to a quiescent memory state before they can be killed, resulting in the establishment of long-lived, latently infected cells. Antiretroviral therapy (ART) blocks the spread of infection by newly synthesized virions. Created with BioRender.com.

state, as the latent reservoir primarily consists of $CD4^+$ central memory and transitional memory T cells subsets (Chomont et al., 2009; Chun et al., 1997). Resting $CD4^+$ T cells are generally refractive to infection and do not typically result in post-integration latency (Bukrinsky et al., 1991; Zack et al., 1990), and HIV-infected, activated $CD4^+$ T cells typically result in productive infection, which causes these cells to quickly die (Ho et al., 1995; Wei et al., 1995). Thus, it is believed that latency arises when an activated $CD4^+$ T cell becomes infected, but transitions into a memory state before it can be killed (Figure 1-2). The transition to quiescence strongly downregulates HIV expression, resulting in integrated, but transcriptionally silent, provirus (Hermankova et al., 2003; Lassen et al., 2004). Because memory cells are long-lived (Combadiere et al., 2004; Finzi et al., 1999; Hammarlund et al., 2003), these latently infected cells can persist, even in the presence of long-term ART. Based on quantitative viral outgrowth assays measuring the reservoir in people on long-term ART, it was previously estimated that the half-life of the reservoir was ~44 months (Siliciano et al., 2003). However, more recent data has shown that after 7 years of ART, the reservoir does not decay, but instead proliferates with an estimated doubling time of 23 years (McMyn et al., 2023). Thus, these latent cells will effectively remain in the body for the lifetime of the individual.

Although resting $CD4^+$ T cells are the most widely recognized source of the HIV reservoir, replication-competent virus can persist in other cell types during ART-suppression, including monocytes and macrophages (Chun et al., 2000). Monocyte and macrophage progenitors express CD4 and CCR5, albeit at very low levels, making them susceptible to HIV infection (Folks et al., 1988). Tissue resident macrophages, including those in the lung and brain, have been shown to harbor virus in ART-suppressed PLWH (Cribbs et al., 2015; Ko et al., 2019). While macrophages are generally short-lived and lack self-renewing capacity (Whitelaw, 1972), microglia may live for

decades (Reu et al., 2017), though their lifespan is much shorter than that of memory $CD4^+$ T cells. Additionally, virions encoding macrophage-tropic envelopes were detected in plasma from PLWH following ART interruption (Andrade et al., 2020). Together, these data support monocytes and macrophages as a potential HIV reservoir that can contribute to viral re-emergence following cessation of treatment.

In addition to cellular reservoirs, anatomical reservoirs such as the central nervous system (CNS), genital tract, and lymph nodes serve as reservoirs of HIV (Coombs et al., 2003; Gras & Kaul, 2010; Yukl et al., 2013). Because many of these anatomical sites are immune-privileged, such as the brain, testis and B cell follicular centers within lymph nodes, viral persistence is likely due to residual replication (Buzón et al., 2011; Chomont et al., 2009; Connick et al., 2007; Eisele & Siliciano, 2012; Fletcher et al., 2014). Understanding and identifying the various reservoirs that can sustain the infection during ART is critical to the development of cure strategies aimed at eliminating latent HIV.

EXPERIMENTAL APPROACHES FOR ELIMINATING HIV RESERVOIRS

Several strategies have been employed in an effort to eliminate the latent reservoir (Figure 1-3). To date, the only successful approach to eliminate the HIV reservoir involves ablative radiotherapy/chemotherapy combined with the transplantation of hematopoietic stem cells that confer resistance to HIV infection. This approach was used on Timothy Ray Brown (the "Berlin patient"), who was infected with HIV, but underwent chemotherapy for leukemia and received a bone marrow transplant from a donor who had a CCR5 Δ32 mutation, which results in cells lacking the CCR5 co-receptor required for HIV entry. Hematopoietic stem cells from the bone marrow donor repopulated his immune system with mature HIV-resistant cells (Allers et al., 2011; Hütter

et al., 2009) allowing him to be the first person known to be cured of HIV. However, because of the health risks and financial costs of such therapy, it is unlikely that this treatment would be a viable option for a majority of PLWH. Potentially safer alternatives, including gene-editing strategies aimed to modify of one's own stem including gene-editing strategies aimed to modify of one's own stem cells to lack CCR5 expression, thus avoiding potential complication associated with graft-versus-host disease (GVHD) caused by donor mismatch (Shen et al., 2013) and more mild conditioning alternatives to harsh radiotherapy/chemotherapy are being investigated (Pace et al., 2011).

Another popular, multi-faceted approach directed towards eliminating infected cells is to utilize

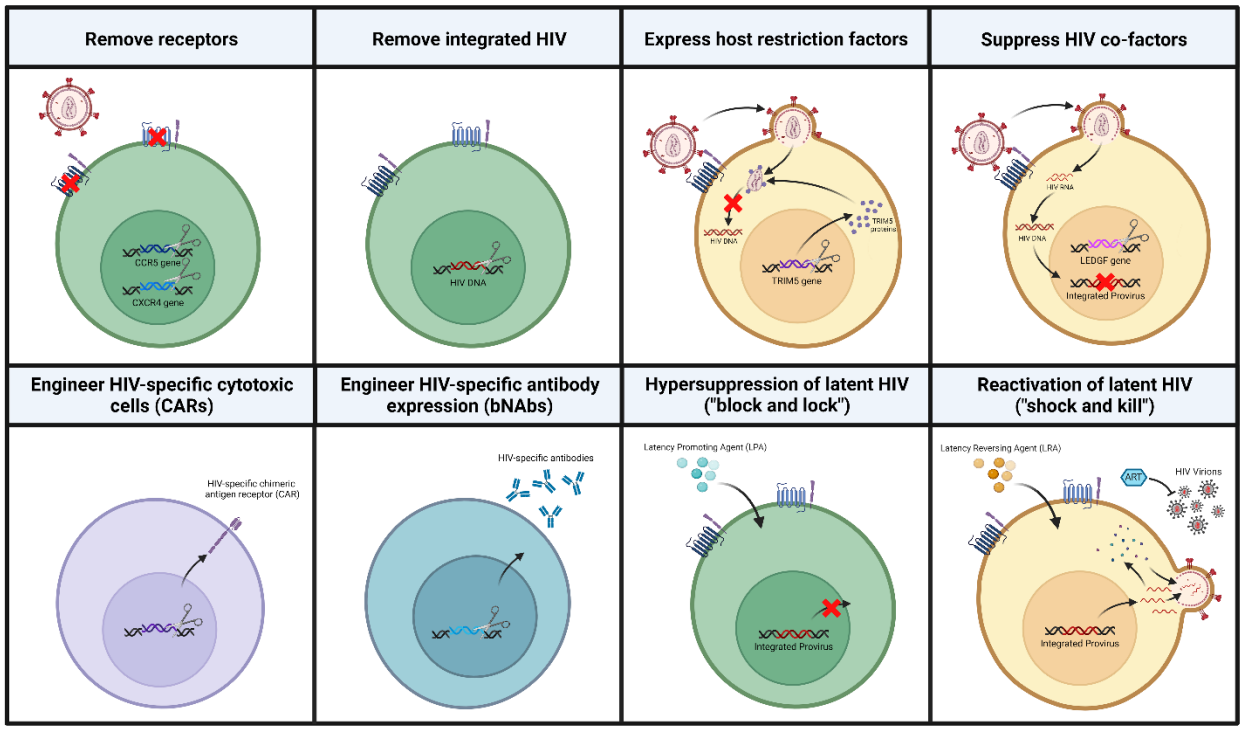

Figure 1-3. Experimental approaches to eliminate latent HIV. Various different strategies aimed at eliminating latent HIV include the removal of CCR5 and/or CXCR4 co-receptors, excising HIV proviral DNA, promoting the expression of host restriction factors, suppressing host co-factors used by HIV to replicate, engineering HIV-specific cytotoxic cells, such as CD8 T-cells or NK cells, engineering B cells to produce HIV-specific antibodies, using latency-inducing agents (LPAs) to induce deep latency and using latency reversing agents (LRAs) to reactivate latent virus. Created with BioRender.com.

gene editing strategies to remove or suppress HIV (Aubert et al., 2011; Qu et al., 2013; Sarkar et al., 2007). The most conceptually straightforward approach involves the excision of latent provirus using DNA-editing enzymes to remove viral DNA from infected cells (Yin et al., 2017). Introduction of genes, such as host restriction factors, could block the replication of HIV without the continued use of ART (Bogerd et al., 2015). Suppression of genes for host cell cofactors that are required for HIV replication, such as LEDGF, are also being investigated (Bobbin et al., 2015). Similarly, inducing stable, long-term transcriptional suppression through epigenetic silencing, referred to as the "block and lock" approach, is being studied (Ahlenstiel et al., 2020). Gene therapies are also being explored in the context of B cells, $CD8^+$ T cells and NK cells, allowing them to specifically target and eliminate HIV-infected cells. Despite the plethora of potential applications for gene therapy in cure studies, challenges associated with the delivery and longevity of such approaches remain problematic.

An alternative approach to gene therapy for eliminating latent virus involves the pharmacological induction of HIV expression followed by the subsequent elimination of reactivated cells. This method, often referred to as the "kick and kill" or "shock and kill" approach, works by stimulating cells with a latency reversing agent (LRA) that activates latently infected cells to express viral proteins, which makes the susceptible to elimination via viral cytopathic effects, immune-mediated clearance or HIV-specific targeted therapeutics (Marsden & Zack, 2015, 2019) (Figure 1-4). When LRAs are administered while maintaining ART, spreading infection by newly produced virions would be inhibited.

USING PKC MODULATORS IN KICK AND KILL STRATEGIES

Several pharmacological LRAs have been identified and demonstrated to reverse HIV latency (Kim et al., 2018; Sadowski & Hashemi, 2019; Spivak & Planelles, 2018). One of the most promising classes of LRAs are protein kinase C (PKC) modulators (Baxter et al., 2016; Beans et al., 2013; Bullen et al., 2014; Darcis et al., 2015; DeChristopher et al., 2012; Jiang et al., 2015; Kinter et al., 1990; Marsden et al., 2017; Pérez et al., 2010; Qatsha et al., 1993). PKC modulators diffuse through the cellular membrane and act as mimetics to diacylglycerol (DAG), which binds to PKC, resulting in downstream phosphorylation of target proteins, including the activation of the transcription factor NF-kappa B (NFκB), which binds to the HIV LTR to promote transcription (Williams et al., 2004)(Figure 1-5). Natural PKC modulators, such as prostratin and bryostatin-1, have been shown to promote transcription activation of latent HIV provirus. Additionally, prostratin can inhibit viral replication by down-regulating the HIV entry receptors CD4, CXCR4 and CCR5 (Gulakowski et al., 1997; Korin et al., 2002; Kulkosky et al., 2001; Marsden et al., 2018). Bryostatin-1 is the only PKC modulator tested in clinical trials (Gutierrez et al., 2016). However, single administration of bryostatin-1 at the low doses tested did not result in PKC activation nor HIV transcription. These results, along with the challenges of a limited therapeutic range and constraints linked to obtaining from natural sources (Schaufelberger et al., 1991),

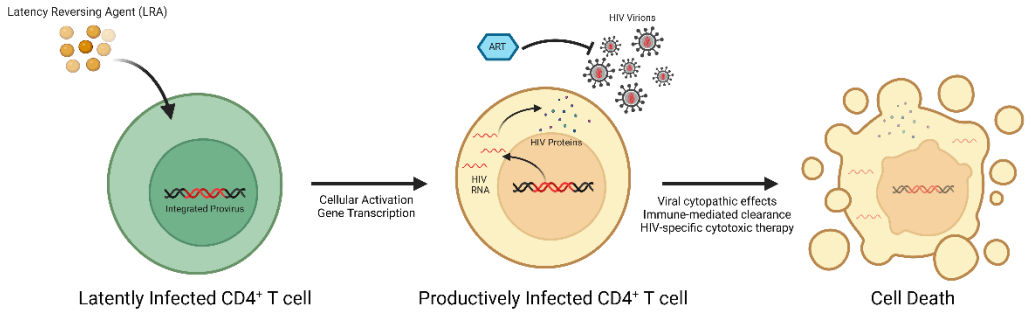

Figure 1-4. HIV "kick and kill" strategy. $CD4^+$ T cells harboring latent provirus can be pharmacologically stimulated by a latency reversing agent (LRA) to induce cellular activation and gene transcription. This results in productive infection, wherein the virus is "reawakened" from latency. Due to the expression of HIV proteins, productively infected cells are quickly eliminated via viral cytopathic effects, immune-mediated clearance or HIV-specific cytotoxic therapies. Created with BioRender.com.

underscore the necessity for improved LRAs.

To address these limitations, recent practical syntheses of the natural PKC modulators prostratin and bryostatin-1 have enabled the creation of designed and synthetic PKC modulator analogs that exhibit superior efficacy and tolerability when compared to their parent compounds

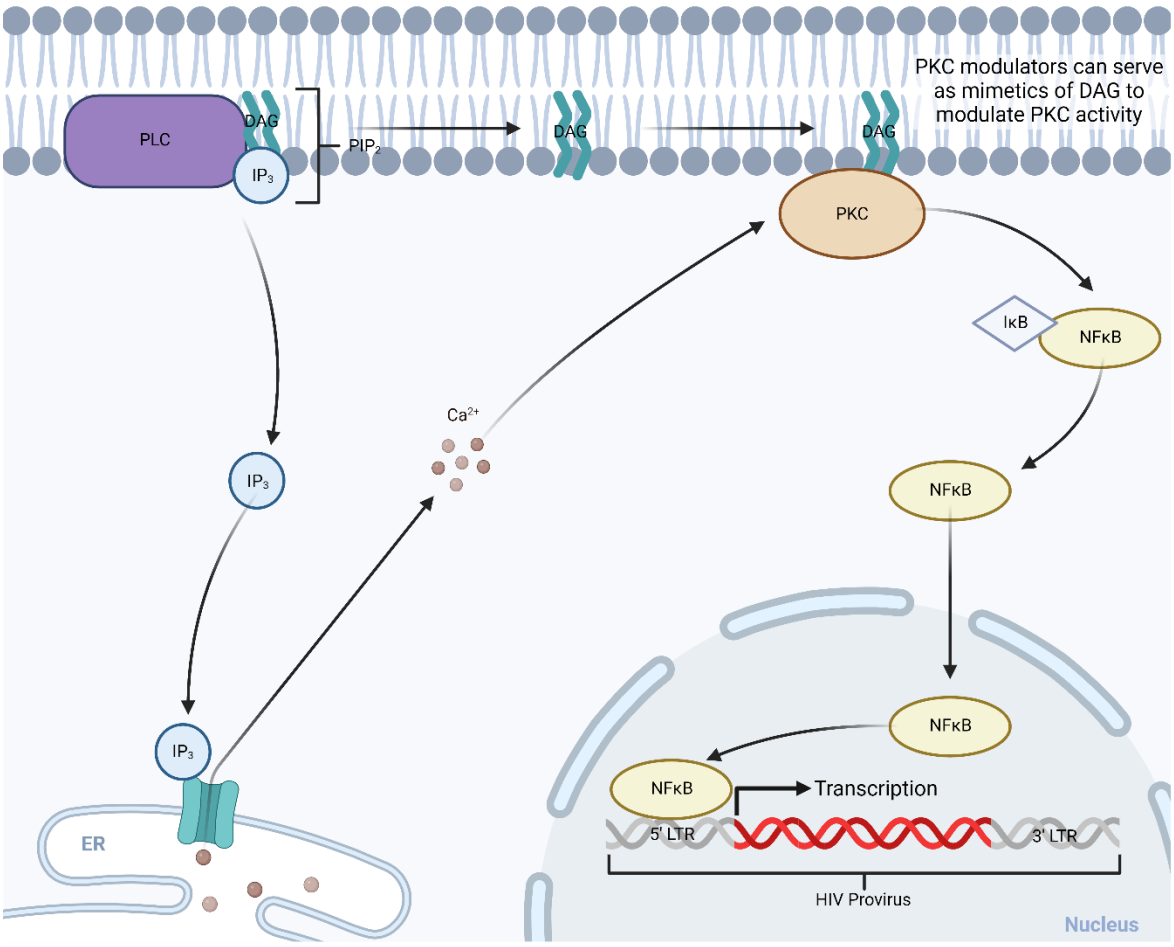

Figure 1-5. Mechanism of HIV latency reversal by protein kinase C (PKC) modulators. Upon cellular activation, phospholipase C (PLC) enzymatically cleaves the membrane phospholipid phosphoatidylinositol-4,5-bisphopshate (PIP_2) into diacylglycerol (DAG) and inositol trisphosphate (IP_3). IP_3 stimulates the release of calcium from intracellular organelles, such as the endoplasmic reticulum (ER) via activation of IP_3-mediated Ca^{2+} channels. DAG remains in the membrane. PKC can become activated in response to cytoplasmic Ca^{2+} and DAG, resulting in phosphorylation of proteins involved in various cellular processes, such as cell proliferation and the regulation of gene expression, including the transcription factor NFκB. PKC modulators, such as prostratin, bryostatin-1 and SUW133 mimic DAG to phosphorylate the NFκB-IκB complex, leading to ubiquitination and proteasomal degradation of IκB and unveiling a nuclear localization sequence on NFκB. Activated NFκB can translocate to the nucleus and bind to the 5' LTR of latent proviruses to initiate transcription. Adapted from "Activation of Protein Kinase C (PKC)", by BioRender.com (2024). Retrieved from https://app.biorender.com/biorender-templates.

(Beans et al., 2013; Marsden et al., 2018; Sloane et al., 2020; Wender, Donnelly, et al., 2015; Wender et al., 2017; Wender et al., 2008; Wender, Quiroz, & Stevens, 2015). One particularly potent bryostatin-1 analog, SUW133, induced latent HIV expression and caused some of the reactivated cells to die 1 day after compound administration *in vivo* in humanized bone marrow-liver-thymus (BLT) mice (Marsden et al., 2017). Moreover, SUW133 has been shown to reverse HIV latency in cell lines and patient-derived cells (Marsden et al., 2018). These findings indicate that the powerful effect produced by SUW133 treatment not only triggers the reactivation of latent provirus but also has the potential to eliminate some of the reactivated cells. Whether this results in a biological impact to the latent reservoir by delaying or eliminating viral rebound remains unknown.

NATURAL KILLER CELLS AND HIV

To date, clinical trials with LRAs have shown that these drugs are capable of inducing viral gene expression *in vivo*, but there has been little to no observed turnover of reactivated cells (Archin et al., 2017; Archin et al., 2012; Elliott et al., 2015; Elliott et al., 2014; Gutierrez et al., 2016; Rasmussen et al., 2014; Sogaard et al., 2015). This underlines the necessity of combining LRAs with an enhanced "kill" strategy aimed to promote elimination of cells following latency reversal. Immune-based strategies, such as broadly neutralizing antibodies, vaccines and enhancing the effector functions of anti-HIV immune cells, are currently in development (Brockman et al., 2015; Marsden & Zack, 2015; Wykes & Lewin, 2018).

Another potential effector cell that may play an important role in antiviral defense are natural killer (NK) cells. NK cells play an important role in antiviral and antitumor immunity (Davis et al., 2015; Jeyaraman et al., 2021; Vivier et al., 2008). They can rapidly kill target cells through contact-

dependent mechanisms, the release of cytotoxic granules and activating death receptor pathways to induce apoptosis (Vivier et al., 2008). They can also eliminate cells via antibody-dependent cell cytotoxicity (ADCC), where the FcγIII receptor (CD16) on the surface of NK cells binds to the constant region of antibodies on the surface of opsonized target cells. This initiates a signaling cascade within the NK cells that results in killing of the antibody-coated cell (Bournazos et al., 2017). Additionally, NK cells can secrete antiviral cytokines and chemokines (Lodoen & Lanier, 2006). NK cells have not been employed for clinical treatment of HIV. However, studies have shown that NK cells can reduce viral transmission and suppress acute infection (Jennes et al., 2013; Ni et al., 2014). Whether they can contribute to elimination of the viral reservoir remains unknown.

SIGNIFICANCE AND DISSERTATION OVERVIEW

In summary, while the advent of antiretroviral therapy has resulted in significant advances in the management of HIV, it is not a cure, due to the persistence of a long-lived reservoir of latently-infected cells. While there are many approaches currently under investigation for how to reduce or eliminate latent provirus, few have advanced to clinical trials and those that have only yielded modest results. This underscores the need for novel therapies and approaches that can potently eliminate latent HIV. We have previously shown that a novel bryostatin-1 analog (SUW133) exhibits increased tolerability and superior efficacy at inducing HIV latency reversal compared to its parent compound. Furthermore, we observed that SUW133 not only triggers the reactivation of latent provirus but also results in the death of some reactivated cells. Whether this translates to clinically relevant outcomes, such as a delay or reduction in viral rebound is unknown. However, prior studies utilizing LRAs alone have shown limited elimination of reactivated cells. Thus, it may be beneficial to couple LRAs with an enhanced kill strategy that can aid in turnover of

reactivated cells. To this extent, NK cells may serve as a promising candidate. As part of the innate immune system, they rapidly eliminate target cells through a variety of mechanisms. Additionally, they have shown to be safely employed in clinical studies for cancer and infectious diseases, though they have not been clinically evaluated against HIV. In this study, we investigate the use of barcoded HIV to evaluate the efficacy of SUW133 alone or in combination with NK cells as a potential therapeutic approach against HIV latency (Chapter 2), examine whether SUW133 improves the activity of NK cells by modulating their capacity to recognize and kill target cells (Chapter 3), and conclude with a forward-looking characterization of synergistic combinations of SUW133 and histone deacetylase inhibitors (HDACi) (Chapter 4). Findings from this study highlight new and exciting opportunities to exploit the beneficial attributes of novel kick and kill approaches for HIV immunotherapy.

REFERENCES

Ahlenstiel, C. L., Symonds, G., Kent, S. J., & Kelleher, A. D. (2020). Block and Lock HIV Cure Strategies to Control the Latent Reservoir. *Front Cell Infect Microbiol*, *10*, 424. https://doi.org/10.3389/fcimb.2020.00424

Allers, K., Hutter, G., Hofmann, J., Loddenkemper, C., Rieger, K., Thiel, E., & Schneider, T. (2011). Evidence for the cure of HIV infection by CCR5Delta32/Delta32 stem cell transplantation. *Blood*, *117*(10), 2791-2799. https://doi.org/10.1182/blood-2010-09-309591

Andrade, V. M., Mavian, C., Babic, D., Cordeiro, T., Sharkey, M., Barrios, L., Brander, C., Martinez-Picado, J., Dalmau, J., Llano, A., Li, J. Z., Jacobson, J., Lavine, C. L., Seaman, M. S., Salemi, M., & Stevenson, M. (2020). A minor population of macrophage-tropic HIV-1 variants is identified in recrudescing viremia following analytic treatment interruption. *Proc Natl Acad Sci U S A*, *117*(18), 9981-9990. https://doi.org/10.1073/pnas.1917034117

Archin, N. M., Kirchherr, J. L., Sung, J. A., Clutton, G., Sholtis, K., Xu, Y., Allard, B., Stuelke, E., Kashuba, A. D., Kuruc, J. D., Eron, J., Gay, C. L., Goonetilleke, N., & Margolis, D. M. (2017). Interval dosing with the HDAC inhibitor vorinostat effectively reverses HIV latency. *J Clin Invest*, *127*(8), 3126-3135. https://doi.org/10.1172/JCI92684

Archin, N. M., Liberty, A. L., Kashuba, A. D., Choudhary, S. K., Kuruc, J. D., Crooks, A. M., Parker, D. C., Anderson, E. M., Kearney, M. F., Strain, M. C., Richman, D. D., Hudgens, M. G., Bosch, R. J., Coffin, J. M., Eron, J. J., Hazuda, D. J., & Margolis, D. M. (2012). Administration of vorinostat disrupts HIV-1 latency in patients on antiretroviral therapy. *Nature*, *487*(7408), 482-485. https://doi.org/10.1038/nature11286

Aubert, M., Ryu, B. Y., Banks, L., Rawlings, D. J., Scharenberg, A. M., & Jerome, K. R. (2011). Successful targeting and disruption of an integrated reporter lentivirus using the engineered homing endonuclease Y2 I-AniI. *PLoS One*, *6*(2), e16825. https://doi.org/10.1371/journal.pone.0016825

Beans, E. J., Fournogerakis, D., Gauntlett, C., Heumann, L. V., Kramer, R., Marsden, M. D., Murray, D., Chun, T. W., Zack, J. A., & Wender, P. A. (2013). Highly potent, synthetically accessible prostratin analogs induce latent HIV expression in vitro and ex vivo. *Proc Natl Acad Sci U S A*, *110*(29), 11698-11703. https://doi.org/10.1073/pnas.1302634110

Bobbin, M. L., Burnett, J. C., & Rossi, J. J. (2015). RNA interference approaches for treatment of HIV-1 infection. *Genome Med*, *7*(1), 50. https://doi.org/10.1186/s13073-015-0174-y

Bogerd, H. P., Kornepati, A. V., Marshall, J. B., Kennedy, E. M., & Cullen, B. R. (2015). Specific induction of endogenous viral restriction factors using CRISPR/Cas-derived

transcriptional activators. *Proc Natl Acad Sci U S A*, *112*(52), E7249-7256. https://doi.org/10.1073/pnas.1516305112

Bournazos, S., Wang, T. T., Dahan, R., Maamary, J., & Ravetch, J. V. (2017). Signaling by Antibodies: Recent Progress. *Annu Rev Immunol*, *35*, 285-311. https://doi.org/10.1146/annurev-immunol-051116-052433

Brockman, M. A., Jones, R. B., & Brumme, Z. L. (2015). Challenges and Opportunities for T-Cell-Mediated Strategies to Eliminate HIV Reservoirs. *Front Immunol*, *6*, 506. https://doi.org/10.3389/fimmu.2015.00506

Bukrinsky, M. I., Stanwick, T. L., Dempsey, M. P., & Stevenson, M. (1991). Quiescent T lymphocytes as an inducible virus reservoir in HIV-1 infection. *Science*, *254*(5030), 423-427. https://doi.org/10.1126/science.1925601

Buzón, M. J., Codoñer, F. M., Frost, S. D., Pou, C., Puertas, M. C., Massanella, M., Dalmau, J., Llibre, J. M., Stevenson, M., Blanco, J., Clotet, B., Paredes, R., & Martinez-Picado, J. (2011). Deep molecular characterization of HIV-1 dynamics under suppressive HAART. *PLoS Pathog.*, *7*(10), e1002314. https://doi.org/10.1371/journal.ppat.1002314

CDC. (2020). *Opportunistic Infections | Living with HIV | HIV Basics | HIV/AIDS | CDC*. https://www.cdc.gov/hiv/basics/livingwithhiv/opportunisticinfections.html#:~:text=AIDS%20(acquired%20immunodeficiency%20syndrome)%20is,called%20opportunistic%20infections%20(OIs).

Chomont, N., El-Far, M., Ancuta, P., Trautmann, L., Procopio, F. A., Yassine-Diab, B., Boucher, G., Boulassel, M. R., Ghattas, G., Brenchley, J. M., Schacker, T. W., Hill, B. J., Douek, D. C., Routy, J. P., Haddad, E. K., & Sekaly, R. P. (2009). HIV reservoir size and persistence are driven by T cell survival and homeostatic proliferation. *Nat Med*, *15*(8), 893-900. https://doi.org/10.1038/nm.1972

Chun, T. W., Carruth, L., Finzi, D., Shen, X., DiGiuseppe, J. A., Taylor, H., Hermankova, M., Chadwick, K., Margolick, J., Quinn, T. C., Kuo, Y. H., Brookmeyer, R., Zeiger, M. A., Barditch-Crovo, P., & Siliciano, R. F. (1997). Quantification of latent tissue reservoirs and total body viral load in HIV-1 infection. *Nature*, *387*(6629), 183-188. https://doi.org/10.1038/387183a0

Chun, T. W., Davey, R. T. J., Engel, D., Lane, H. C., & Fauci, A. S. (1999). Re-emergence of HIV after stopping therapy. *Nature*, *401*(6756), 874-875. https://doi.org/10.1038/44755

Chun, T. W., Davey, R. T. J., Ostrowski, M., Shawn Justement, J., Engel, D., Mullins, J. I., & Fauci, A. S. (2000). Relationship between pre-existing viral reservoirs and the re-emergence of plasma viremia after discontinuation of highly active anti-retroviral therapy. *Nat Med*, *6*(7), 757–761. https://doi.org/10.1038/77481

Combadiere, B., Boissonnas, A., Carcelain, G., Lefranc, E., Samri, A., Bricaire, F., Debre, P., & Autran, B. (2004). Distinct time effects of vaccination on long-term proliferative and IFN-gamma-producing T cell memory to smallpox in humans. *J Exp Med*, *199*(11), 1585-1593. https://doi.org/10.1084/jem.20032083

Connick, E., Mattila, T., Folkvord, J. M., Schlichtemeier, R., Meditz, A. L., Ray, M. G., McCarter, M. D., Mawhinney, S., Hage, A., White, C., & Skinner, P. J. (2007). CTL fail to accumulate at sites of HIV-1 replication in lymphoid tissue. *J Immunol*, *178*(11), 6975-6983. https://doi.org/10.4049/jimmunol.178.11.6975

Coombs, R. W., Reichelderfer, P. S., & Landay, A. L. (2003). Recent observations on HIV type-1 infection in the genital tract of men and women. *AIDS*, *17*(4), 455-480. https://doi.org/10.1097/00002030-200303070-00001

Cribbs, S. K., Lennox, J., Caliendo, A. M., Brown, L. A., & Guidot, D. M. (2015). Healthy HIV-1-infected individuals on highly active antiretroviral therapy harbor HIV-1 in their alveolar macrophages. *AIDS Res Hum Retroviruses*, *31*(1), 64-70. https://doi.org/10.1089/AID.2014.0133

Davis, Z. B., Felices, M., Verneris, M. R., & Miller, J. S. (2015). Natural Killer Cell Adoptive Transfer Therapy: Exploiting the First Line of Defense Against Cancer. *Cancer J*, *21*(6), 486-491. https://doi.org/10.1097/PPO.0000000000000156

Desai, M., Iyer, G., & Dikshit, R. K. (2012). Antiretroviral drugs: critical issues and recent advances. *Indian J Pharmacol*, *44*(3), 288-298. https://doi.org/10.4103/0253-7613.96296

Eisele, E., & Siliciano, R. F. (2012). Redefining the viral reservoirs that prevent HIV-1 eradication. *Immunity*, *37*(3), 377-388. https://doi.org/10.1016/j.immuni.2012.08.010

Elliott, J. H., McMahon, J. H., Chang, C. C., Lee, S. A., Hartogensis, W., Bumpus, N., Savic, R., Roney, J., Hoh, R., Solomon, A., Piatak, M., Gorelick, R. J., Lifson, J., Bacchetti, P., Deeks, S. G., & Lewin, S. R. (2015). Short-term administration of disulfiram for reversal of latent HIV infection: a phase 2 dose-escalation study. *Lancet HIV*, *2*(12), e520-529. https://doi.org/10.1016/S2352-3018(15)00226-X

Elliott, J. H., Wightman, F., Solomon, A., Ghneim, K., Ahlers, J., Cameron, M. J., Smith, M. Z., Spelman, T., McMahon, J., Velayudham, P., Brown, G., Roney, J., Watson, J., Prince, M. H., Hoy, J. F., Chomont, N., Fromentin, R., Procopio, F. A., Zeidan, J., . . . Lewin, S. R. (2014). Activation of HIV transcription with short-course vorinostat in HIV-infected patients on suppressive antiretroviral therapy. *PLoS Pathog*, *10*(10), e1004473. https://doi.org/10.1371/journal.ppat.1004473

Fatkenheuer, G., Pozniak, A. L., Johnson, M. A., Plettenberg, A., Staszewski, S., Hoepelman, A. I., Saag, M. S., Goebel, F. D., Rockstroh, J. K., Dezube, B. J., Jenkins, T. M., Medhurst, C., Sullivan, J. F., Ridgway, C., Abel, S., James, I. T., Youle, M., & van der Ryst, E. (2005). Efficacy of short-term monotherapy with maraviroc, a new CCR5 antagonist, in

patients infected with HIV-1. *Nat Med*, *11*(11), 1170-1172. https://doi.org/10.1038/nm1319

Finzi, D., Blankson, J., Siliciano, J. D., Margolick, J. B., Chadwick, K., Pierson, T., Smith, K., Lisziewicz, J., Lori, F., Flexner, C., Quinn, T. C., Chaisson, R. E., Rosenberg, E., Walker, B., Gange, S., Gallant, J., & Siliciano, R. F. (1999). Latent infection of CD4+ T cells provides a mechanism for lifelong persistence of HIV-1, even in patients on effective combination therapy. *Nat Med*, *5*(5), 512-517. https://doi.org/10.1038/8394

Fletcher, C. V., Staskus, K., Wietgrefe, S. W., Rothenberger, M., Reilly, C., Chipman, J. G., Beilman, G. J., Khoruts, A., Thorkelson, A., Schmidt, T. E., Anderson, J., Perkey, K., Stevenson, M., Perelson, A. S., Douek, D. C., Haase, A. T., & Schacker, T. W. (2014). Persistent HIV-1 replication is associated with lower antiretroviral drug concentrations in lymphatic tissues. *Proc Natl Acad Sci U S A*, *111*(6), 2307-2312. https://doi.org/10.1073/pnas.1318249111

Folks, T. M., Kessler, S. W., Orenstein, J. M., Justement, J. S., Jaffe, E. S., & Fauci, A. S. (1988). Infection and replication of HIV-1 in purified progenitor cells of normal human bone marrow. *Science*, *242*(4880), 919-922. https://doi.org/10.1126/science.2460922

Gras, G., & Kaul, M. (2010). Molecular mechanisms of neuroinvasion by monocytes-macrophages in HIV-1 infection. *Retrovirology*, *7*, 30. https://doi.org/10.1186/1742-4690-7-30

Grinsztejn, B., Nguyen, B. Y., Katlama, C., Gatell, J. M., Lazzarin, A., Vittecoq, D., Gonzalez, C. J., Chen, J., Harvey, C. M., Isaacs, R. D., & Team, P. (2007). Safety and efficacy of the HIV-1 integrase inhibitor raltegravir (MK-0518) in treatment-experienced patients with multidrug-resistant virus: a phase II randomised controlled trial. . *Lancet*, *369*(9569), 1261–1269. https://doi.org/10.1016/S0140-6736(07)60597-2

Gulick, R. M., Mellors, J. W., Havlir, D., Eron, J. J., Gonzalez, C., McMahon, D., Richman, D. D., Valentine, F. T., Jonas, L., Meibohm, A., Emini, E. A., & Chodakewitz, J. A. (1997). Treatment with indinavir, zidovudine, and lamivudine in adults with human immunodeficiency virus infection and prior antiretroviral therapy. *N Engl J Med*, *337*(11), 734-739. https://doi.org/10.1056/NEJM199709113371102

Gutierrez, C., Serrano-Villar, S., Madrid-Elena, N., Perez-Elias, M. J., Martin, M. E., Barbas, C., Ruiperez, J., Munoz, E., Munoz-Fernandez, M. A., Castor, T., & Moreno, S. (2016). Bryostatin-1 for latent virus reactivation in HIV-infected patients on antiretroviral therapy. *AIDS*, *30*(9), 1385-1392. https://doi.org/10.1097/QAD.0000000000001064

Hammarlund, E., Lewis, M. W., Hansen, S. G., Strelow, L. I., Nelson, J. A., Sexton, G. J., Hanifin, J. M., & Slifka, M. K. (2003). Duration of antiviral immunity after smallpox vaccination. *Nat Med*, *9*(9), 1131-1137. https://doi.org/10.1038/nm917

Hammer, S. M., Squires, K. E., Hughes, M. D., Grimes, J. M., Demeter, L. M., Currier, J. S., Eron, J. J., Jr, Feinberg, J. E., Balfour, H. H., Jr, Deyton, L. R., Chodakewitz, J. A., & Fischl, M. A. (1997). A controlled trial of two nucleoside analogues plus indinavir in persons with human immunodeficiency virus infection and CD4 cell counts of 200 per cubic millimeter or less. AIDS Clinical Trials Group 320 Study Team. *N Engl J Med*, *337*(11), 725-733. https://doi.org/10.1056/NEJM199709113371101

Hermankova, M., Siliciano, J. D., Zhou, Y., Monie, D., Chadwick, K., Margolick, J. B., Quinn, T. C., & Siliciano, R. F. (2003). Analysis of human immunodeficiency virus type 1 gene expression in latently infected resting CD4+ T lymphocytes in vivo. *J Virol*, *77*(13), 7383-7392. https://doi.org/10.1128/jvi.77.13.7383-7392.2003

Hirsch, M. S., Conway, B., D'Aquila, R. T., Johnson, V. A., Brun-Vézinet, F., Clotet, B., Demeter, L. M., Hammer, S. M., Jacobsen, D. M., Kuritzkes, D. R., Loveday, C., Mellors, J. W., Vella, S., & Richman, D. D. (1998). Antiretroviral Drug Resistance Testing in Adults With HIV Infection. *JAMA*, *279*, 1984-1991. https://doi.org/10.1001/jama.279.24.1984

Ho, D. D., Neumann, A. U., Perelson, A. S., Chen, W., Leonard, J. M., & Markowitz, M. (1995). Rapid turnover of plasma virions and CD4 lymphocytes in HIV-1 infection. *Nature*, *373*(6510), 123-126. https://doi.org/10.1038/373123a0

Hull, M. W., & Montaner, J. (2011). Antiretroviral therapy: a key component of a comprehensive HIV prevention strategy. *Curr HIV/AIDS Rep*, *8*(2), 85-93. https://doi.org/10.1007/s11904-011-0076-6

Hütter, G., Nowak, D., Mossner, M., Ganepola, S., Müssig, A., Allers, K., Schneider, T., Hofmann, J., Kücherer, C., Blau, O., Blau, I. W., Hofmann, W. K., & Thiel, E. (2009). Long-term control of HIV by CCR5 Delta32/Delta32 stem-cell transplantation. *N Engl J Med*, *360*(7), 692-298. https://doi.org/10.1056/NEJMoa0802905

Jennes, W., Verheyden, S., Mertens, J. W., Camara, M., Seydi, M., Dieye, T. N., Mboup, S., Demanet, C., & Kestens, L. (2013). Inhibitory KIR/HLA incompatibility between sexual partners confers protection against HIV-1 transmission. *Blood*, *121*(7), 1157-1164. https://doi.org/10.1182/blood-2012-09-455352

Jeyaraman, M., Muthu, S., Bapat, A., Jain, R., Sushmitha, E. S., Gulati, A., Channaiah Anudeep, T., Dilip, S. J., Jha, N. K., Kumar, D., Kesari, K. K., Ojha, S., Dholpuria, S., Gupta, G., Dureja, H., Chellappan, D. K., Singh, S. K., Dua, K., & Jha, S. K. (2021). Bracing NK cell based therapy to relegate pulmonary inflammation in COVID-19. *Heliyon*, *7*(7), e07635. https://doi.org/10.1016/j.heliyon.2021.e07635

Kim, Y., Anderson, J. L., & Lewin, S. R. (2018). Getting the "Kill" into "Shock and Kill": Strategies to Eliminate Latent HIV. *Cell Host Microbe*, *23*(1), 14-26. https://doi.org/10.1016/j.chom.2017.12.004

Ko, A., Kang, G., Hattler, J. B., Galadima, H. I., Zhang, J., Li, Q., & Kim, W. K. (2019). Macrophages but not Astrocytes Harbor HIV DNA in the Brains of HIV-1-Infected Aviremic Individuals on Suppressive Antiretroviral Therapy. *J Neuroimmune Pharmacol.*, *14*, 110-119. https://doi.org/10.1007/s11481-018-9809-2

Lassen, K. G., Bailey, J. R., & Siliciano, R. F. (2004). Analysis of human immunodeficiency virus type 1 transcriptional elongation in resting CD4+ T cells in vivo. *J Virol*, *78*(17), 9105-9114. https://doi.org/10.1128/JVI.78.17.9105-9114.2004

Lodoen, M. B., & Lanier, L. L. (2006). Natural killer cells as an initial defense against pathogens. *Curr Opin Immunol*, *18*(4), 391-398. https://doi.org/10.1016/j.coi.2006.05.002

Marsden, M. D., Loy, B. A., Wu, X., Ramirez, C. M., Schrier, A. J., Murray, D., Shimizu, A., Ryckbosch, S. M., Near, K. E., Chun, T. W., Wender, P. A., & Zack, J. A. (2017). In vivo activation of latent HIV with a synthetic bryostatin analog effects both latent cell "kick" and "kill" in strategy for virus eradication. *PLoS Pathog*, *13*(9), e1006575. https://doi.org/10.1371/journal.ppat.1006575

Marsden, M. D., Wu, X., Navab, S. M., Loy, B. A., Schrier, A. J., DeChristopher, B. A., Shimizu, A. J., Hardman, C. T., Ho, S., Ramirez, C. M., Wender, P. A., & Zack, J. A. (2018). Characterization of designed, synthetically accessible bryostatin analog HIV latency reversing agents. *Virology*, *520*, 83-93. https://doi.org/10.1016/j.virol.2018.05.006

Marsden, M. D., & Zack, J. A. (2015). Experimental Approaches for Eliminating Latent HIV. *For Immunopathol Dis Therap*, *6*(1-2), 91-99. https://doi.org/10.1615/forumimmundisther.2016015242

Marsden, M. D., & Zack, J. A. (2019). HIV cure strategies: a complex approach for a complicated viral reservoir? *Future Virology*, *14*(1), 5-8. https://doi.org/10.2217/fvl-2018-0205

McMyn, N. F., Varriale, J., Fray, E. J., Zitzmann, C., MacLeod, H., Lai, J., Singhal, A., Moskovljevic, M., Garcia, M. A., Lopez, B. M., Hariharan, V., Rhodehouse, K., Lynn, K., Tebas, P., Mounzer, K., Montaner, L. J., Benko, E., Kovacs, C., Hoh, R., . . . Siliciano, J. M. (2023). The latent reservoir of inducible, infectious HIV-1 does not decrease despite decades of antiretroviral therapy. *J Clin Invest*, *133*(17). https://doi.org/10.1172/JCI171554

Ni, Z., Knorr, D. A., Bendzick, L., Allred, J., & Kaufman, D. S. (2014). Expression of chimeric receptor CD4zeta by natural killer cells derived from human pluripotent stem cells improves in vitro activity but does not enhance suppression of HIV infection in vivo. *Stem Cells*, *32*(4), 1021-1031. https://doi.org/10.1002/stem.1611

Pace, M. J., Agosto, L., Graf, E. H., & O'Doherty, U. (2011). HIV reservoirs and latency models. *Virology*, *411*(2), 344-354. https://doi.org/10.1016/j.virol.2010.12.041

Perelson, A. S., Essunger, P., Cao, Y., Vesanen, M., Hurley, A., Saksela, K., Markowitz, M., & Ho, D. D. (1997). Decay characteristics of HIV-1-infected compartments during combination therapy. *Nature*, *387*(6629), 188-191. https://doi.org/10.1038/387188a0

Pomerantz, R. J., & Horn, D. L. (2003). Twenty years of therapy for HIV-1 infection. . *Nat Med*, *9*(7), 867–873. https://doi.org/10.1038/nm0703-867

Qu, X., Wang, P., Ding, D., Li, L., Wang, H., Ma, L., Zhou, X., Liu, S., Lin, S., Wang, X., Zhang, G., Liu, S., Liu, L., Wang, J., Zhang, F., Lu, D., & Zhu, H. (2013). Zinc-finger-nucleases mediate specific and efficient excision of HIV-1 proviral DNA from infected and latently infected human T cells. *Nucleic Acids Res*, *41*(16), 7771-7782. https://doi.org/10.1093/nar/gkt571

Rasmussen, T. A., Tolstrup, M., Brinkmann, C. R., Olesen, R., Erikstrup, C., Solomon, A., Winckelmann, A., Palmer, S., Dinarello, C., Buzon, M., Lichterfeld, M., Lewin, S. R., Østergaard, L., & Søgaard, O. S. (2014). Panobinostat, a histone deacetylase inhibitor, for latent-virus reactivation in HIV-infected patients on suppressive antiretroviral therapy: a phase 1/2, single group, clinical trial. *Lancet*, *1*(1), e13–e21. https://doi.org/10.1016/S2352-3018(14)70014-1

Reu, P., Khosravi, A., Bernard, S., Mold, J. E., Salehpour, M., Alkass, K., Perl, S., Tisdale, J., Possnert, G., Druid, H., & Frisen, J. (2017). The Lifespan and Turnover of Microglia in the Human Brain. *Cell Rep*, *20*(4), 779-784. https://doi.org/10.1016/j.celrep.2017.07.004

Sadowski, I., & Hashemi, F. B. (2019). Strategies to eradicate HIV from infected patients: elimination of latent provirus reservoirs. *Cell Mol Life Sci*, *76*(18), 3583-3600. https://doi.org/10.1007/s00018-019-03156-8

Sarkar, I., Hauber, I., Hauber, J., & Buchholz, F. (2007). HIV-1 Proviral DNA Excision Using an Evolved Recombinase. *Science*, *316*(5833), 1912-1915. https://doi.org/10.1126/science.1141453

Schaufelberger, D. E., Koleck, M. P., Beutler, J. A., Vatakis, A. M., Alvarado, A. B., Andrews, P., Marzo, L. V., Muschik, G. M., Roach, J., & Ross, J. T. (1991). The large-scale isolation of bryostatin 1 from Bugula neritina following current good manufacturing practices. *J Nat Prod*, *54*(5), 1265-1270. https://doi.org/10.1021/np50077a004

Shen, A., Baker, J. J., Scott, G. L., Davis, Y. P., Ho, Y. Y., & Siliciano, R. F. (2013). Endothelial cell stimulation overcomes restriction and promotes productive and latent HIV-1 infection of resting CD4+ T cells. *J Virol*, *87*(17), 9768-9779. https://doi.org/10.1128/JVI.01478-13

Siliciano, J. D., Kajdas, J., Finzi, D., Quinn, T. C., Chadwick, K., Margolick, J. B., Kovacs, C., Gange, S. J., & Siliciano, R. F. (2003). Long-term follow-up studies confirm the stability of the latent reservoir for HIV-1 in resting CD4+ T cells. *Nat Med*, *9*(6), 727-728. https://doi.org/10.1038/nm880

Sloane, J. L., Benner, N. L., Keenan, K. N., Zang, X., Soliman, M. S. A., Wu, X., Dimapasoc, M., Chun, T. W., Marsden, M. D., Zack, J. A., & Wender, P. A. (2020). Prodrugs of PKC modulators show enhanced HIV latency reversal and an expanded therapeutic window. *Proc Natl Acad Sci U S A*, *117*(20), 10688-10698. https://doi.org/10.1073/pnas.1919408117

Sogaard, O. S., Graversen, M. E., Leth, S., Olesen, R., Brinkmann, C. R., Nissen, S. K., Kjaer, A. S., Schleimann, M. H., Denton, P. W., Hey-Cunningham, W. J., Koelsch, K. K., Pantaleo, G., Krogsgaard, K., Sommerfelt, M., Fromentin, R., Chomont, N., Rasmussen, T. A., Ostergaard, L., & Tolstrup, M. (2015). The Depsipeptide Romidepsin Reverses HIV-1 Latency In Vivo. *PLoS Pathog*, *11*(9), e1005142. https://doi.org/10.1371/journal.ppat.1005142

Spivak, A. M., & Planelles, V. (2018). Novel Latency Reversal Agents for HIV-1 Cure. *Annu Rev Med*, *69*, 421-436. https://doi.org/10.1146/annurev-med-052716-031710

Vivier, E., Tomasello, E., Baratin, M., Walzer, T., & Ugolini, S. (2008). Functions of natural killer cells. *Nat Immunol*, *9*(5), 503-510. https://doi.org/10.1038/ni1582

Wei, X., Ghosh, S. K., Taylor, M. E., Johnson, V. A., Emini, E. A., Deutsch, P., Lifson, J. D., Bonhoeffer, S., Nowak, M. A., & Hahn, B. H. (1995). Viral dynamics in human immunodeficiency virus type 1 infection. *Nature*, *373*(6510), 117-122. https://doi.org/10.1038/373117a0

Wender, P. A., Donnelly, A. C., Loy, B. A., Near, K. E., & Staveness, D. (2015). Rethinking the role of natural products: Function-oriented synthesis, bryostatin, and bryologs. In S. Hanessian (Ed.), *Natural Products in Medicinal Chemistry* (pp. 473–544). Wiley-VCH. https://doi.org/10.1002/9783527676545.ch14

Wender, P. A., Hardman, C. T., Ho, S., Jeffreys, M. S., Maclaren, J. K., Quiroz, R. V., Ryckbosch, S. M., Shimizu, A. J., Sloane, J. L., & Stevens, M. C. (2017). Scalable synthesis of bryostatin 1 and analogs, adjuvant leads against latent HIV. *Science*, *358*, 218–223. https://doi.org/10.1126/science.aan7969

Wender, P. A., Kee, J. M., & Warrington, J. M. (2008). Practical synthesis of prostratin, DPP, and their analogs, adjuvant leads against latent HIV. *Science*, *320*(5876), 649-652. https://doi.org/10.1126/science.1154690

Wender, P. A., Quiroz, R. V., & Stevens, M. C. (2015). Function through synthesis-informed design. *Acc Chem Res*, *48*(3), 752-760. https://doi.org/10.1021/acs.accounts.5b00004

Whitelaw, D. M. (1972). Observations on human monocyte kinetics after pulse labeling. *Cell Tissue Kinet.*, *5*(4), 311-317. https://doi.org/doi:10.1111/j.1365-2184.1972.tb00369.x

WHO. (2023a). HIV. https://www.who.int/health-topics/hiv-aids#tab=tab_1

WHO. (2023b). *WHO | HIV & AIDS*. https://www.who.int/news-room/fact-sheets/detail/hiv-aids

Williams, S. A., Chen, L. F., Kwon, H., Fenard, D., Bisgrove, D., Verdin, E., & Greene, W. C. (2004). Prostratin antagonizes HIV latency by activating NF-kappaB. *J Biol Chem*, *279*(40), 42008-42017. https://doi.org/10.1074/jbc.M402124200

Wykes, M. N., & Lewin, S. R. (2018). Immune checkpoint blockade in infectious diseases. *Nat Rev Immunol*, *18*(2), 91-104. https://doi.org/10.1038/nri.2017.112

Yin, C., Zhang, T., Qu, X., Zhang, Y., Putatunda, R., Xiao, X., Li, F., Xiao, W., Zhao, H., Dai, S., Qin, X., Mo, X., Young, W. B., Khalili, K., & Hu, W. (2017). In Vivo Excision of HIV-1 Provirus by saCas9 and Multiplex Single-Guide RNAs in Animal Models. *Mol Ther*, *25*(5), 1168-1186. https://doi.org/10.1016/j.ymthe.2017.03.012

Yukl, S. A., Shergill, A. K., Ho, T., Killian, M., Girling, V., Epling, L., Li, P., Wong, L. K., Crouch, P., Deeks, S. G., Havlir, D. V., McQuaid, K., Sinclair, E., & Wong, J. K. (2013). The distribution of HIV DNA and RNA in cell subsets differs in gut and blood of HIV-positive patients on ART: implications for viral persistence. *J Infect Dis*, *208*(8), 1212-1220. https://doi.org/10.1093/infdis/jit308

Zack, J. A., Arrigo, S. J., Weitsman, S. R., Go, A. S., Haislip, A., & Chen, I. S. (1990). HIV-1 Entry into Quiescent Primary Lymphocytes: Molecular Analysis Reveals a Labile, Latent Viral Structure. *Cell*, *61*(2), 213-222. https://doi.org/10.1016/0092-8674(90)90802-l

CHAPTER 2

Assessing the efficacy of kick and kill strategies using barcoded HIV

ABSTRACT

Despite advances in the treatment and management of HIV infection with antiretroviral therapy (ART), curative strategies remain elusive due to the persistence of latently infected cells. One strategy for eliminating latently infected cells, known as the "kick and kill" strategy, involves the pharmacological induction of viral protein expression via latency-reversing agents (LRAs) followed by the elimination of cells harboring reactivated virus via viral cytopathic effects or immune clearance. Natural killer (NK) cells have been shown to play an important role in inhibiting HIV infection, but it remains unclear whether NK cells can contribute to a reduction of rebounding viremia when ART is stopped. Here, we utilize a barcoded HIV virus swarm in the context of a humanized mouse model to study the effects of a designed, synthetic protein kinase C modulating LRA (SUW133) plus NK cells on HIV rebound. We show that mice treated with SUW133 during ART exhibit a delay in rebound following ART interruption. Furthermore, we observed a reduction in the number of unique barcoded viruses in SUW133-treated animals compared to control-treated animals, suggesting that LRA treatment eliminated some reservoir cells that would have contributed to viral rebound. Moreover, treating mice with a combination of SUW133 and allogeneic human peripheral blood natural killer cells during anti-retroviral therapy resulted in greater delay in rebound and further reduction in viral rebounding clones, even potentially eliminating the viral reservoir in a subset of mice. Together, these data support the use of barcoded virus to study the efficacy of treatment modalities against HIV latency and suggest that combination therapy utilizing SUW133 and allogenic NK cells may be an effective approach to reducing and eradicating the viral reservoir.

INTRODUCTION

In 2022, approximately 39 million individuals worldwide were reported to be living with HIV, while approximately 40 million had succumbed to HIV-related illnesses since the onset of the epidemic (UNAIDS, 2023). Treatment of HIV infection with antiretroviral therapy (ART) can inhibit viral replication and prevent disease progression. However, ART does not cure HIV infection (Chun et al., 2000; Davey et al., 1999), as the virus persists within latently infected cells, which, upon ART interruption, can rebound and rekindle clinical progression of infection. While HIV has been shown to infect many different cell types, including monocytes and macrophages, the virus preferentially infects $CD4^+$ T cells (Chun, Stuyver, et al., 1997; Finzi et al., 1997). It is believed that upon infection, a small subset of infected cells survives viral cytopathic effects and adopt a memory phenotype, allowing for the persistence of very-long-lived cells that harbor intact, integrated HIV genomes, but express little or no viral RNA and no viral proteins (Marsden & Zack, 2013), allowing them to evade immune detection and rendering them unsusceptible to ART. However, if ART is stopped, these latently infected cells can cause re-emergence of virus and spread of infection.

Humanized mice serve as powerful models to study HIV infection and evaluate therapeutic strategies aimed to reduce or eliminate the latent reservoir. Perhaps the most advanced small animal model of the human immune system is the bone marrow-liver-thymus (BLT) mouse (Marsden & Zack, 2017), which is generated by implanting human fetal liver and thymus tissue under the kidney capsule of an immunodeficient [typically Nod-SCID-common gamma chain (NSG) knockout] mouse, followed by sublethal irradiation to precondition the mice for efficient engraftment, then transfusion of human hematopoietic stem cells (Melkus et al., 2006). This results in reconstitution of a mouse with multilineage human immune cells, including $CD4^+$ and $CD8^+$ T

cells, natural killer (NK) cells, monocytes, macrophages, and dendritic cells (Marsden et al., 2012; Melkus et al., 2006). The humanized BLT mouse model can be successfully infected with HIV and form a post-integration latent reservoir in resting $CD4^+$ T cells (Denton et al., 2012; Llewellyn et al., 2019; Marsden et al., 2012; Marsden et al., 2017; Tsai et al., 2016). Infected mice can be treated with clinically relevant ART to suppress viral loads, and upon ART cessation, exhibit viral rebound similar to people living with HIV (PLWH).

Humanized mice have proven particularly valuable in evaluating the efficacy of pharmacological strategies aimed at depleting the latent reservoir. One such approach known as "kick and kill" aims to awaken, or “kick”, non-expressing HIV proviruses to induce expression of viral RNA and proteins using an LRA, thereby making these cells susceptible to elimination, or “kill”, by viral cytopathic effects and immune clearance (Marsden, 2020). Many different classes of LRAs that function through various mechanisms have been tested using *in vitro* or *in vivo* models (Archin et al., 2012; Brooks et al., 2003; Chun, Engel, et al., 1999; Jiang et al., 2015; Kulkosky et al., 2001; Marsden et al., 2018; Spivak et al., 2018; Zhu et al., 2012). One of the most potent classes of LRAs are protein kinase C (PKC) modulators, which activate NFκB to induce viral transcription of latent provirus (Laird et al., 2015). We have previously shown that the latency-reversing capabilities of naturally occurring PKC modulators, including bryostatin-1 and prostratin, can be improved by designing synthetic analogs of these compounds (Beans et al., 2013; DeChristopher et al., 2012; Marsden et al., 2018), which can improve their tolerability and bioactivity *in vivo*. One particularly potent bryostatin-1 analog (SUW133) induced latent HIV expression and caused some of the reactivated cells to die 1 day after compound administration *in vivo* in BLT mice (Marsden et al., 2017). These findings suggest that the potent “kick” induced by SUW133 treatment not only results in the reactivation of latent provirus, but is capable of inducing elimination of some reactivated

cells. However, it remains unknown whether this translates into clinically relevant outcomes, such as delaying or eliminating HIV rebound.

Allogeneic NK cells have been widely and safely used in the treatment of cancer due to their strong alloreactivity toward leukemic cells (Davis et al., 2015). Additionally, there are currently five clinical trials evaluating the use of allogeneic NK cells to treat COVID-19 (Jeyaraman et al., 2021). To date, allogeneic NK cells have not been used to clinically treat HIV infection. However, clinical studies have found that killer cell immunoglobulin like receptors (KIRs) and human leukocyte antigen (HLA) mismatches between HIV-1 discordant sexual partners correlate with protection against HIV transmission (Jennes et al., 2013). Similarly, allogeneic NK cells from healthy donors have been shown to inhibit HIV infection *in vitro* (Jennes et al., 2013). Additionally, adoptive transfer of allogeneic NK cells derived from human embryonic stem cells (hESC) inhibited acute HIV infection in humanized mice (Ni et al., 2014). Whether adoptive transfer of allogeneic NK cells can aid in the elimination of the viral reservoir remains unknown.

Thus, we sought to develop an accurate means of tracking viral replication and reservoir formation in order to quantify the efficacy of LRAs (and potential combination with separate "kill" approaches) on the latent reservoir. Prior studies have utilized "genetic barcodes", or short, unique nucleotide sequences used to tag individual molecules and track their behavior in a heterogeneous pool of cells, to study expression of a non-replicating HIV-based vector *in vitro* (Chen et al., 2017) or replication and rebound of simian immunodeficiency virus *in vivo* (Fennessey et al., 2017). In this study, we have devised a barcoded HIV system for tracking individual viral lineages as they establish latent reservoirs in BLT mice under ART treatment, and subsequently reactivate upon cessation of ART. Using this barcoded system in the context of humanized BLT mice, our findings

demonstrate that SUW133 can significantly influence the HIV reservoir under ART, resulting in a decrease in barcode diversity, suggesting a depletion of the reservoir. This depletion, in turn, led to a delay or prevention of viral rebound. Similarly, we also show that adoptive transfer of allogeneic NK cells following SUW133 administration further delays rebound and reduces barcode diversity to a greater extent than treatment with LRA or NK cells alone. These findings demonstrate the utility of barcoded HIV technology in a humanized mouse model to study the efficacy of curative strategies and highlight the combined use of SUW133 and NK cells as a potential approach against HIV latency.

RESULTS

Generation of barcoded HIV plasmid library

To track and quantify individual HIV clones during latency and rebound, we constructed a swarm of genetically barcoded HIV viruses, using the NL-hemagglutinin (HA) backbone plasmid as template for modification. The NL-HA virus contains a near-full-length, replication-competent, pathogenic HIV strain derived from NL4-3, which has been modified to express an HA epitope in place of Vpr (Ali & Yang, 2006), and has been utilized in previous *in vivo* latency studies (Llewellyn et al., 2019; Marsden et al., 2017). Expression of the HA tag allows for the identification of productively infected cells and the enrichment/depletion of latently infected cells. However, because it lacks a function Vpr gene, the virus cannot be used to study the effects of Vpr in latency studies. A unique, 21-nucleotide barcode sequence was inserted in a non-expressed region of this vector immediately upstream of the HA tag and outside any known cis elements or splice sites (Figure 2-1A). Each 3rd nucleotide of this barcode was constrained to a thymidine to avoid random strings of consecutive GC bases and premature stop codons, providing an overall

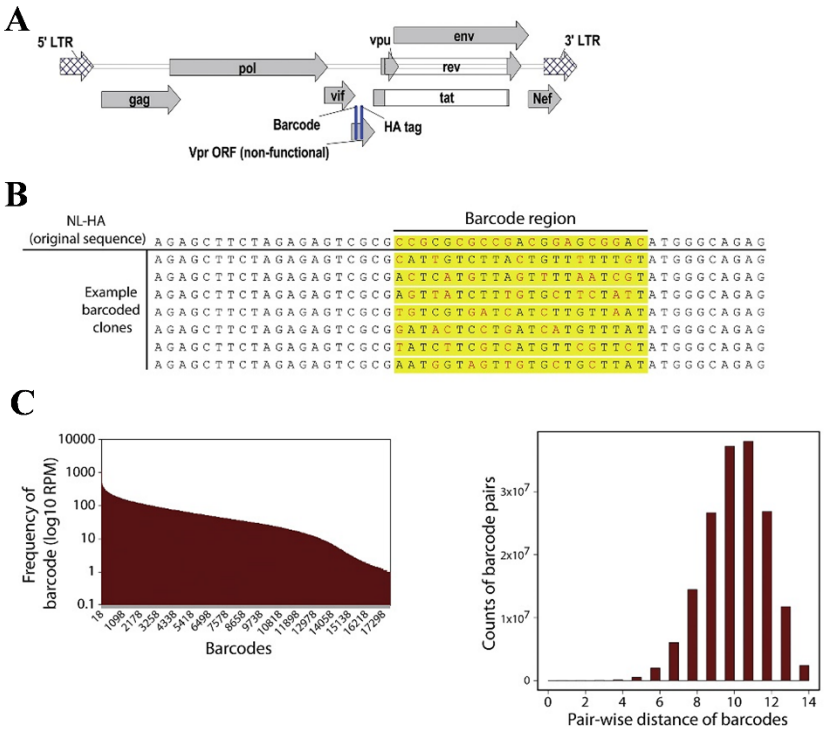

Figure 2-1. Generation of barcoded HIV plasmid library. A) Location of barcode upstream of the HA tag in the genome of HIV strain NL-HA. **B)** Example of individual 21 nucleotide "barcode" sequences in which each 3rd nucleotide is constrained to a thymine. **C)** Complexity of barcode region as quantified by HiSeq sequencing, showing ~18,000 barcodes with relatively equal distribution. **D)** Average pairwise distance between barcodes is ~11 bp.

---

theoretical complexity of 414 unique sequences (Figure 2-1B). The pool of plasmids was expanded in bacteria, with >20,000 bacterial colonies harvested, and then subjected to Illumina HiSeq deep sequencing, which revealed a barcode complexity of ~18,000 unique sequences with relatively similar frequencies (Figure 2-1C). There was an average difference of 11 base pairs between any 2 barcode sequences (Figure 2-1D), allowing for easy distinction between original barcodes in downstream virologic analyses. The library of barcoded plasmids (NL-HABC) was transfected into 293FT cells in parallel with the parental NL-HA plasmid to generate virions and yielded similar amounts of cell-free, as quantified by ELISA specific for HIV p24 (Figure 2-2A). Virions were collected and treated with DNase, followed by viral RNA extraction, then amplification and deep sequencing of the barcode region. As anticipated, the virions maintained a comparable

complexity and frequency of barcodes to those found in the original plasmid preparation. This correlation shows that individual barcodes are not strongly selected for or against during viral replication (Spearman correlation ρ = 0.99; Figure 2-2B).

In vitro analysis of barcoded HIV swarm shows similar activity to parental virus

To validate whether introduction of the genetic barcode affected infectivity of the virus *in vitro*,

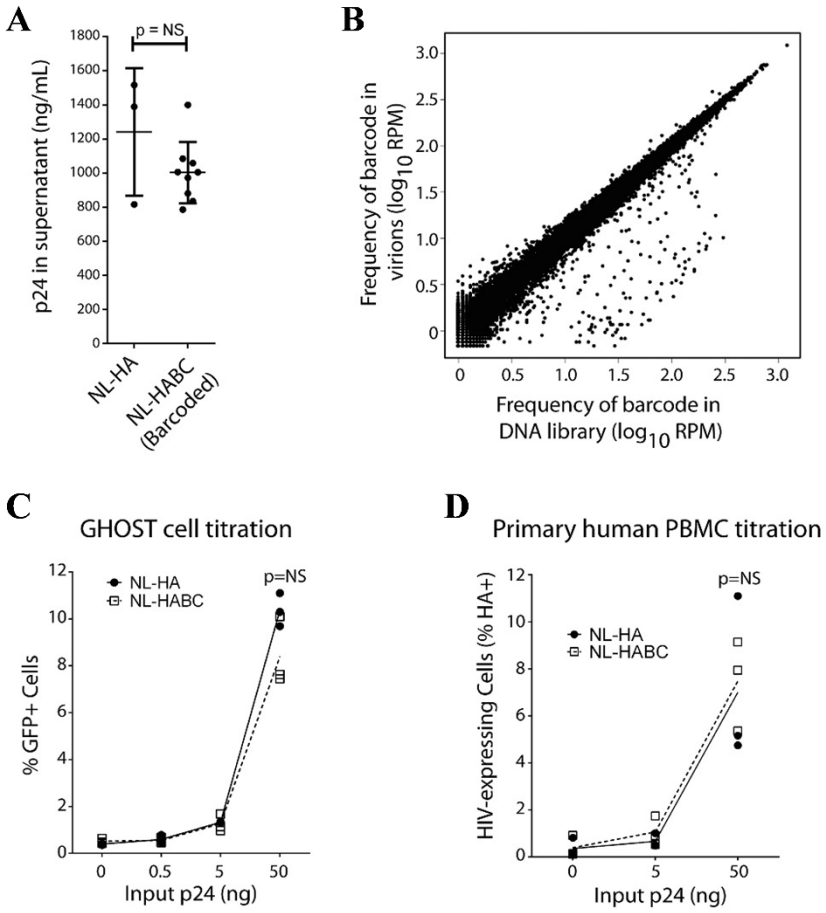

Figure 2-2. *In vitro* analysis of barcoded HIV swarm. A) Transfection with NLHABC plasmid produces similar HIV virion concentrations to transfection with the parental NL-HA plasmid as quantified by HIV p24 protein levels. n = 3 transfections (biological replicates) for NL-HA and 9 transfections (biological replicates) for NLHABC. Error bars, mean ± 1 SD. **B)** Comparison between barcode occurrence in original plasmid DNA and resultant virion-associated viral RNA after HIV production in 293FT cells (Spearman correlation ρ= 0.99). **C)** Infection of GHOST cells for 2 days show similar infectivity between NL-HA and NLHABC in a cell line model (n = 3 independent experiments). **D)** Infection of costimulated primary human PBMCs (n = 3 biological replicate infections per condition using cells from different human donors) for 3 days shows similar *in vitro* replication rate between NL-HA and NLHABC. Statistical comparisons in **(A)**, **(C)**, and **(D)** performed with unpaired, 2-sided t test.

we infected GHOST CXCR4^{+}CCR5^{+} cells, which carries an HIV LTR linked to a green fluorescent protein (GFP) gene allowing it to express GFP upon productive HIV infection, with parental NL-HA virus in parallel with the barcoded NL-HABC virus. Both viruses yielded similar frequencies of infected (GFP^{+}) after 2-day infections (Figure 2-2C and Supplemental Figure 2-1A). A similar experiment was conducted using human peripheral blood mononuclear cells (PBMCs) and different concentrations of either NL-HA or NL-HABC (Figure 2-2D and Supplemental Figure 2-1B) to assess infectivity in primary cells, resulting in statistically similar frequencies of HIV-expressing (HA^{+}) cells. Virus produced by primary PBMCs after 3 days of infection was harvested, and the barcode region was amplified by RT-PCR and deep sequenced to compared relative barcode diversity with that of the input viral RNA. Good correlation between barcode frequencies pre- and post-PBMC infection (Spearman correlation $\rho = 0.74$; Supplemental Figure 2-1C and 2-1D), confirm the neutrality of individual barcodes for viral replication.

Ultra-sensitive PCR assay with Primer ID is able to identify individual barcode sequences from *in vivo* samples

In order to utilize barcode technology in the context of studying reservoir dynamics, an ultra-sensitive detection method had to be developed, such that individual clones, including those expressed at very low frequencies, could be accurately identified and tracked. To do this, we developed and optimized a hemi-nested PCR assay combining Primer ID with our barcode library (Supplemental Figure 2-2). The Primer ID tags each viral RNA template with a unique molecular identifier (UMI) that is carried along with the barcode throughout downstream amplification and sequencing, allowing for construction and quantification of consensus sequences, which show the sampling depth of the viral population and greatly reduces PCR and sequencing errors that may convolute the quantification of clonal diversity (Zhou et al., 2015).

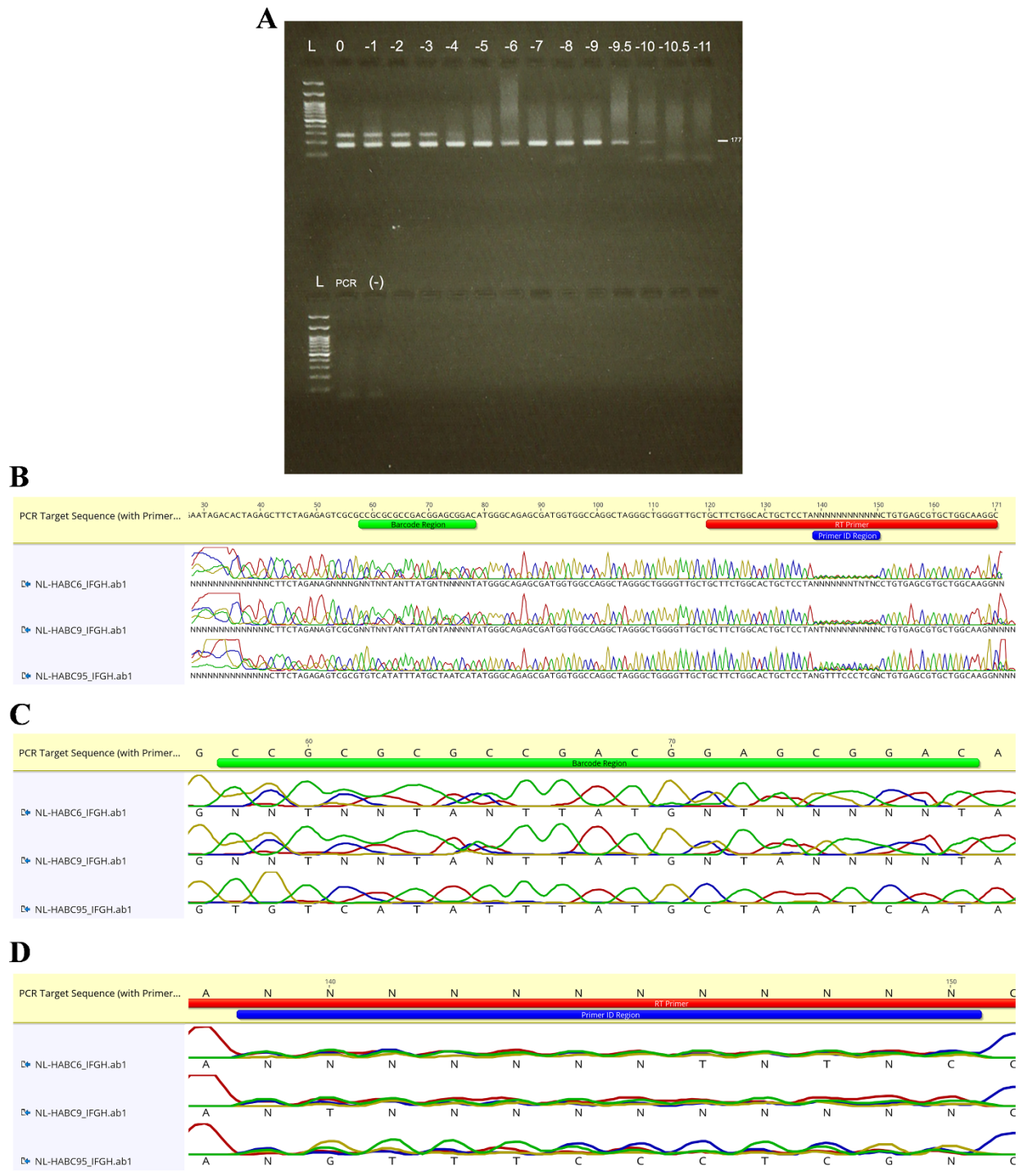

Figure 2-3. Limiting dilution PCR to identify single barcode sequences. A) Gel image of amplified PCR products. Numbers above each well indicate RNA dilution. L = 100 bp DNA ladder, PCR = no RT control, (-) = no template control (water). 177 bp band corresponds to target fragment. Sanger sequencing chromatograms of target fragment **(B)**, barcode region **(C)** and Primer ID region **(D)** for 10^{-6}, 10^{-9} and $10^{-9.5}$ dilutions.

To test the sensitivity of our PCR assay, a sample containing 31.36 ng HIV RNA (equivalent to 6.385×10^9 copies of HIV) was serially diluted down to single copy. Each dilution was amplified and sequenced, using Sanger sequencing, to examine whether we could achieve single nucleotide resolution in the barcode and Primer ID regions (Figure 2-3A). As expected, all of the sequences were identical at the non-barcode and non-Primer ID regions (Figure 2-3B). At higher RNA concentrations, the nucleotide sequences at the barcode and Primer ID regions were unreadable. However, at the lowest concentration ($10^{-9.5}$), both the barcode and Primer ID sequences were able to be read (Figure 2-3C & D). Furthermore, as expected, the barcode sequence accurately displayed a thymine in every 3rd nucleotide position (Figure 2-3C). This suggests that the PCR assay is able to detect and identify HIV RNA down to single copy sensitivity. However, the peaks from the sequence chromatograms appeared lower at the Primer ID region than the rest of the amplicon, implying impurities within the sample. To address this, we modified the PCR purification protocol following RT-PCR to include a "dry spin" after the final wash step, wherein the column was centrifuged at 16,000 x *g* to ensure complete removal of any residual flow-through that may contain excess RT primer and contaminate the sample in the column. Splenic RNA samples of known RNA concentration were diluted to single copy and tested with this modified PCR assay (Figure 2-4A). The resulting Sanger sequences yielded improved resolution of the Primer ID region, suggesting increased sample purity and optimized assay conditions for the detection of individual barcode sequences (Figure 2-4B-D).

SUW133 delays viral rebound and decreases viral diversity *in vivo*

To test the effects of SUW133 on the viral reservoir, humanized BLT mice were constructed and infected with barcoded HIV. Because primary infection with HIV is known to exhibit a large genetic bottleneck of viral populations, we devised a strategy that utilizes cell-associated viral

A

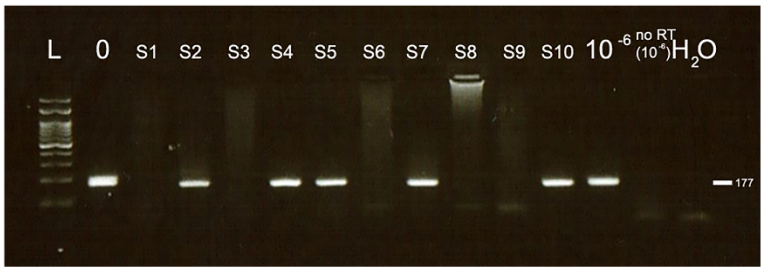
L
0
S1
S2
S3
S4
S5
S6
S7
S8
S9
S10
10 -6
no RT (10 -6)
H2O
177

B

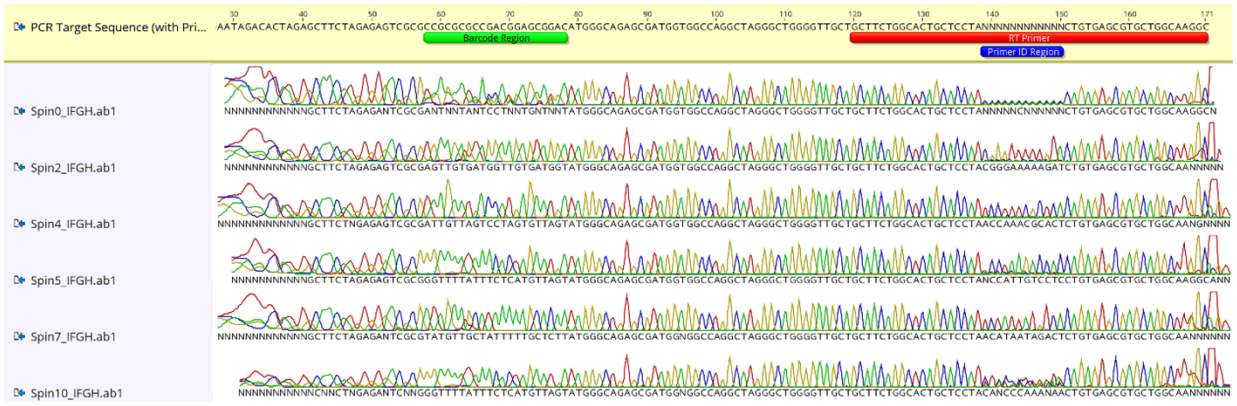
PCR Target Sequence (with Pri...
Barcode Region
RT Primer
Primer ID Region
Spin0_IFGH.ab1
Spin2_IFGH.ab1
Spin4_IFGH.ab1
Spin5_IFGH.ab1
Spin7_IFGH.ab1
Spin10_IFGH.ab1

C

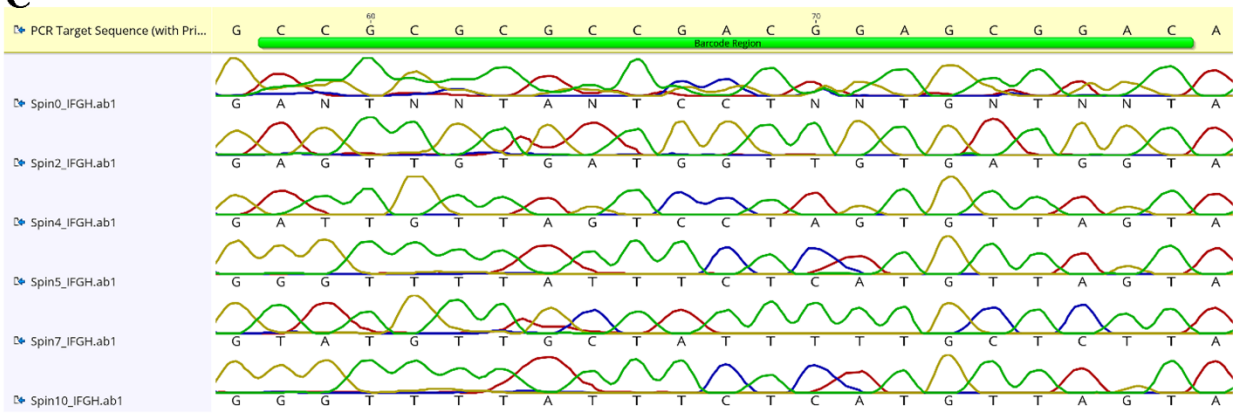
PCR Target Sequence (with Pri...
Barcode Region
Spin0_IFGH.ab1
Spin2_IFGH.ab1
Spin4_IFGH.ab1
Spin5_IFGH.ab1
Spin7_IFGH.ab1
Spin10_IFGH.ab1

D

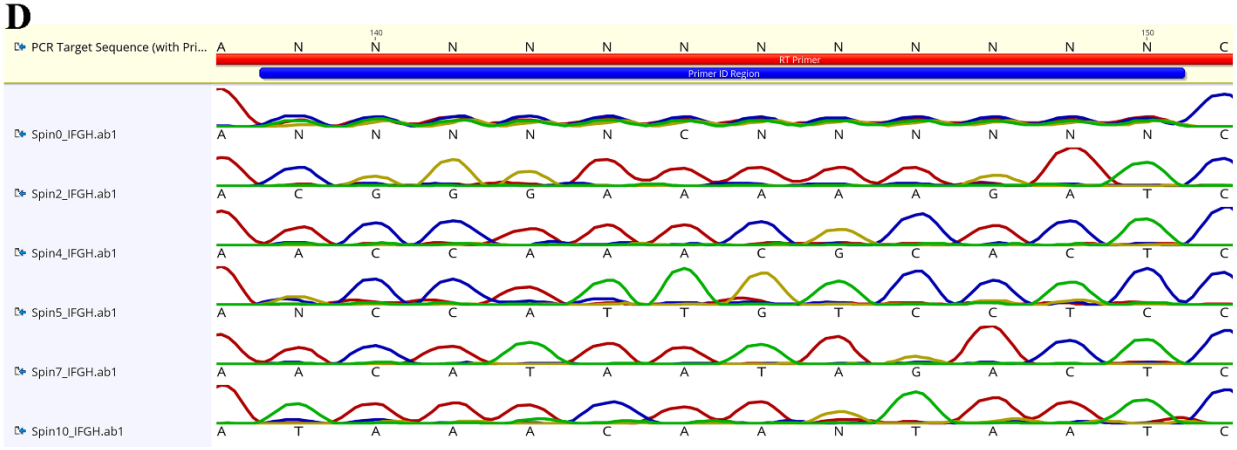
PCR Target Sequence (with Pri...
RT Primer
Primer ID Region
Spin0_IFGH.ab1
Spin2_IFGH.ab1
Spin4_IFGH.ab1
Spin5_IFGH.ab1
Spin7_IFGH.ab1
Spin10_IFGH.ab1

Figure 2-4. Addition of "dry spin" to optimize of barcode PCR. A) Gel image of amplified PCR products. Numbers above each well indicate sample ID. 0 = undiluted control sample, S = spin, L = 100 bp DNA ladder, 10^{-6} = 6-log dilution of control sample, no RT 10^{-6} = no RT control, H_2O = no template control (water). 177 bp band corresponds to target fragment. Sanger sequencing chromatograms of target fragment **(B)**, barcode region **(C)** and Primer ID region **(D)** for PCR positive samples.

infection to establish infections with a large number of barcoded HIV variants wherein $CD4^+$ T cells were isolated from a subset of mice within a series, co-stimulated with CD3 and CD28 Dynabeads, infected with HIV using standard procedures, suspended in free virus, and then transplanted into other mice from the same series harboring syngeneic human tissue (Figure 2-5A). This approach yielded efficient infection of the mice (Figures 2-5B and Supplemental Figure 2-3A). Three mice were sacrificed at 4 weeks post-infection and were found to harbor between 18 and 42 unique original barcode sequences in spleen and between 28 and 49 barcode sequences in plasma (Supplemental Figure 2-3B & C). For other animals, after 4–5 weeks of infection, we initiated ART (Figure 2-5B), which was administered in animal feed for an additional 6–7 weeks to allow for viral load suppression. Once confirmed to be suppressed by RT-PCR, mice were then treated intraperitoneally with either vehicle (DMSO) control or SUW133, which we have previously demonstrated can induce the expression of latent HIV in BLT mice and cause some of the newly HIV-expressing cells to die (Marsden et al., 2017). We observed no significant differences in humanization between the control and LRA-treated mice as measured by the percentage of human $CD45^+$ cells either before or after LRA administration ($p > 0.05$), and the levels of humanization did not significantly change after treatment administration in either group compared with the pre-administration time point (Supplemental Figure 2-3D; Supplemental Table 2-1). Prior to stopping ART, we allowed 4 days for potential reactivation and death of latently infected cells to occur. Following ART cessation, mice were bled and monitored for viral rebound over the next several weeks (Figures 2-5B, Supplemental Figure 2-4A & B). Among the 15 animals

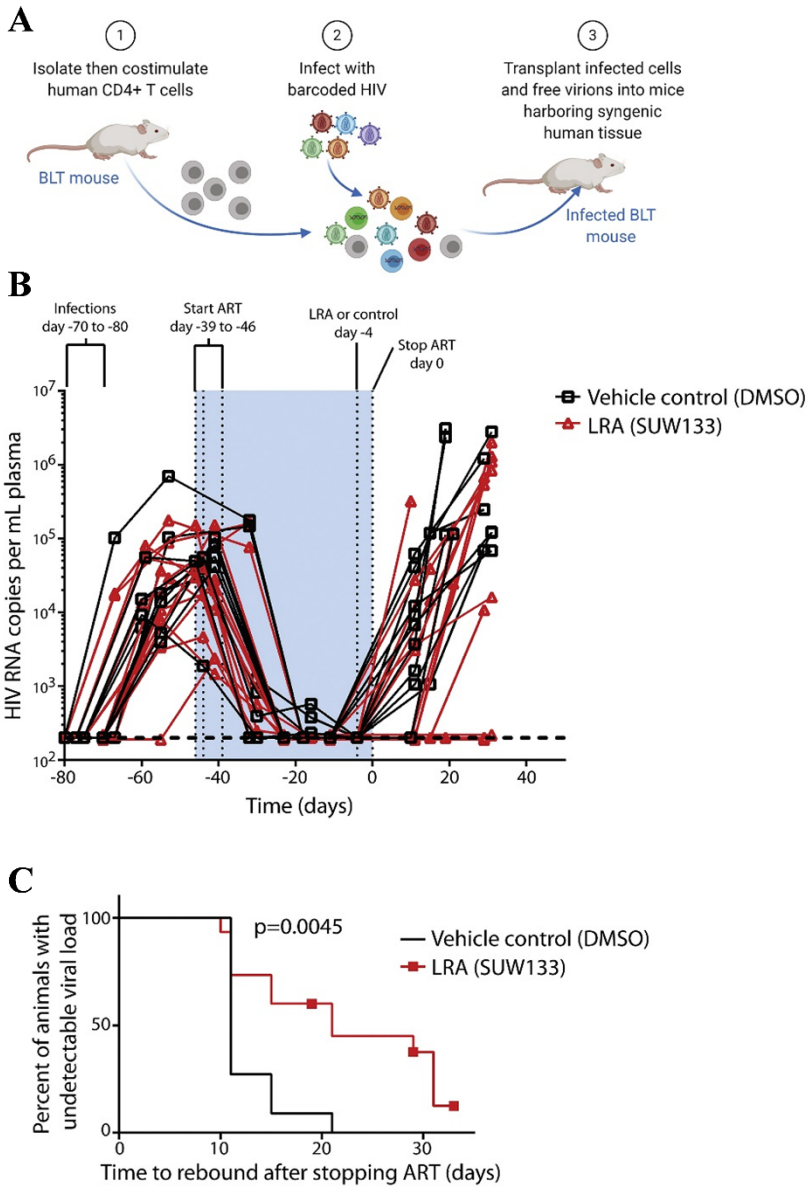

Figure 2-5. ***In vivo*** **barcode virus infection and effects of LRA on rebound. A)** Schematic representation of infection procedure intended to overcome potential transmission bottlenecks and increase barcode diversity during initial infection of humanized mice. **B)** Viral loads of mice at each phase of infection. Primary infections lasted 4–5 weeks, followed by 6–7 weeks of antiretroviral therapy (ART). SUW133 (LRA) (n = 15 mice) or control injections (n = 11 mice) were administered 4 days before stopping ART, to allow latently infected cells sufficient time to die after reactivation. See Supplemental Figure 2-4 for individual viral load plots for each animal. **C)** Delay in viral rebound induced by SUW133 versus DMSO control-treated animals compared using a log-rank (Mantel-Cox) test.

---

treated with SUW133, 4 did not experience rebound within this timeframe, contributing to an overall delay in rebound within this group. (p = 0.0045, log-rank [Mantel-Cox] test) compared to

DMSO-treated animals (Figure 2-5C).

To further explore the impact of SUW133 the viral reservoirs, splenocytes from both control and treated animals underwent *ex vivo* co-stimulation, followed by co-culturing with CEM cells to facilitate viral outgrowth. HIV p24 concentrations were measured in the supernatants following 14–15 days of culture. Replication-competent HIV was detected from all of the splenocyte cultures, including mouse #26 that did not exhibit viral rebound (Supplemental Figure 2-5). This result indicates that although LRA treatment was sufficient to delay viral rebound, it does not completely eliminate the viral reservoir. Thus, it is presumed that rebound would eventually occur in all mice, if the experiments were extended longer.

To evaluate whether peak viral load prior to LRA administration differed between treatment groups or whether there was any correlation with time to rebound, we measured the peak viral load and area under the curve (AUC: viral load over time) before LRA administration. We observed no significant differences in peak viral load or AUC between groups (Supplemental Figures 2-6A & B), and no correlation with time to rebound (Supplemental Figures 2-6C–F). However, 2 of the 3 mice with the lowest peak viral loads and AUC did not rebound after treatment. This aligns with the idea that reduced pre-ART viral replication leads to a smaller reservoir that is easier to reduce, resulting in delayed rebound. This scenario resembles the case of the "Mississippi baby," who received potent ART shortly after birth and demonstrated markedly delayed rebound upon cessation of ART (Persaud et al., 2013).

In order to assess whether LRA treatment reduced the number of barcoded HIV variants, we quantified the number of barcodes in both the plasma and spleen. In both compartments, we observed a reduction in the number of rebounding barcoded viral clones in the SUW133-treated

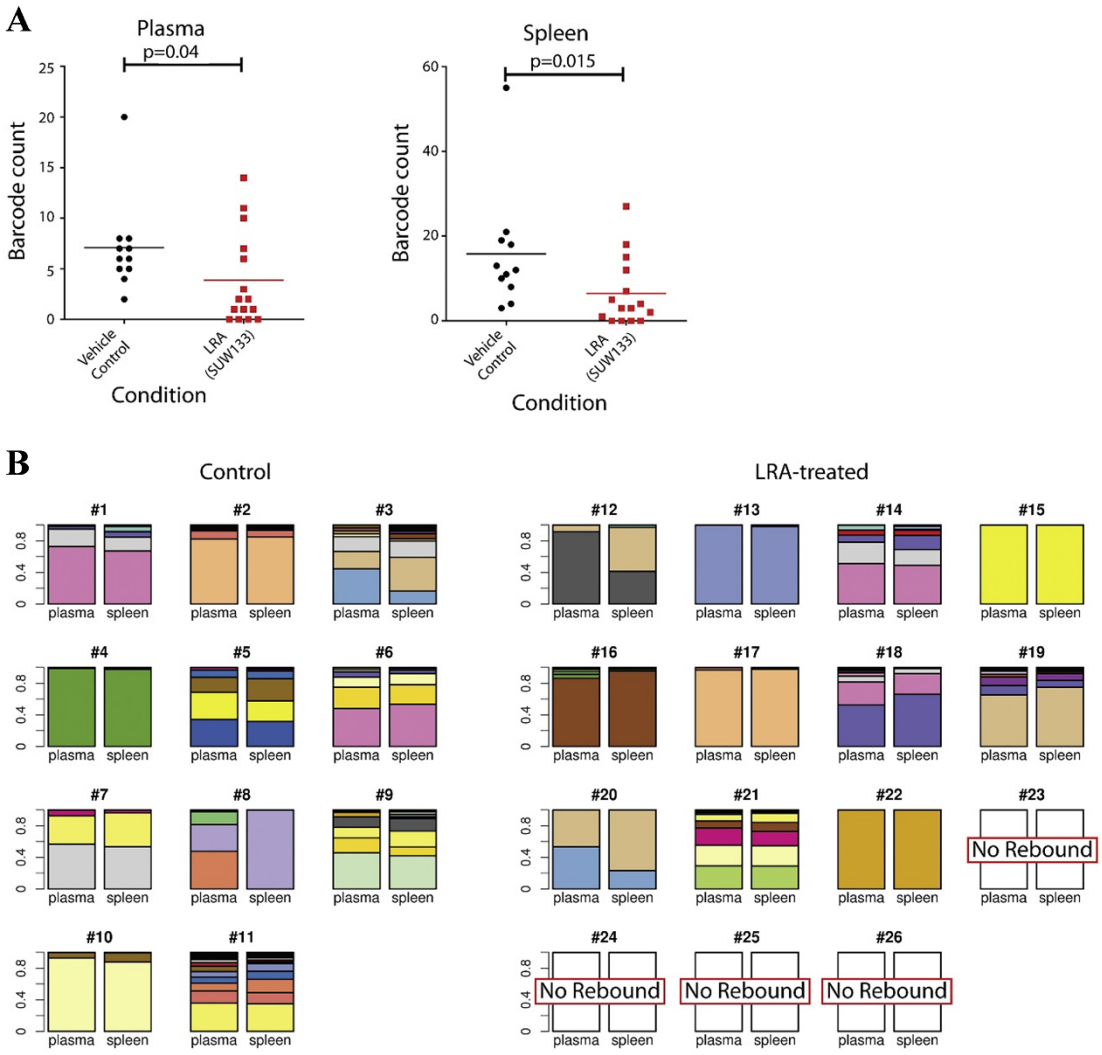

Figure 2-6. HIV barcode diversity present in plasma and spleen at necropsy. A) Plasma and spleen barcode diversity quantified by deep sequencing of viral RNA. Statistical comparisons between groups performed using a 2-tailed Mann-Whitney test. If the 4 non-rebounding mice are excluded from analysis, then comparisons yield a trend lower in the LRA-treated group ($p > 0.05$). **B)** Stacked bar plots showing the relationship between plasma and spleen virus. For each animal, the relative frequencies of major barcoded variants identified in the plasma and spleen are shown. Each plasma-spleen tissue pair shares a unique color scheme, with individual barcodes represented by 1 color.

mice compared to the controls (Figure 2-6A). Interestingly, if we eliminate the 4 non-rebounding mice from these calculations, the statistical significance is lost and the difference is reduced to a trend, which could be explained by the reduced sample size or suggest that complex factors regulate the number of reactivating cells. Comparing the barcode variants between the different compartments, we found that, in general, following rebound, the major barcoded HIV variants

present in the spleen also predominated in the plasma and vice versa (Figure 2-6B). Furthermore, the barcode diversities were significantly lower in the SUW133-treated group compared to the DMSO-treated group ($p = 0.028$ for plasma, $p = 0.022$ for spleen, 2-sided Mann-Whitney U test on Shannon entropy). This approach may be useful in future LRA studies, in which the animals are maintained on ART during the stimulation process, to determine the tissue origin of plasma virus induced by LRA stimulation in the absence of subsequent HIV replication.

Kick and kill comprised of SUW133 and NK cells delays viral rebound

We hypothesized that combining SUW133 with and added "kill" step would effectively diminish the viral reservoir, as elimination of reactivated cells would be enhanced. To test this hypothesis, we infected TKO-BLT mice with NL-HABC, followed by ART to halt productive infection (Figure 2-7A and Supplemental Table 2-2). TKO-BLT mice were used in these experiments, as they can be robustly infected with HIV and are less susceptible to graft versus host disease (GVHD) compared to NSG-BLT mice (Lavender et al., 2013), which allowed us to monitor the mice for an extended interval after ART disruption. Once mice were suppressed on ART, mice were treated with SUW133 or vehicle control (DMSO). A subset of mice from each treatment group received an injection of allogeneic human NK cells 8 hours later. We then allowed five days for the reactivation and killing of activated infected cells to occur while the mice were maintained on ART. When ART was stopped, some mice were administered an additional injection of NK cells. Plasma viral loads were monitored for up to 12.1 weeks following ART interruption (Figure 2-7B). Interestingly, 4 out of 10 mice receiving the combination of SUW133 plus NK cells displayed no rebound viremia during the period of the study. In contrast, all control mice receiving SUW133 alone, NK cells alone, or DMSO alone rebounded (Figure 2-7B). Mice receiving SUW133 plus NK cells demonstrated a significant or trend towards delay to rebound after ART interruption in

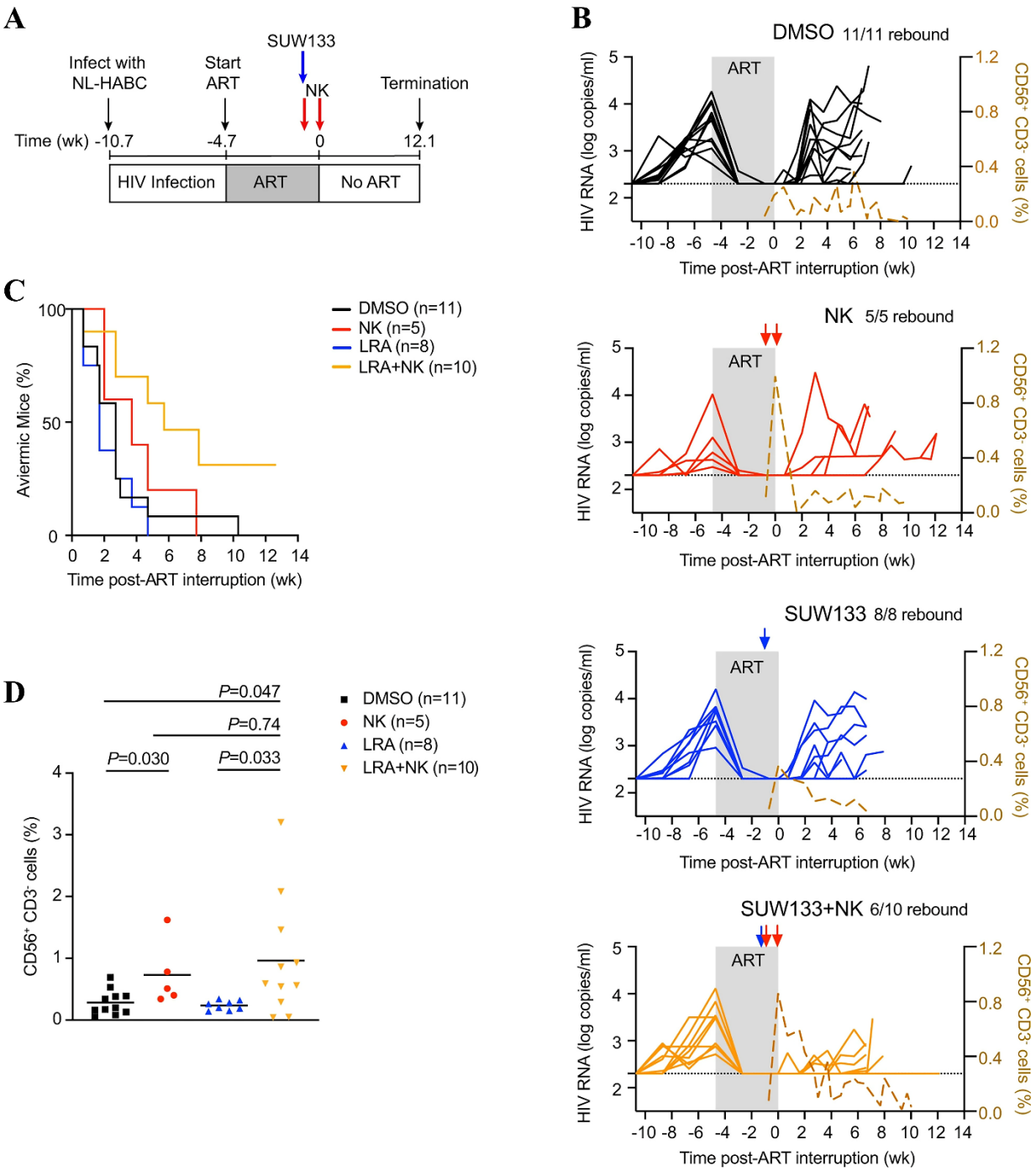

Figure 2-7. SUW133 plus NK cells delay viral rebound after ART interruption. A) Schematic representation of experiment; acute infection of TKO-BLT mice with NL-HABC. ART for 4.7 weeks. SUW133 (blue arrow) or control vehicle DMSO was administered 5 days prior to stopping ART. 5×10^6 allogeneic human peripheral blood NK cells (red arrows) were injected the same day as injection of SUW133 or DMSO and another homologous dose of cells were given 5 days later on the day of ART discontinuation. **B)** Longitudinal plasma viral loads for each infected animal at various timepoints in the DMSO only (black), NK only (red), LRA only (blue), and LRA plus NK (orange) groups. Gray shading indicates an ART treatment period of 4.7 weeks. A dashed brown line indicates the median frequency of $CD56^+CD3^-$ cells detected in the blood. The black dotted line indicates the detection limit of 2.3 log RNA copies per mL. **C)** Kaplan–Meier curves showing the frequency of aviremic mice after ART interruption. **D)** Frequency of

$CD56^+CD3^-$ cells in the blood 5 days after the first injection of NK cells. Horizontal bars represent the means. P values were calculated using the two-tailed Mann–Whitney test. n = 11 biologically independent animals in DMSO group, n = 5 biologically independent animals in NK group, n = 8 biologically independent animals in the LRA group, n = 10 biologically independent animals in LRA plus NK group (B-D). Results are pooled from two independent experiments.

---

comparison to the other groups (P = 0.012, SUW133 plus NK vs DMSO; P = 0.037, SUW133 plus NK vs SUW133; P = 0.09, SUW133 plus NK vs NK; long-rank Mantel-Cox test; Figure 2-7C). There was no observed difference in time to rebound between mice receiving SUW133 alone or NK cells alone compared to mice receiving DMSO alone (P = 0.59, SUW133 vs DMSO; P = 0.47, NK vs DMSO, log-rank Mantel–Cox test, Figure 2-7C). All of the mice receiving NK cells alone eventually rebounded, and no significant delay to viral rebound was observed compared to control mice receiving DMSO alone (Figure 2-7). These mice initially appeared to have a delay in rebound compared to mice receiving DMSO alone during the first two to four weeks post-ART interruption, but as viral loads were monitored for a longer period after ART was discontinued this trend did not reach statistical significance. A potential explanation for this may be because NK cells were injected and the level of peripheral blood $CD56^+CD3^-$ cells peaked while animals were on ART (Figure 2-7B), HIV-expressing cells may not have been present for NK cells to target in the absence of an LRA.

To evaluate whether SUW133 was activating latent cells *in vivo*, we measured the expression of CD69, an early activation marker expressed on the surface of T cells, and found that CD69 expression was significantly elevated on peripheral $CD4^+$ T cells in the blood five days after LRA treatment in mice that received either SUW133 plus NK cells or SUW133 alone (Supplemental Figure 2-7A). There was no significant difference in CD69 expression on $CD4^+$ T cells between mice that received SUW133 plus NK cells or SUW133 alone. These results are consistent with our previous findings (Marsden et al., 2017).

To evaluate the relative timing of NK cell engraftment with latency reactivation, we measured the level of $CD56^{+}CD3^{-}$ cells in the blood of mice following injection with NK cells. As expected, mice that received NK cells alone or in combination with SUW133 showed increased levels of $CD56^{+}CD3^{-}$ cells over the five days post-NK cell injection (Figure 2-7B & D). For the mice receiving SUW133 plus NK cells, the engraftment period of NK cells likely coincided with the period of latency reversal induced by SUW133, thereby sensitizing latent cells for NK cell killing via upregulation of activation or stress markers.

Next, we assessed whether there was a correlation between time to rebound and pre-ART viral loads among the groups of mice. There was no significant difference between the pre-ART viral loads among the different treatment groups (Supplemental Figure 2-7B). Pre-ART viral loads were inversely correlated with time to rebound in mice that received DMSO only ($r = -0.65$; $P = 0.030$, Pearson correlation test, Supplemental Figure 2-7C), suggesting the extent of viral infection before ART initiation was important in determining the time to viral rebound after ART interruption. Similar trends were seen in mice that received SUW133 alone or NK cells alone, but not LRA plus NK cells (Supplemental Figure 2-7C). These findings suggest that the effectiveness of the kick and kill approach may not significantly correlate to the extent of the initial seeding of the reservoir. Additionally, human immune cell engraftment, as measured by the frequencies and absolute counts of human immune cells, was not significantly different between the different treatment groups (Supplemental Figure 2-8), indicating that human immune reconstitution did not contribute to the observed differences in viral rebound between treatment groups.

SUW133 plus NK cells reduce viral diversity greater than single treatment

Next, we analyzed plasma and cell-associated HIV RNA. There was no significant difference in

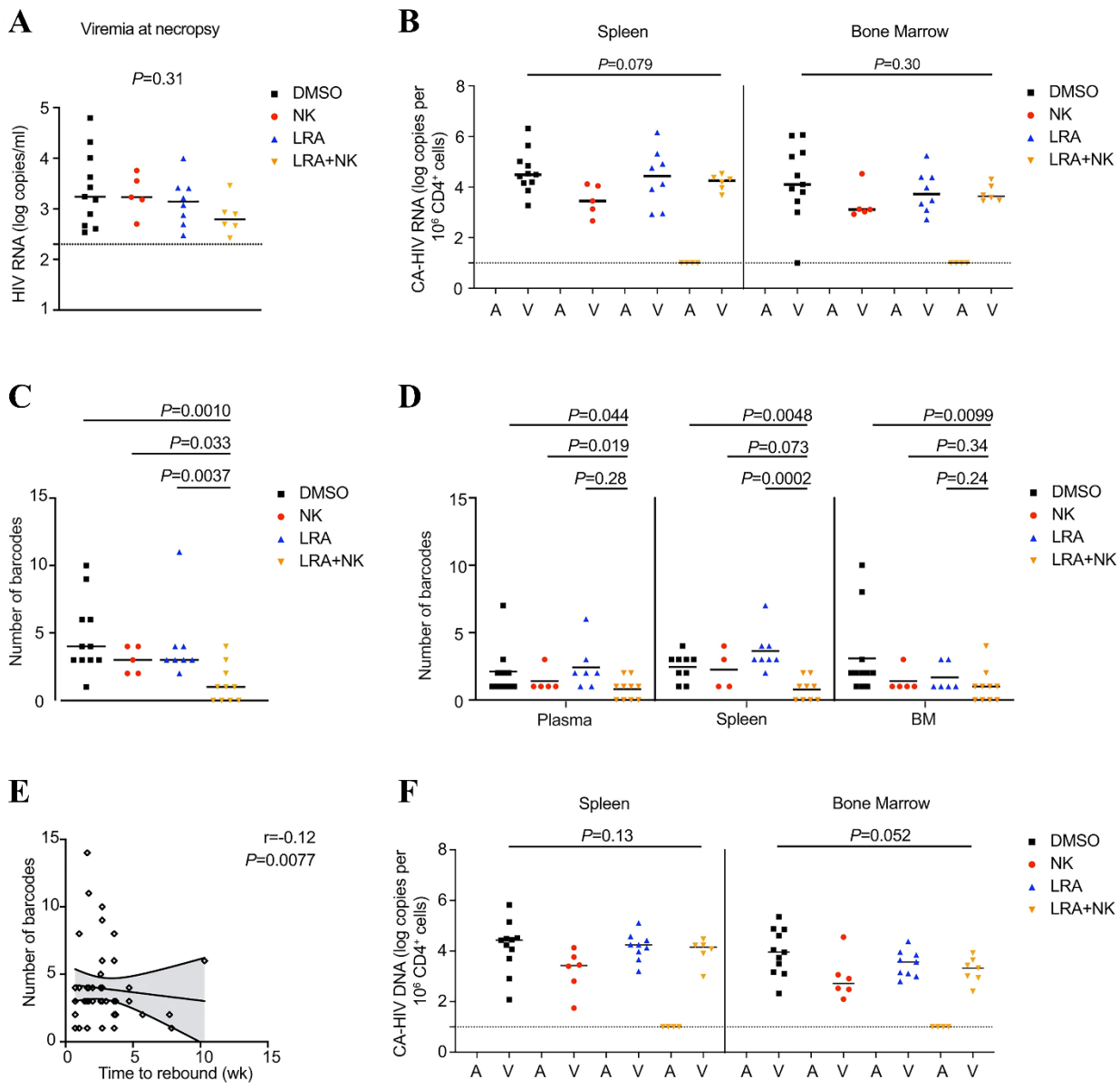

Figure 2-8. Levels of viral RNA, barcode diversity, and HIV DNA from infected mice treated with SUW133 and NK cells. A) Plasma viral loads of rebounding mice. n = 11 biologically independent animals in DMSO (black) group, n = 5 biologically independent animals in NK only (red) group, n = 8 biologically independent animals in LRA only (blue) group, n = 6 biologically independent animals in LRA plus NK (orange) group. **B)** Cell-associated "CA" HIV RNA from the spleen and bone marrow "BM" of mice that were aviremic "A" or had rebound viremia "V" at necropsy. **C, D)** Number of unique barcodes quantified by deep sequencing of viral RNA from pooled organs per mouse **(C)** or from the plasma, spleen, and BM of each mouse **(D)**. **E)** Scatterplot of a number of unique barcodes per mouse and time to rebound among all mice that rebounded after ART interruption. n = 48 biologically independent rebounding animals. Lines are linear predictions of time to rebound on the number of barcodes. The 95% confidence intervals of the fitted values are shown by gray areas. r Pearson correlation coefficient. **F)** Total CA-HIV DNA from the spleen and BM of mice that were aviremic or had rebound viremia at necropsy. n = 11 biologically independent animals in DMSO only group, n = 5 biologically independent animals in NK only group, n = 8 biologically independent animals in LRA only group, n = 10 biologically independent animals in LRA plus NK group **(B–D, F)**. Black dotted line indicates the detection limit of 2.3 log RNA copies per mL (a) or 1.0 log RNA or DNA copies **(B, F)**. Horizontal bars

represent the means (**A-D, F**). P values were calculated using one-way ANOVA Kruskal–Wallis test **(A, B, F)**, two-tailed Mann–Whitney (**C, D**), or Pearson correlation test (**E**). Results are pooled from two independent experiments.

---

the rebounding viral loads between treated and control mice at necropsy (Figure 2-8A & B). To assess the effect of treatment on viral diversity, viral RNA was deep sequenced to measure the barcode frequency of the rebounding virus in each mouse. Notably, mice receiving the combination of SUW133 plus NK cells exhibited a significantly lower number of unique barcodes per mouse (mean = 1.1) compared to mice receiving DMSO alone, NK cells alone or SUW133 alone (mean = 4.7, 3.0, and 4.1, respectively; Figure 2-8C). Additionally, there were no statistical differences in the numbers of unique barcodes between the groups of mice receiving NK cells alone, SUW133 alone, and DMSO alone ($P = 0.25$, NK vs DMSO; $P = 0.52$, SUW133 vs DMSO; $P = 0.65$, NK vs SUW133; two-tailed Mann–Whitney test; Figure 2-8C). Similar trends in barcode diversity were observed in the plasma, spleen, and bone marrow of these groups (Figure 2-8D), indicating the combination of SUW133 plus NK cells more effectively diminished the diversity of rebounding viral clones compared to other treatment groups, irrespective of compartment. There was a significant inverse correlation between time to rebound and the number of unique barcodes among all rebounding animals in this study (Figure 2-8E), suggesting that the breadth of barcode diversity correlates with the time to rebound after ART interruption.

Cell-associated HIV DNA was detectable in the spleen and bone marrow of all rebounding animals. However, among the 4 non-rebounding mice that received the combination of SUW133 plus NK cells, cell-associated HIV DNA was not detected in the tissues (Figure 2-8F). Furthermore, when splenocytes from the 4 non-rebounding mice were co-stimulated *ex vivo*, followed by co-culturing with CEM cells to facilitate viral outgrowth, we were unable to detect replication-competent virus (Supplemental Table 2-3). Remarkably, these results suggest that the administration of SUW133

plus NK cells efficiently eliminated cells harboring replication-competent virus in the spleens in a subset of mice.

DISCUSSION

In this study, we successfully demonstrate the utility of barcoded HIV in the context of a humanized mouse model to evaluate the efficacy of kick and kill strategies. We showed that administration of SUW133 delays viral rebound and reduces viral diversity and the addition of allogeneic human peripheral blood NK cells after LRA treatment further enhances these effects, even eliminating infected cells from the splenocytes of a subset of mice.

The results of this study are significant because previous clinical trials employing kick and kill approaches have not yielded promising results (Thorlund et al., 2017). However, newer and more recent kick and kill approaches have generated exciting findings in a few preclinical studies. The combination of LRAs plus broadly neutralizing antibodies (bNAbs) effectively delayed rebound after ART interruption in humanized mice infected with HIV (Halper-Stromberg et al., 2014). Similarly, TLR7 agonist plus Ad26/MVA vaccine (Borducchi et al., 2016) or bNAb PGT121 (Borducchi et al., 2018) delayed viral rebound in rhesus monkeys infected with SIV or SHIV. The current study shows use of a potent, novel bryostatin-1 analog (SUW133) combined with allogeneic NK cells delays viral rebound in humanized mice. These findings support the continued investigation of kick and kill approaches as a valuable treatment towards HIV cure.

We suspect that timing of NK cellular injections relative to LRA administration is important in our kick and kill approach. We observed a decrease in barcode diversity of rebounding viruses when mice received treatment of SUW133 plus NK cells, suggesting that NK cells eliminate the

reactivated T cells before the virus can spread to new cells. This suggests that optimal NK cell activity is achieved after activation of T cells by the LRA but before viral replication can occur. This may explain why treatment with NK cells alone resulted in a delay in viral rebound and decrease in viral diversity when administered after ART interruption, while NK cells administered alone while virus replication was suppressed on ART failed to significantly delay viral rebound (Figure 2-7C). It is also possible that the diminished basal immune activation state of TKO-BLT mice (Lavender et al., 2018; Marsden et al., 2020) may have reduced the likelihood that NK cells would recognize any spontaneously activating latently infected cells on ART. Future studies evaluating the scheduling and lengthening of NK cellular engraftment may be helpful in optimizing their utility in eliminating latently infected cells.

Important limitations of this study include the use of NL-HABC, which encodes a reporter gene and barcode in place of Vpr. While we have previously shown that the lack of functional Vpr does not affect the infectivity or reactivation of virus in humanized mice (Marsden et al., 2017; Marsden & Zack, 2017; Pache et al., 2020), this virus is not suitable for evaluating the effect of Vpr on latency. Notably, it has been reported that Vpr results in upregulation of ULBP2 in HIV-infected T cells, which may sensitize them for elimination via interaction with the NKG2D receptor on NK cells (Richard et al., 2010; Ward et al., 2009). However, we observed that allogeneic NK cells effectively delayed viral rebound of NL-HABC, which does not express Vpr, suggesting that multiple interactions involving inhibitory and activating receptors likely mediate the response of NK cells against infected target cells *in vivo*. Further evaluation is required to determine the exact mechanism of the observed response. In addition, our interpretation of the results may be affected by the limited sensitivity of our viral load assay, which may not have been able to detect small viral blips, intermittent viral replication, or a low level of productive infection. Inherent limitations

of the mouse models, including the restricted capacity to humanely collect large longitudinal volumes and the narrow window of experimentation before the mice exhibit GVHD, influenced the experimental design of the study. Because of this, we were unable to track viral barcode diversity in the plasma over time. Similarly, we were unable to extend the duration of ART treatment to mimic the "deep latency" that is observed in PLWH. Additionally, the humanized mouse models used in this study may not accurately recapitulate the immune response in PLWH. Further evaluation of the efficacy of this kick and kill approach as a potential therapeutic strategy would involve related studies on cells from HIV-positive individuals.

Overall, this proof-of-concept study demonstrates that a kick and kill strategy comprised of SUW133 plus allogeneic human peripheral blood NK cells substantially target the HIV reservoir in humanized mouse models more potently than single treatment alone and validates the use of barcoded HIV as a tool for tracking HIV latency reversal and rebound *in vivo*. Results from this study outline the utility of combining novel LRAs and NK cells, opening a new paradigm for the HIV cure field.

METHODS

Cells and animal models. 293FT cells were obtained from Invitrogen. These cells were maintained in Dulbecco's modified Eagle medium (Invitrogen) containing 10% fetal bovine serum (FBS: Omega Scientific), 100 U/mL of penicillin, and 100 µg/mL of streptomycin (pen/strep: Invitrogen). Cells were cultured at 37°C in 5% CO_2.

GHOST (3) $CXCR4^+CCR5^+$ cells were obtained through the NIH AIDS Reagent Program, Division of AIDS, NIAID, NIH, from Dr. Vineet N. KewalRamani and Dr. Dan R. Littman (Cat#

3942). These were cultured in DMEM containing 10% FBS, 500 μg/mL G418 (GIBCO Cat#10131-27) 100 μg/mL hygromycin (Sigma Cat#H3274-100MG), pen/strep, and 1 μg/mL puromycin (Sigma Cat#P8833-10MG). Cells were cultured at 37°C in 5% CO_2.

Cell lines were obtained directly from NIH AIDS Reagent repository or Invitrogen. Their phenotype and characteristics were as expected therefore they were not subjected to further authentication procedures.

De-identified PBMCs were provided by the UCLA AIDS Institute Virology Core Laboratory following IRB approval. Cells were costimulated for 3 days by culturing in RF10 medium (consisting of RPMI 1640 medium supplemented with 10% FBS and pen/strep) containing 20 U/mL of interleukin-2 (IL-2) in the presence of plate-bound anti-CD3 (1 μg/mL, Fisher Scientific Cat#50-105-5018) (adhered via pre-treatment of plates with Goat Anti-Mouse antibody [Fisher Scientific Cat#PI-31160]) and soluble anti-CD28 (100 ng/mL) using previously described procedures (Marsden et al., 2012). Cells were cultured at 37°C in 5% CO_2.

NK cells were isolated using CD56 MicroBeads (Miltenyi) with 75-90% purity (Supplemental Figure 2-9A). Cells were stained with CD158(KIR)-FITC (clone HP-MA4), CD244(2B4)-PE (clone C1.7), NKp80-APC (clone 5D12), CD336(NKp44)-PerCp/Cy5.5 (clone P44-8), CD314(NKG2D)-PE-Dazzle594 (clone 1D11), CD159a(NKG2A)-PE/Cy7 (clone S19004C), CD56-Brilliant Violet421 (clone HCD56), CD3-Brilliant Violet 510 (clone Hit3a), CD337(NKp30)-Brilliant Violet605 (clone P30-15), CD335(NKp46)-Brilliant Violet650 (clone 9E2), CD57-Brilliant Violet711 (clone QA17A04), and CD16-Brilliant Violet785 (clone B73.1) (all from Biolegend) and Ghost Dye Red 780 (Tonbo Biosciences) prior to analysis by flow cytometry for UMAP analysis. To isolate $CD4^+$ T cells, adherent macrophages were removed from

PBMCs by culturing in flasks overnight in C10 (RPMI 1640 media supplemented with 10% vol/vol FBS (Omega Scientific), 1% l-glutamine, 1% penicillin/streptomycin (Invitrogen), 500 mM 2-mercaptoethanol (Sigma), 1 mM sodium pyruvate (Gibco), 0.1 mM MEM nonessential amino acids (Gibco), 10 mM HEPES (Gibco), and 20 ng per mL of recombinant human interleukin-2 (IL-2) (Peprotech). $CD4^+$ T cells were isolated using CD4 MicroBeads (Miltenyi). 293 T cell line was purchased from the American Type Culture Collection (ATCC) (ATCC CRL-11268).

Animal experiments conformed to all local and national guidelines and regulations (including the Public Health Service Policy on Humane Care and Use of Laboratory Animals, the Guide for the Care and Use of Laboratory Animals, and the AVMA Guidelines for the Euthanasia of Animals), and procedures were approved by the UCLA Animal Research Committee (Approval number ARC #1996–058). Euthanasia was performed by anesthetizing animals with isoflurane followed by cervical dislocation.

Humanized bone marrow liver thymus (BLT) mice (Melkus et al., 2006) were constructed by the UCLA humanized mouse core using techniques described previously (Bristol et al., 1997; Marsden et al., 2012; Marsden et al., 2017; McCune et al., 1988). In brief, NOD.Cg-PrkdcscidIl2rgtm1wjl (Nod-SCID-common gamma chain knockout [NSG]) mice were irradiated with 270 rads and then transplanted under the kidney capsule with pieces of fetal thymus and liver tissue. Mice were then infused intravenously by retro-orbital injection with $5x10^5$ human fetal liver-derived $CD34^+$ cells isolated by immunomagnetic separation as previously described (Marsden et al., 2017; Shimizu et al., 2015). At 8 weeks post-transplantation and approximately every 2 weeks thereafter mice were evaluated for reconstitution with human cells. Mice were bled as previously described (Marsden

et al., 2012; Marsden et al., 2017) and peripheral blood mononuclear cells analyzed by flow cytometry. To reduce the effects of potential donor-to-donor variability, results are derived from series of mice constructed with tissue from 4 different human donors. Only animals with undetectable plasma viral loads at the end of ART treatment and no graft-versus-host disease were included in analysis. Mouse groups were randomized to ensure similar pre-ART viral loads between groups and eliminate the possibility of variations in pre-ART viral load affecting post-ART results. This was pre-defined because these experimental factors would confound study of HIV latency and rebound. Both male and female mice were included in this study to avoid systematic biases associated with sex as a biological variable. Mice were purchased from The Jackson Laboratory and bred at UCLA. Mice were maintained in HEPA-filtered mouse racks in groups of up to 5 animals per cage. Mice were 3 months of age at time of initial transplant.

C57BL/6 Rag2$^{-/-}\gamma c^{-/-}$CD47$^{-/-}$ (TKO) mice (Lavender et al., 2018) were obtained from Jackson Laboratories and bred at UCLA. Male and female mice were age-matched and between 6 and 8 weeks old were irradiated with 270 rads, and then pieces of fetal thymus and liver tissue were transplanted under the kidney capsule. Mice were then injected intravenously with 5×10^4 human fetal liver-derived CD34$^+$ cells isolated by immunomagnetic separation.

Construction of HIV-1 barcode library. We utilized the HIV-1 construct NL43-HA (Ali & Yang, 2006; Marsden et al., 2017) as the backbone, which has a hemagglutinin (HA) tag inserted in place of the vpr gene, and expresses the HA epitope on the infected cell surface with a murine heat stable antigen. The barcode was inserted into a non-translated region before the HA tag start codon. This region does not contain known cis element or splicing sites, thus should be neutral for viral replication. The barcode is designed to be 21 base pairs in length, with 14 random nucleotides that

contain a ‘T’ at each 3rd position to avoid unwanted start or stop codons. This randomization strategy allows a total complexity of 268,435,456 (414) unique barcodes. The barcode region was amplified by 2-step PCR with the following primers:

1st PCR:

Primer 1 (Supplemental Table 2-4) Forward:

agagcttctagagagtcgcgNNTNNTNNTNNTNNTNNTNNTATGggcagagcgatggtg

Primer 2 Reverse: cgcctattctgctatgtcgacaccc

Amplicon: 336bp

Primer 3 2nd PCR Forward: GAAGCAGAGCTAGAACTGGCAGA

Reverse: PCR product of first PCR

Amplicon: 2,513 bp

The randomized nucleotides were inserted into the forward primer of the 1st PCR. Then the amplified region was digested using AgeI and EcoRI and ligated back to NL43-HA vector and transformed into MegaX DH10B T1R cells (ThermoFisher Cat# C640003).

We anticipated that 10,000 barcodes would be more than sufficient for our *in vivo* experiments, thus we harvested plasmid DNA from > 20,000 bacteria colonies post transformation, each representing a uniquely barcoded virus, resulting in a very complex barcoded HIV-1 plasmid library. Plasmids from collected bacteria were midi-prepped as the input plasmid library. Classic Sanger sequencing across the barcode region were performed to examine the diversity at expected nucleotide positions.

Sequencing and analysis of *in vitro* barcode library. For *in vitro* samples, the barcode region was amplified by PCR. The PCR was performed using Phusion High-Fidelity DNA Polymerase (ThermoFisher Cat#F530L) and thermal cycling conditions of 98°C 30 sec, 98°C 10 sec, 59°C 20 sec, 72°C 30 sec" for 27 cycles, 72°C 5 min with the following primers:

Primer 4 1st PCR Forward: ggactggttttatagacatcactatg

Primer 5 Reverse: cgcctattctgctatgtcgacaccc

2nd PCR Primer 6 Forward: ccccagaagaccaagggc

Primer 7 Reverse: ctgcgtgggtaggagcag

For 1st round amplification of *in vitro* RNA samples by RT-PCR the One-Step RT-PCR kit (Bioland Sci Cat#RT01-01) was used with the same primers listed above. Thermal cycling conditions for the first-round PCR were 42°C 30 min, 94°C 3 min, "94°C 30 sec, 54°C 20 sec, 72°C 30 sec" for 27 cycles, then 72°C for 5 min. For the second-round PCR we utilized Phusion High-Fidelity DNA Polymerase (ThermoFisher Cat#F530L) and thermal cycling of 98°C 30 sec, 98°C 10 sec, 59°C 20 sec, 72°C 30 sec" for 35 cycles, then 72°C for 5 min.

The amplified fragment was ligated with the sequencing adaptor, which had six-nucleotide multiplexing ID to distinguish among different samples (NEBNext Ultra II DNA Library Prep Kit for Illumina Cat# E7645). Deep sequencing was performed with Illumina HiSeq PE150. Raw sequencing reads were de-multiplexed using the six-nucleotide ID. Sequencing error within the barcode region was corrected by filtering out low quality reads (quality score < 30) and un-matched base-pairs between forward and reverse reads. Barcodes with read depth < 10 were filtered.

Transfections. To generate HIV-1 virus supernatant, plasmids were transfected into 293 T cells in T-150 flasks, following the manufacturer's protocol for the BioT transfection reagent (Bioland).

Virus-containing supernatant was harvested at day 2 post-transfection and passed through a 0.45 μm filter. Aliquots of virus were frozen at −80 °C and thawed immediately prior to use.

PCR amplification of *in vivo* samples from humanized NSG-BLT mice. Viral RNA was extracted from plasma samples using a QIAamp viral RNA minikit and tissue RNA was extracted from lysed splenic cells using an RNeasy minikit (QIAGEN). Prior to extraction, plasma samples were spiked with 250 ng of carrier RNA. Splenic RNA was treated with DNase during extraction (QIAGEN) while plasma RNA was treated with DNase post-extraction (Invitrogen). 8 μL of plasma RNA or 500 ng of splenic RNA was used as template for cDNA synthesis. cDNA was synthesized using a SuperScript IV first-strand synthesis kit (ThermoFisher Cat#18091050). The cDNA primer was Primer 8: 5′- GCCTTGCCAGCACGCTCACAGNNNNNNNNNNNNTAGG AGCAGTGCCAGAAGC-3′. We used a Primer ID strategy to accurately quantify RNA copy numbers (Zhou et al., 2015). The cDNA primer was synthesized by Integrated DNA Technologies with machine mixing of random nucleotides and standard desalting for purification. Each cDNA reaction mixture contained 2 μM cDNA primer, 10 mM deoxynucleoside triphosphates (dNTPs), 100 mM dithiothreitol (DTT), 40 U of RNase inhibitor and 200 U of Superscript IV in a total volume of 20 μL. The primers, dNTPs, and templates were mixed and heated at 65°C for 5 min then cooled on ice for 1 min. The reaction mixtures were incubated at 52.5°C for 10 min and then at 80°C for 10 min to inactivate the enzymes. To remove the RNA template, 1 μL of RNase H (Invitrogen) was added to each reaction mixture, followed by incubation at 37°C for 20 min. To remove unused cDNA primer, samples were purified using an RNA clean and concentrator kit (Zymo Research Cat#R1017). cDNA was eluted in RNase/DNase-free water and the entire sample was used for PCR amplification.

cDNA was amplified using a hemi-nested PCR. We used Phusion DNA polymerase (ThermoFisher Cat#F530L) for both rounds of PCR. The first-round PCR forward primer was Primer 9: 5′-CTGACAGAGGACAGGTGGAACAAGC-3′ and the reverse primer was Primer 10: 5′-GCCTTGCCAGCACGCTCACAG-3′. Each first-round PCR reaction mixture contained 10 mM deoxynucleoside triphosphates (dNTPs), 0.4 μM forward primer, 0.4 μM reverse primer and 1U of Phusion in a total volume of 50 μL. The first-round PCR cycling protocol had an initial denaturation at 98°C for 30 s, 30 cycles of 98°C for 10 s, 69.4°C for 20 s, and 72°C for 7 s and a final extension at 72°C for 5 min. 2 μL of first-round PCR product was used as input for second-round PCR. The second-round forward primer was Primer 11: 5′-AAGGGCCACAGAGGGAGC −3′, and the reverse primer was Primer 12: 5′-GCCTTGCCAGCACGCTCACAG −3′. Each second-round PCR reaction mixture contained 10 mM deoxynucleoside triphosphates (dNTPs), 0.4 μM forward primer, 0.4 μM reverse primer and 1U of Phusion in a total volume of 100 μL. The second-round PCR cycling protocol had an initial denaturation at 98°C for 30 s, 35 cycles of 98°C for 10 s, 66.6°C for 20 s, and 72°C for 6 s and a final extension at 72°C for 5 min. PCR products were purified using a DNA clean and concentrator kit (Zymo Research Cat#D4033). Purified DNA was eluted in RNase/DNase-free water and 500 ng in 25 μL was sent for deep sequencing.

PCR product was phosphorylated and A-tailed by Ultra II End Repair Module (NEB). A sequencing adaptor with 6-nucleotide multiplexing tag was ligated to PCR product to distinguish different samples. Deep sequencing was performed on HiSeq3000 platform (Illumina) with PE150 settings.

PCR amplification of *in vivo* samples from humanized TKO-BLT mice. RNA was extracted from the barcoded virus supernatant using QIAamp Viral RNA Mini Kit (Qiagen) and from cells using RNeasy Mini Kit (Qiagen). cDNA was generated using SuperScript IV First-Strand Synthesis Kit (Invitrogen). The same amount of input RNA that was used for viral load measurement was also used for cDNA synthesis for barcode analysis. The barcode region was amplified by hemi-nested PCR using Phusion High-Fidelity DNA Polymerase (ThermoFisher Scientific). Each RNA molecule was tagged with a Primer ID (Jabara et al., 2011; Zhou et al., 2015). Primer ID removal and cDNA purification was performed using an PureLink Quick PCR Purification Kit (Invitrogen). For the first PCR reaction, a fixed volume of 11 μL of cDNA was used along with the following primers: FW-5′-CTGACAGAGGACAGGTGGAACAAGC-3′ and BW-5′-GCCTTGCCAGCACGCTCACAG-3′. The second PCR reaction used 2 μL of the first PCR reaction, the same reverse primer, and the following forward primer: FW-5′-AAGGGCCACAGAGGGAGC-3′. The amplified fragment was ligated with the sequencing adapter, which had a six-nucleotide multiplexing ID to distinguish among different samples. Deep sequencing was performed with Illumina HiSeq3000 PE150. We ensured sequencing depth is tenfold higher than viral genome copies. Raw sequencing reads were de-multiplexed using the six-nucleotide ID. Sequencing error within the barcode region was corrected by filtering out low-quality reads (quality score < 30) and unmatched base pairs between forward and reverse reads. We also used Primer IDs to correct sequencing errors. We found the frequency of Primer ID reads follows a bimodal distribution (Supplemental Figure 2-10C). We filtered the Primer IDs using the frequency cutoff between the Poisson distribution of errors and normal distribution of real Primer IDs. For each Primer ID, the most frequently observed barcode was called. We then grouped the similar barcodes into clusters. Clustered barcodes represent sequences with ≥4 bp differences from

one another (Supplemental Figure 2-10B). Barcode clusters with less than 400 occurrences were filtered to remove handling and sequencing errors. To prove our barcodes quantification are an absolute number of clones, we sampled RNA molecules from the same population twice and found the number of barcodes is identical in the two samples (Supplemental Figure 2-10D).

Cell associated- (CA) HIV RNA was extracted from lysed splenocytes and bone marrow cells using RNeasy Mini Kit (Qiagen). CA-HIV DNA was extracted from cell pellets using DNeasy Blood & Tissue Kits (Qiagen). Viral loads were measured by qPCR using 500 ng of CA-HIV RNA and DNA with the same primers as above. CA-HIV RNA and DNA are reported as the number of HIV-1 RNA or DNA copies per 10^6 $CD4^+$ cells. The same amount of input RNA that was used for viral load measurement was used for Primer ID and barcode analysis. All cDNA was used as the template for the first round of PCR during the barcode analysis.

Data analysis of *in vivo* sequences. Barcode sequences and Primer ID sequences were extracted by mapping flanking sequences. Barcodes and Primer IDs with ambiguous base, or base quality score lower than 30 were filtered out. Barcodes with inconsistent forward and reverse reads were also filtered out. We calculated the read depth of Primer IDs and filtered out low occurrence Primer IDs according to the bimodal distribution of their read depth (Melkus et al., 2006). For each Primer ID, the most dominantly linked barcode was counted. We used CD-hit to cluster barcodes with less than 3-nucleotides difference (Huntington et al., 2009). Mice sacrificed at week 4 post-infection (Supplemental Figure 2-3C) were analyzed without incorporation of Primer ID.

Production of barcoded virions. For transfection, 107 293FT cells were seeded into 150 cm^2 tissue culture flask and the next day were transfected with30 μg of barcoded HIV plasmid using lipofectamine 2000 reagent (Invitrogen) according to the manufacturer's instructions. One day

after transfection the media was replaced with 20 mL of Opti-MEM media (GIBCO) containing 10% FBS. Virus-containing supernatant was harvested at day 2 post-transfection and passed through a 0.45 μm filter. Aliquots of virus were frozen at −80°C and thawed immediately prior to use.

***In vitro* infections.** During infection of costimulated PBMC, $5x10^5$ cells were exposed to virus in a screw-capped 1.5 mL tube containing 250 μL of RF10 medium and 10 μg/mL of Polybrene. This was incubated on a rocking platform for 2 h at 37°C. After infection, cells were washed and resuspended in 1 mL of RF10 medium containing 20 U/mL of IL-2, and viral growth was quantified by analyzing supernatant samples using an HIV p24 enzyme-linked immunosorbent assay kit (Perkin Elmer Alliance Cat#NEK050).

GHOST (3) $CXCR4^+CCR5^+$ were seeded into 24-well tissue culture plates at $5x10^4$ cells/well prior to infection. The next day media was aspirated and 250 μL of virus suspended in fresh media containing 10 μg/mL of Polybrene was added to cells. Plates were incubated for 2h at 37°C and then the media was replaced with 1 mL of fresh media without polybrene. Cells were incubated for a further 2 days and then harvested by exposure to 0.05% trypsin (GIBCO Cat#5400-54) in PBS for 5 min, and then removed by agitation with media. After removal from plate cells were pelleted and resuspended in 2-3% paraformaldehyde then analyzed for GFP expression by flow cytometry as described below (Supplemental Figure 2-9B).

$CD4^+$ T cells were isolated from PBMCs by immunomagnetic selection (Miltenyi) following the manufacturer's instructions, then were costimulated with Dynabead CD3/CD28 human T-activator (ThermoFisher Scientific) per manufacturer's instructions and cultured in C10 media containing 20 ng per mL of IL-2 (Peprotech). For infection, 5×10^5 cells were exposed to HIV-1 in 200 μL of

C10 media containing IL-2 and 10 μg per mL of polybrene. Cells were spin inoculated by centrifugation at 1200 × *g* for 1.5 h at 22°C. After spin-inoculation, cells were washed and resuspended in 200 μL of fresh C10 media containing IL-2. Viral infection was quantified by staining cells for p24 using PE-conjugated antibody to HIV core antigen (clone KC57) and analyzed by flow cytometry (Supplemental Figure 2-9C). Cell-free supernatant samples were analyzed using HIV p24 enzyme-linked immunosorbent assay kit (Beckman Coulter).

Infection and analysis of NSG-BLT mice. *Ex vivo* infection of $CD4^+$ T cells was performed by sacrificing 2-4 animals from a humanized NSG-BLT mouse series to isolate human cells. Mice were anesthetized with isoflurane and bled by cardiac puncture then euthanized and spleens removed. Spleen tissues was disaggregated and filtered through a 40 μm filter to produce a single-cell suspension. Splenocytes and peripheral blood mononuclear cells from all animals were then pooled and subjected to positive immunomagnetic selection using human-CD4 MicroBeads (Miltenyi Biotec Cat#130-045-101) following the manufacturer's instructions. Cells were costimulated for 3 days as described above and then infected with barcoded HIV (182-560 ng of p24). Infections were conducted by spinoculating 2 million costimulated $CD4^+$ T cells per well of a 24-well plate in 400 μL of virus containing 10 μg/mL of polybrene. Plates were centrifuged at 1200 x *g* for 2 hours at 25°C.

After infection an aliquot of cells was removed for overnight culture in RF10 media to quantify infection efficacy by flow cytometry specific for the HA reporter gene, and the remaining cells were resuspended in 500 μL of barcoded HIV virions (ranging from 280-700ng of p24 in different experiments) and then injected intraperitoneally into mice from the same series (i.e., syngeneic mice generated with cells from the same human donor tissue).

HIV RNA copy numbers in plasma at each bleed were quantified using RT-PCR performed by the UCLA AIDS Institute virology core as previously described (Marsden et al., 2012). For interval biweekly or weekly bleeds, 50 µl of blood was collected using EDTA-coated capillary tubes by retro-orbital bleed for viral load measurements. Whole blood was spun at 300 × *g* for 5 min to separate plasma from the cellular fraction. Total RNA was extracted from plasma using QIAamp Viral RNA Mini Kit (Qiagen) per the manufacturer's protocol. HIV-1 RNA was quantified by qRT-PCR. The reaction mixture was prepared using Taqman Fast Virus 1-Step Mastermix (ThermoFisher Scientific) with 20 µl eluted RNA and a sequence-specific targeting a conserved region of the HIV-1 gag gene probe (FAM 5′-CCTTTTAGAGACATCAGAAGGCTGTAGACA AATACTGGG-3′). The forward and reverse primers sequences were FW-5′-GGGAGCTAGAAC GATTCGCAGTTAAT-3′ and BW-5′-ATAATGATCTAAGTTCTTCTGATCCTGTCTGAAGGG A-3′, respectively. Cycle threshold values were calibrated using standard samples with known amounts of absolute plasmid DNA copies. The quantitation limit was determined to be 200 copies per mL. At necropsy, more than 100 µl of blood was collected from each mouse, which allowed at least 50 µl of plasma to be analyzed for barcode analysis.

After 4-5 weeks of infection, NSG-BLT mice were treated with ART in animal feed consisting of emtricitibine (FTC) at 0.5 mg/g of feed, tenofovir disoproxil fumarate (TDF) at 0.75 mg/gram of feed, and raltegravir at 1 mg/g of feed for a further 6-7 weeks. PKC modulator for injection (2 µg/mouse) was initially suspended in 0.6 µL of DMSO and then this was added to 500 µL of phosphate buffered saline before administration to mice by intraperitoneal injection. Control animals were injected with the same concentration of DMSO in PBS without compound.

At the time of necropsy, the mice were anesthetized with isoflurane and then exsanguinated by intracardiac bleed using a 1 mL syringe and 25G ½ inch needle rinsed with 0.5M EDTA to prevent clotting, and then transferred into a 1.5 mL screw-capped tube containing 2 µL of 0.5M EDTA. Animals were then euthanized and spleens removed. Blood was centrifuged at 1300 x *g* and the upper plasma layer was collected, aliquoted and stored at −80°C. The central 150 µL layer containing white blood cells was transferred into a new 1.5 mL screw-capped tube and then 1 mL of Ammonium Chloride Solution lysis buffer (StemCell Technologies, Inc.) was added to each tube. Tubes were then briefly vortexed and incubated for 5 min at room temperature, before pelleting by centrifugation at 1300 x *g*. Splenocytes were obtained by passing disaggregated tissue through a 40 µm filter. Bone marrow cells were obtained by grinding bones using a mortar and pestle. Blood, spleen and bone marrow cells were then washed with RF10 media and either used for flow cytometry as described below, frozen as cell pellets, or suspended in RLT buffer (QIAGEN) for RNA storage and then frozen at −80°C.

***Ex vivo* stimulations of splenocytes from NSG-BLT mice.** During *ex vivo* stimulations for virus outgrowth, splenocytes comprising approximately 60% of spleen tissue were costimulated in RF10 medium containing 20 U/mL of interleukin-2 (IL-2) in the presence of plate-bound anti-CD3 (1 µg/mL) and soluble anti-CD28 (100 ng/mL) and then 10^6 CEM cells were added to the cultures to facilitate replication of any released virus. At day 3 post-stimulation cells were washed and stimulatory antibodies removed. Cultures were split every 3 to 4 days and p24 levels in the supernatant were quantified using an HIV p24 enzyme-linked immunosorbent assay kit (Perkin Elmer Alliance Cat:NEK050) at 14- or 15-days post-stimulation.

Ex vivo **stimulations of splenocytes from TKO-BLT mice.** The spleens were aseptically collected from mice at the time of necropsy, passed through a 40 μm cell filter to achieve single-cell suspensions, and lysed using RBC Lysis Buffer (Biolegend). About 2.5×10^6 to 36×10^6 splenocytes were resuspended in C10 media containing Piperacillin/tazobactam (Wockhardt), 2.5 μg per mL Amphotericin B (Fisher), and 20 ng per mL recombinant human IL-2 (Peprotech) at a concentration of 5×10^5 to 2×10^6 cells per mL. The splenocytes were cocultured with 1×10^6 CEM cells and costimulated with 1 μg per mL anti-CD28 antibody (Tonbo biosciences; In Vivo Ready™ Anti-Human CD28 (clone CD28.2) on 6-well tissue culture plates pre-coated with 50 μg/mL goat anti-mouse antibody (Invitrogen; Goat anti-Mouse IgG (H + L) Secondary Antibody) and 1 μg per mL of OKT3 antibody (Tonbo biosciences; Purified Anti-Human CD3 (clone OKT3))4. Twenty-four hours after co-stimulation, the culture media were doubled. After 3 days of activation, the cells were resuspended in fresh media at 5×10^5 cells per mL. For each subsequent passaging, the cells were cultured in a 17:3 ratio of fresh culture media and prior culture media at 5×10^5 cells per mL. The supernatants were sampled on days 7, 10, and 14 days post-costimulation and diluted in Triton X-100 (Sigma) in PBS at a final working concentration of 0.5% Triton X. The samples were sent to the CFAR Virology Core at UCLA for HIV p24 antigen ELISA.

Flow cytometry. During cell staining 10^5 cells were suspended in a 50 μL volume of 1:1 dilution of phosphate buffered saline (PBS):Human AB serum (Sigma). For 2-step staining to detect cell surface HA expression, cells were first stained with Anti-HA-Biotin, High Affinity antibody (Sigma Cat#12158167001) at 4°C for 20 min and then after washing were stained with the secondary Streptavidin, R-PE Conjugate (FisherSci Cat#S866A) before resuspension in 2% paraformaldehyde in PBS. PBMC from humanized NSG-BLT mice were evaluated for the presence of human immune cells by staining with either anti-human CD45 e450 (eBioscience

Cat#48-0459-42) or Pacific Blue anti-human CD45 Antibody (HI30) (Biolegend Cat#304029). Stained samples were stored at 4°C, then samples were run using a Cytomics FC 500 flow cytometer (Beckman Coulter). PBMCs from humanized TKO-BLT mice were stained with fluorescently conjugated antibodies: CD69-Brilliant Violet 510 (clone FN50) or CD14-Brilliant Violet 510 (clone M5E2), CD3-Pacific Blue (clone Hit3a), CD8a-FITC (clone Hit8a), CD4-PE (clone RPA-T4), CD19-PE-Cy5 (clone SJ25C1), CD45-APC (clone 2D1), CD56-PE-Cy7 (clone MEM-188) (all from Biolegend) and Ghost Dye Red 780 (Tonbo Biosciences), then samples were run using a MACSQuant Analyzer 10 flow cytometer (Miltenyi) or Attune NxT (Beckman Coulter) (Supplemental Figure 2-9D). All data was analyzed using FlowJo software (version 7 or later).

SUW133 compound. PKC modulator SUW133 was synthesized as previously described (DeChristopher et al., 2012).

Quantification and statistical Analysis. Statistical analyses were performed using FlowJo (version 7 or later), GraphPad Prism software (version 8.4.3), Microsoft Excel or Python (version 2.7). Statistical details of experiments and significance can be found in the figure legends.

ACKNOWLEDGEMENTS

Equipment used for this project was provided by the James B. Pendleton Charitable Trust and the McCarthy Family Foundation. ART drugs for humanized mouse studies were kindly provided by Merck (RAL) and Gilead Sciences (TDF and FTC). The illustrations were created with https://biorender.com/.

FUNDING SOURCES

This work was supported by the National Institutes of Health (P01 AI131294 to J.A.Z., CA31845 to P.A.W., AI124763 to M.D.M., AI124743 to J.A.Z. and P.A.W., AI155232 to J.T.K., K08CA235525 to C.S.S., and AI145038 to R.S.), the National Center for Advancing Translational Sciences UCLA CTSI Grant (UL1TR001881 and UL1TR000124), the American Foundation for AIDS Research (110057-69-RGRL to J.A.Z.), the National Science Foundation (DMS1662146/1662096 to N.L.K. and D.W.), and the UCLA Center for AIDS Research (AI28697). The UCLA AIDS Institute, UCLA Charity Treks and UCLA Department of Medicine also provided support.

CONFLICTS OF INTEREST

Stanford University has filed patent applications on SUW133 and related technology, which has been licensed by Neurotrope BioScience (Synaptogenix, Inc.) for the treatment of neurological disorders and by BryoLogyx, Inc. for use in HIV/AIDS eradication and cancer immunotherapy. Paul A. Wender is an adviser to both companies and a cofounder of the latter. Jerome A. Zack is on the scientific advisory board for BryoLogyx, Inc. and is a cofounder of CDR3 Therapeutics. The remaining authors declare no competing interests.

SUPPLEMENTARY FIGURES & TABLES

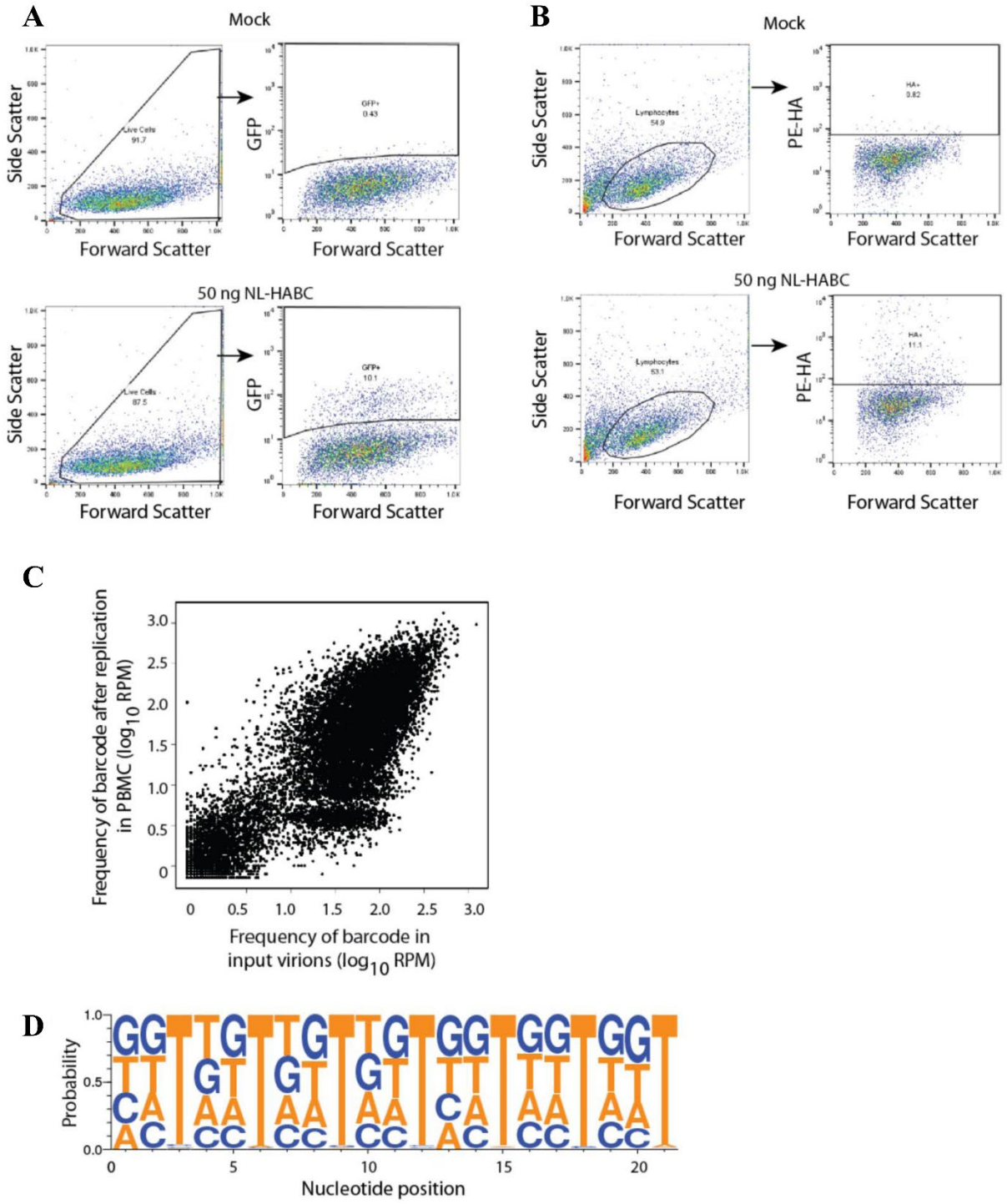

Supplemental Figure 2-1. Example flow cytometry profile/gating strategy and additional sequence analysis. Related to Fig 2-2. A) GHOST cell infections. GHOST cells encode GFP under the control of an HIV promoter and express GFP when newly infected by HIV (after expression of the Tat gene). Consequently, they are used as indicator cell lines for HIV titrations. Upper panels show mock-infected control cells and lower panels show cells exposed to 50 ng of barcoded NL-HABC virus at 48 h post-infection. **B)** Human PBMC mock infections (upper panel) or NL-

HABC infections (lower panel). Percentages of gated cells shown. **C)** Scatter plot showing comparison between barcode occurrence in virions before and after replication for 3 days in primary human PBMC. Spearman correlation rho = 0.74. **D)** Plot showing frequency of different nucleotides within barcode sequence after passage in PBMC, indicating no strong bias towards any particular nucleotide in varied bases (the height of each letter represents the probability of occurrence).

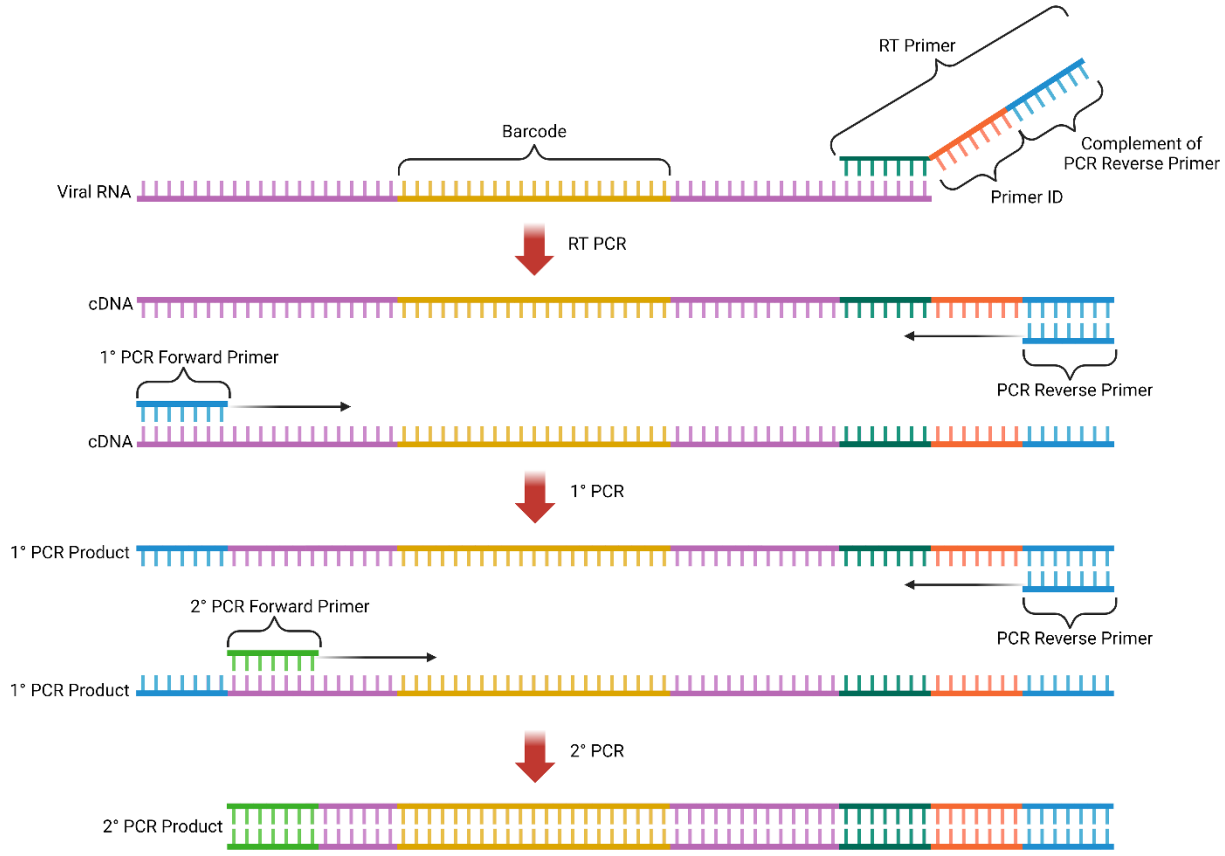

Supplemental Figure 2-2. Schematic of hemi-nested barcode PCR with Primer ID. Related to Figs 2-3 and 2-4. Graphical schematic of RT- and hemi-nested PCR protocol with Primer ID used to amplify viral RNA from *in vivo* samples.

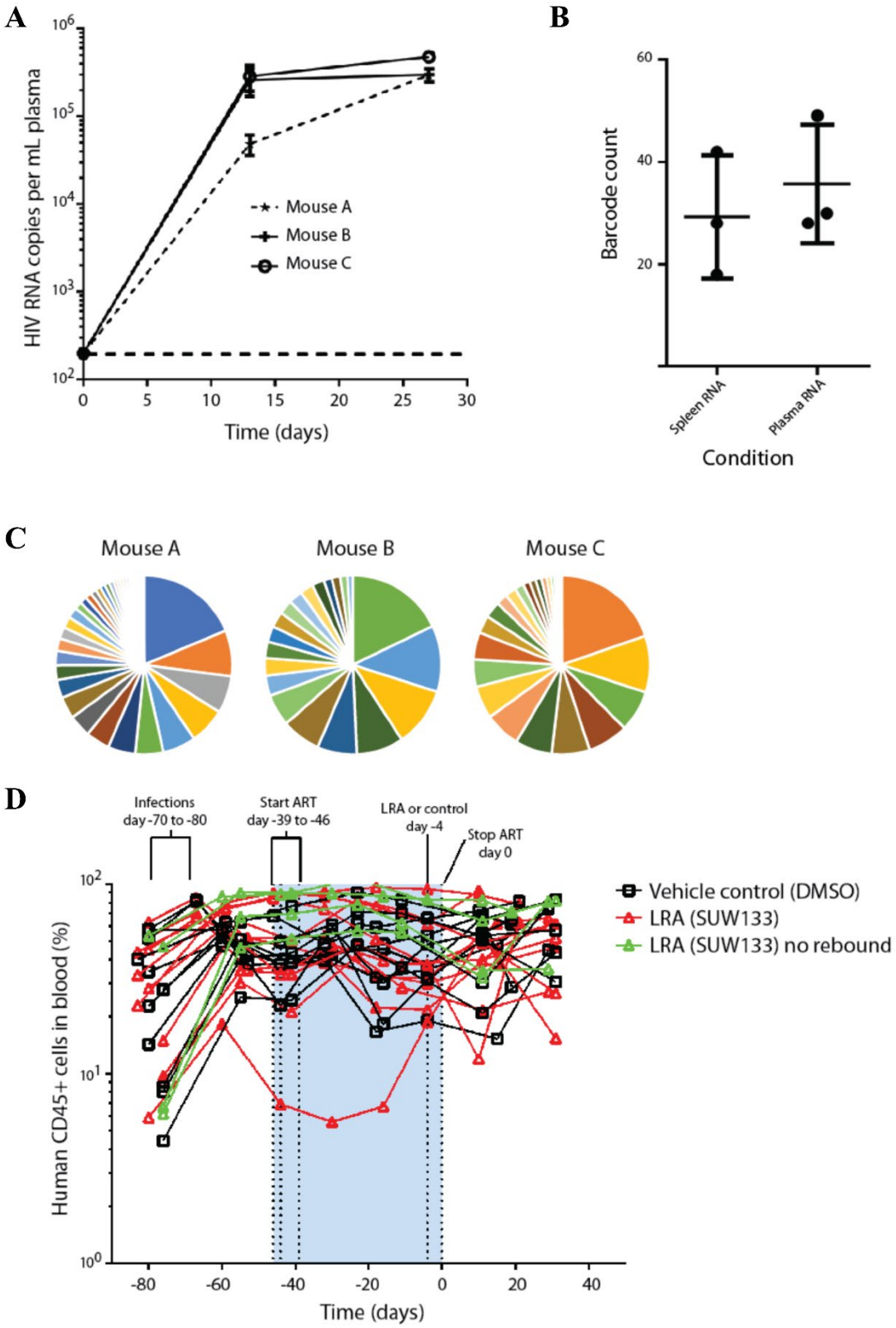

Supplemental Figure 2-3. ***In vivo*** **analysis in humanized BLT mice. Related to Figs 2-5 and 2-6. A)** Plasma viral loads showing virus replication after primary infection in 3 mice. **B)** Barcode count of individual viral sequences in plasma and spleen at the time of necropsy in these 3 animals (week 4 post-infection). Error bars represent mean+/-

SEM. **C)** Pie charts showing barcode frequency distribution in mice A-C with each color representing a unique barcoded sequence present in plasma. **D)** Humanization in mice 1-26 (Fig 2-5) over time. Percentages of human $CD45^+$ cells were analyzed by flow cytometry. See Supplemental Table 2-1 for statistical comparisons between groups before and after LRA administration.

A DMSO control

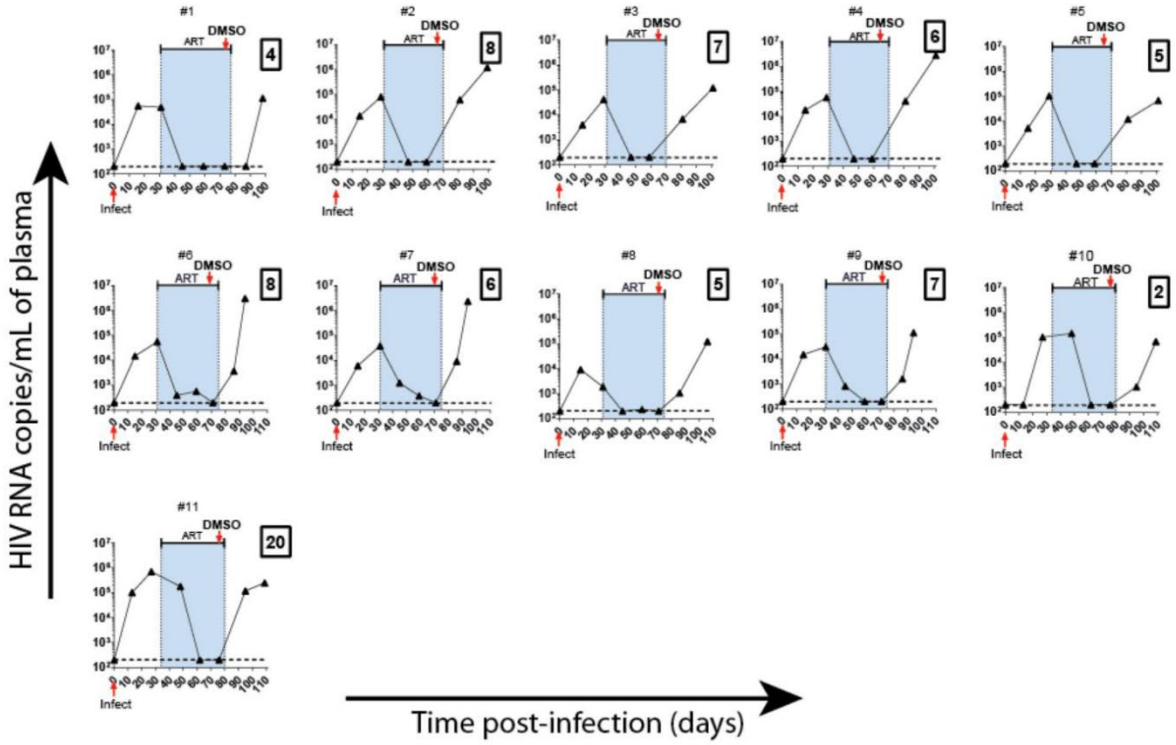

B LRA-treated

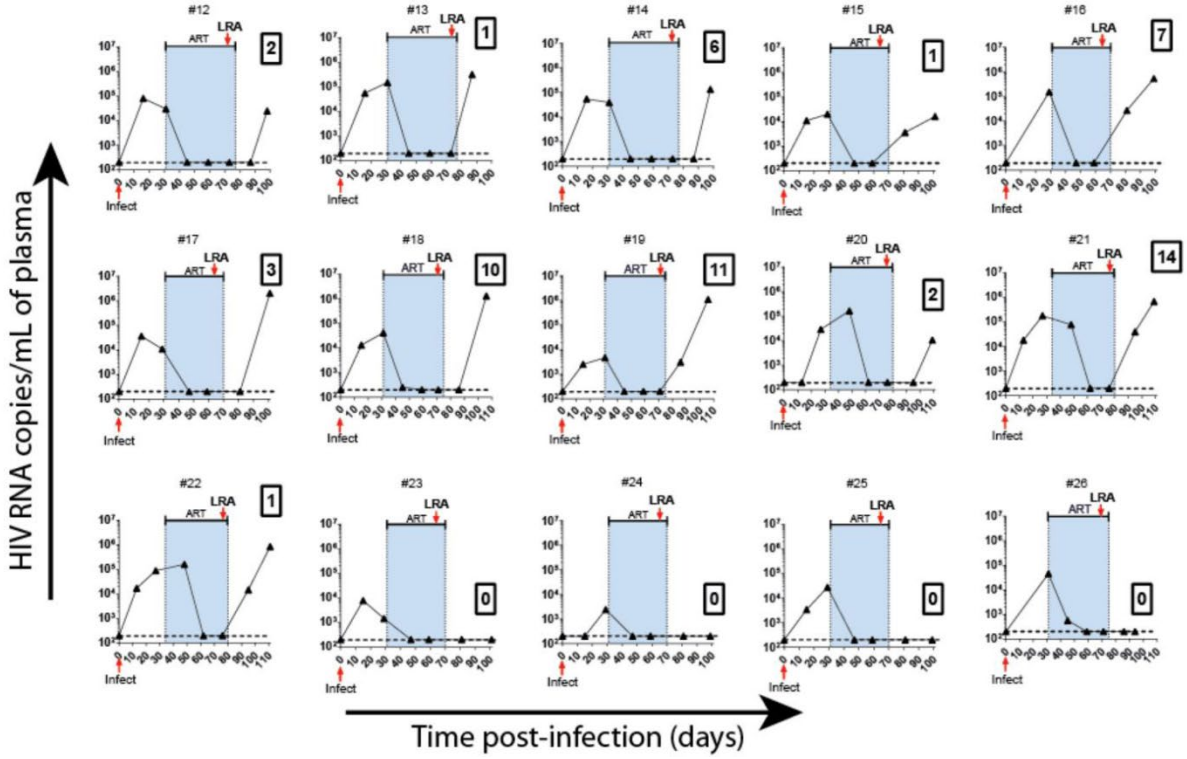

Supplemental Figure 2-4. Viral loads and *ex vivo* outgrowth assays. Related to Figs 2-5 and 2-6. A) Viral loads of individual control (DMSO) treated animals. **B)** Viral loads of LRA-treated animals. Plasma barcodes identified in each animal indicated within boxes.

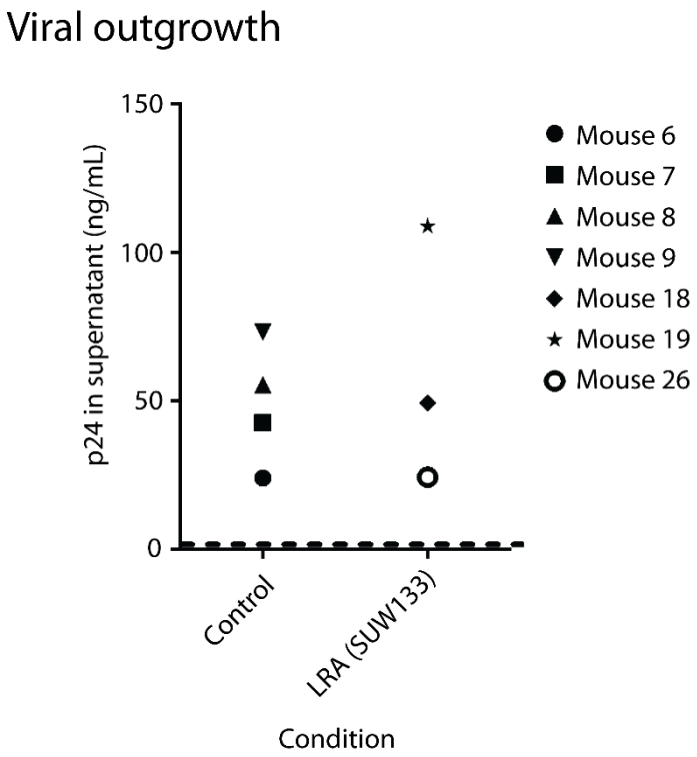

Supplemental Figure 2-5. *Ex vivo* viral outgrowth from spleen. Related to Figs 2-5 and 2-6. Splenocytes were costimulated and then incubated with CEM cells to support viral outgrowth from infected tissue. The concentration of HIV p24 in culture supernatant following 14-15d of culture is shown. Notably, cells from non-rebounding mouse #26 (open circle) did produce replicating virus under these conditions, indicating that LRA treatment delayed rebound but did not entirely eliminate viral reservoirs in this animal

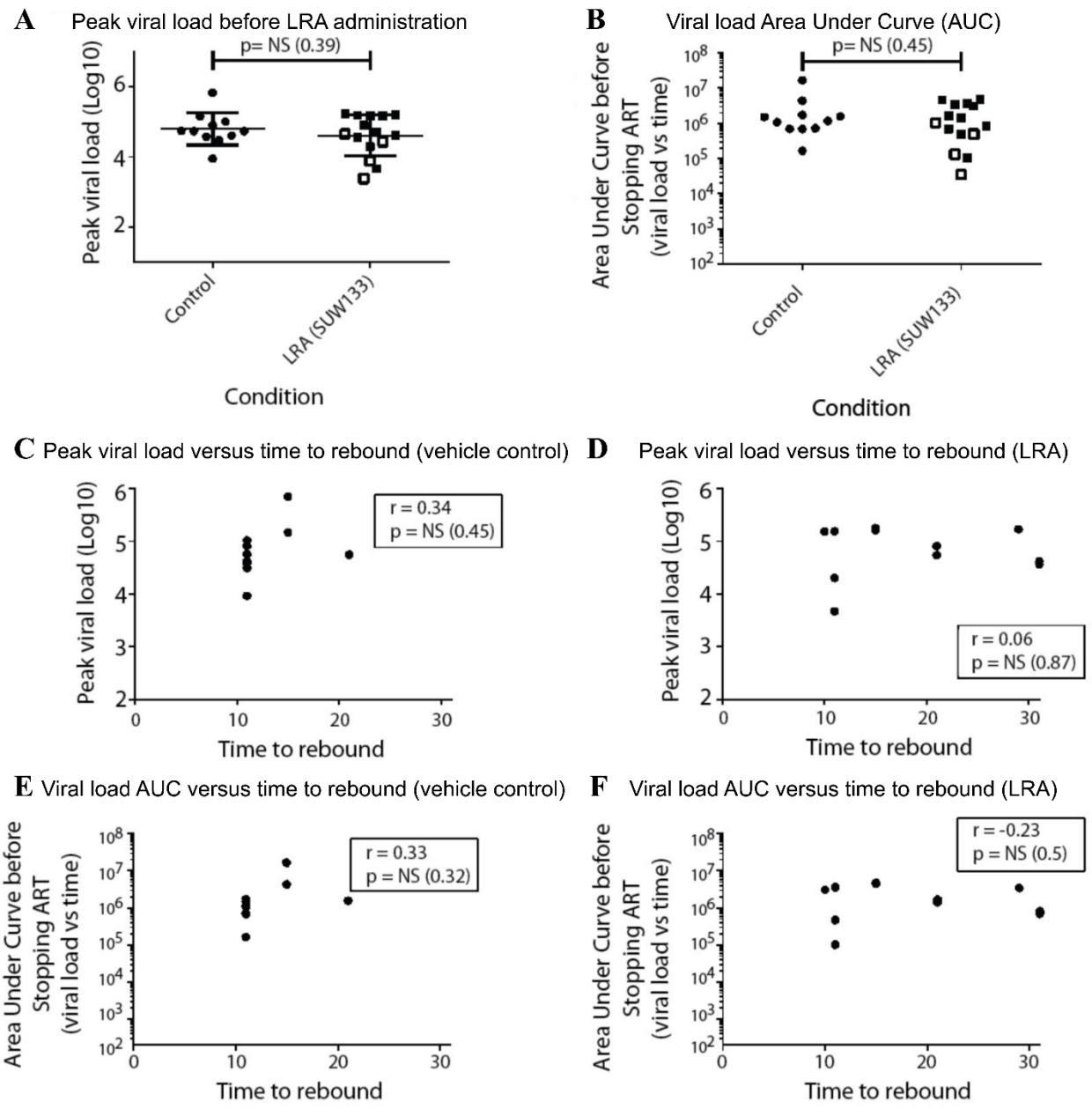

Supplemental Figure 2-6. Peak viral load and viral load vs time Area Under Curve (AUC) comparisons. Related to Figs 2-5 and 2-6. A) Peak viral load before LRA administration in each animal group. **B)** AUC before stopping ART in each animal group (viral load versus time). **C)** Peak viral load versus time to rebound (control-treated animals). **D)** Peak viral load versus time to rebound (LRA-treated animals). **E)** Viral load AUC versus time to rebound (control-treated animals). **F)** Viral load AUC versus time to rebound (LRA-treated animals). Open squares in panels A and B represent mice non-rebounding mice. A 2-sided equal variance t test was used for comparisons in panels A and B, and Pearson r (2 tailed) for panels C-F. Four non-rebounding mice are not included in panels D and F as no x value is available. Other datapoints are shown but in some cases overlap.

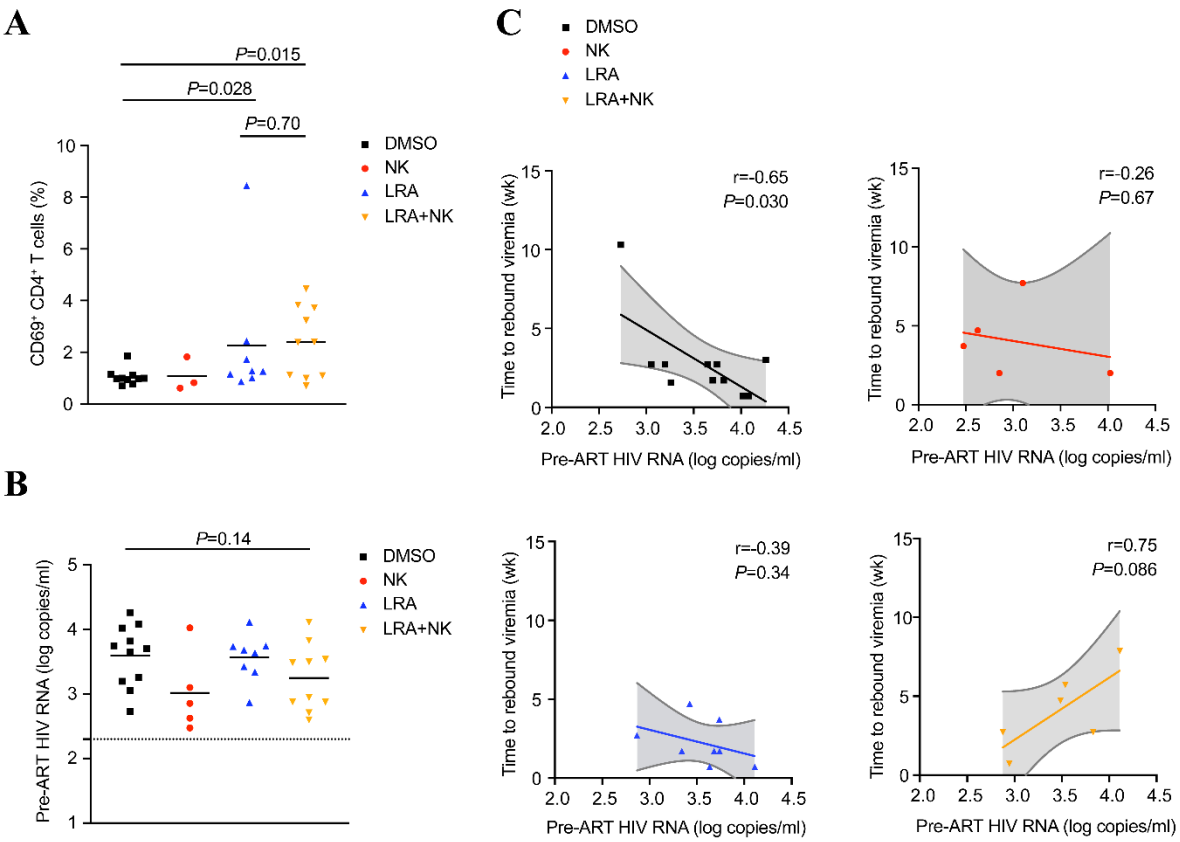

Supplemental Figure 2-7. T cell activation and correlation between pre-ART viral loads and time to rebound. **A)** Frequency of $CD69^+$ $CD4^+$ T cells in the blood five days after the injection of DMSO only (black), NK only (red), LRA only (blue), and LRA plus NK (orange) groups. n=10 biologically independent animals in DMSO only group, n=3 biologically independent animals in NK only group, n=8 biologically independent animals in LRA only group, n=10 biologically independent animals in LRA plus NK group. P values were calculated using two-tailed Mann-Whitney test. **B)** Plasma viral loads for each animal before ART was initiated. Black dotted line indicates the detection limit of 2.3 log RNA copies per mL. P values were calculated using one way ANOVA Kruskal-Wallis test. n=11 biologically independent animals in DMSO only group, n=5 biologically independent animals in NK only group, n=8 biologically independent animals in LRA only group, n=10 biologically independent animals in LRA plus NK group. Horizontal bars represent the means **(A, B)**. **C)** Scatterplot of pre-ART HIV levels and time to rebound after ART discontinuation of the rebounding animals. Among the rebounding animals, n=11 biologically independent animals in DMSO only group, n=5 biologically independent animals in NK only group, n=8 biologically independent animals in LRA only group, n=6 biologically independent animals in LRA plus NK group. Lines are linear predictions of time to rebound on pre-ART viral loads. The 95% confidence intervals of the fitted values are shown by grey areas. r = Pearson correlation coefficient. *P* values were calculated using Pearson correlation test. Results are pooled from two independent experiments.

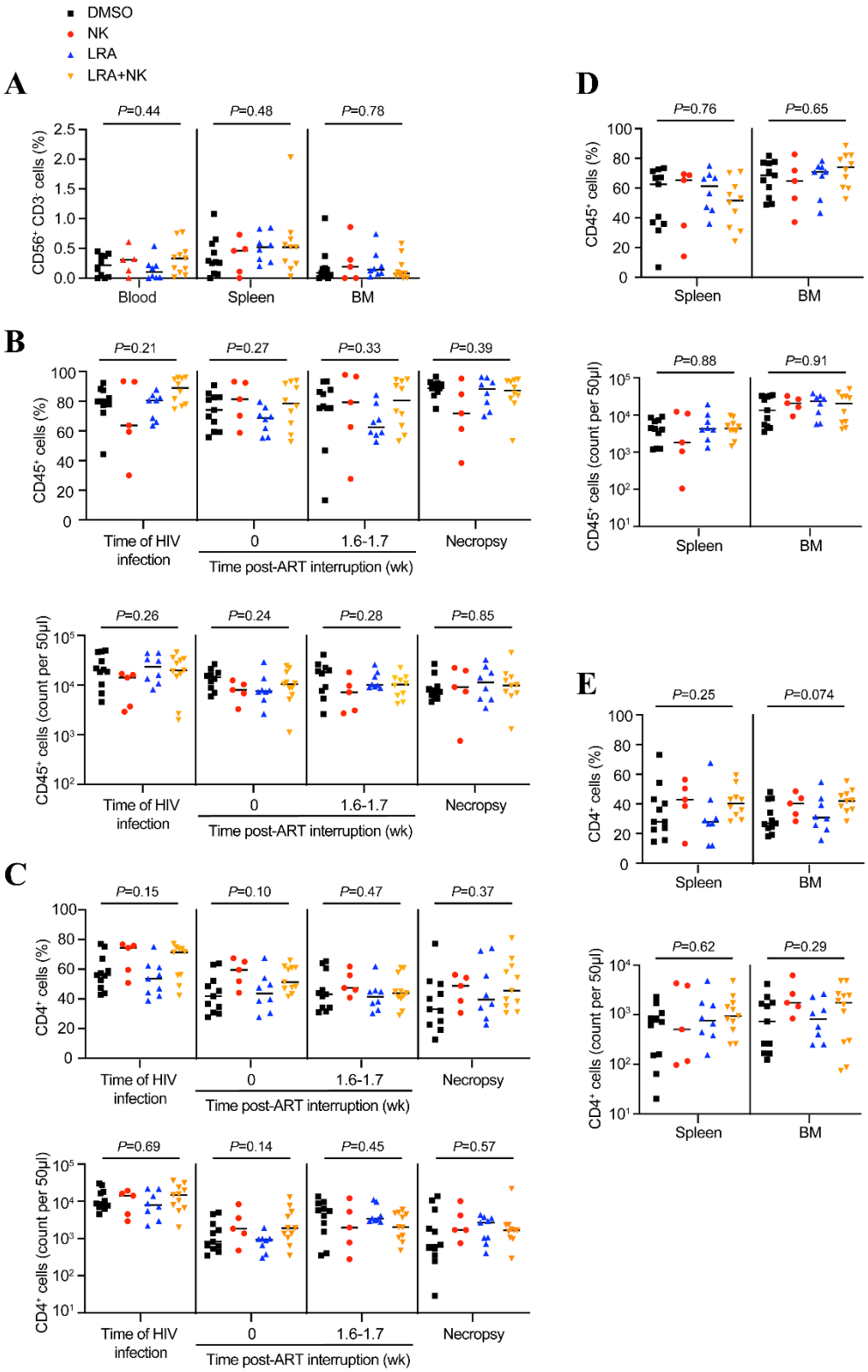

Supplemental Figure 2-8. Human immune engraftment in infected mice treated with SUW133 and NK cells. A) Frequency of human $CD56^+$ $CD3^-$ cells in the blood, spleen, and bone marrow "BM" at necropsy of the DMSO only (black), NK only (red), LRA only (blue), and LRA plus NK (orange) groups. **B, C)** Longitudinal frequencies and absolute counts of human $CD45^+$ cells **(B)** and $CD4^+$ T cells **(C)** in the blood at various timepoints. **D, E)** Frequencies

and absolute counts of human $CD45^+$ cells **(D)** and $CD4^+$ T cells **(E)** in the spleen, and BM at necropsy (right). n=11 biologically independent animals in DMSO only group, n=5 biologically independent animals in NK only group, n=8 biologically independent animals in LRA only group, n=10 biologically independent animals in LRA plus NK group. Horizontal bars represent the medians. P values were calculated using one-way ANOVA Kruskal-Wallis test. Results are pooled from two independent experiments.

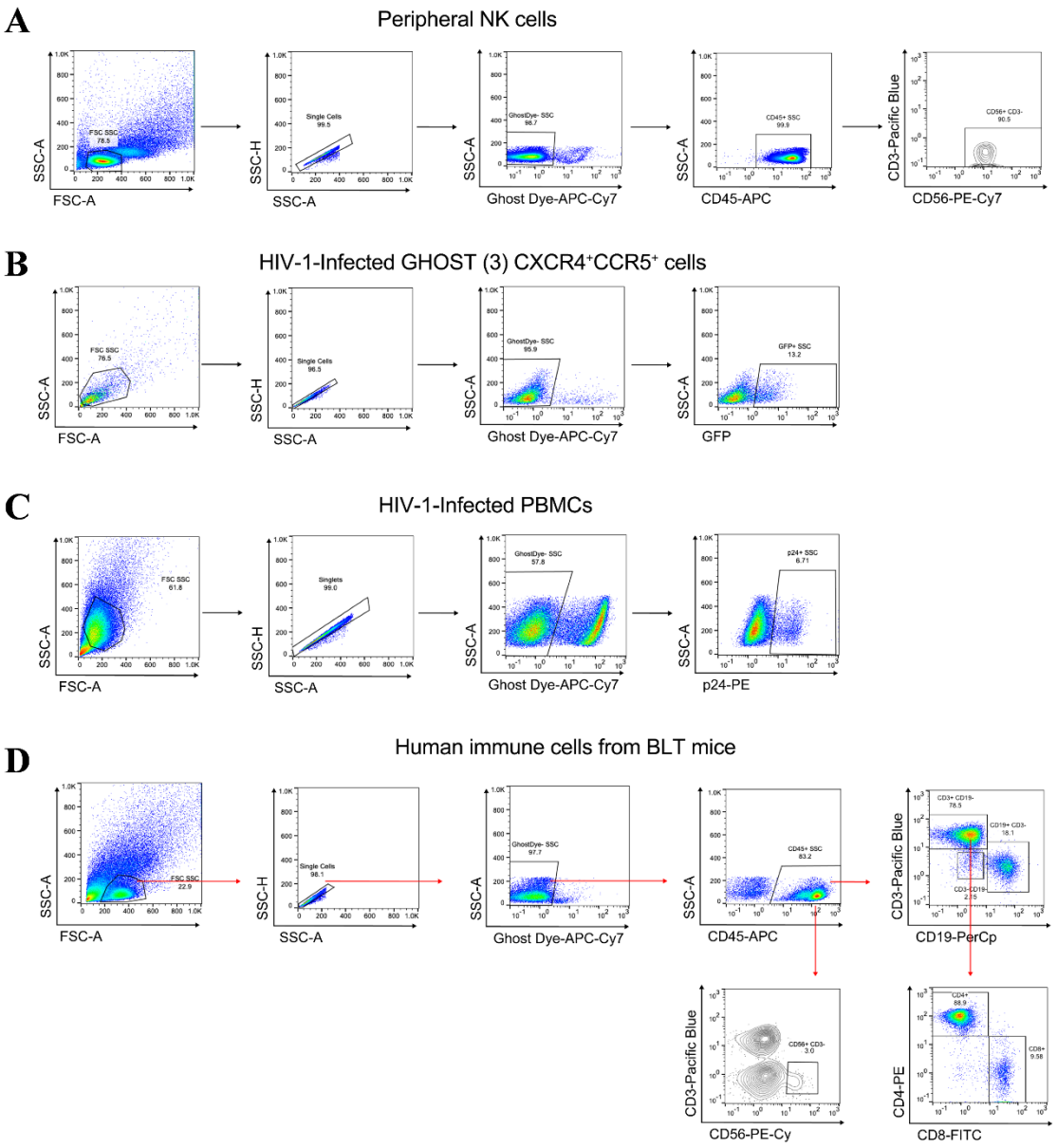

Supplemental Figure 2-9. Flow cytometry gating strategies. A, B) Flow cytometric analysis of human PBMCs **(A)**, HIV-infected Ghost CXCR4^{+}CCR5^{+} cells **(B)**, HIV-infected PBMCs **(C)**, and human immune cells from TKO-BLT mice **(D)**.

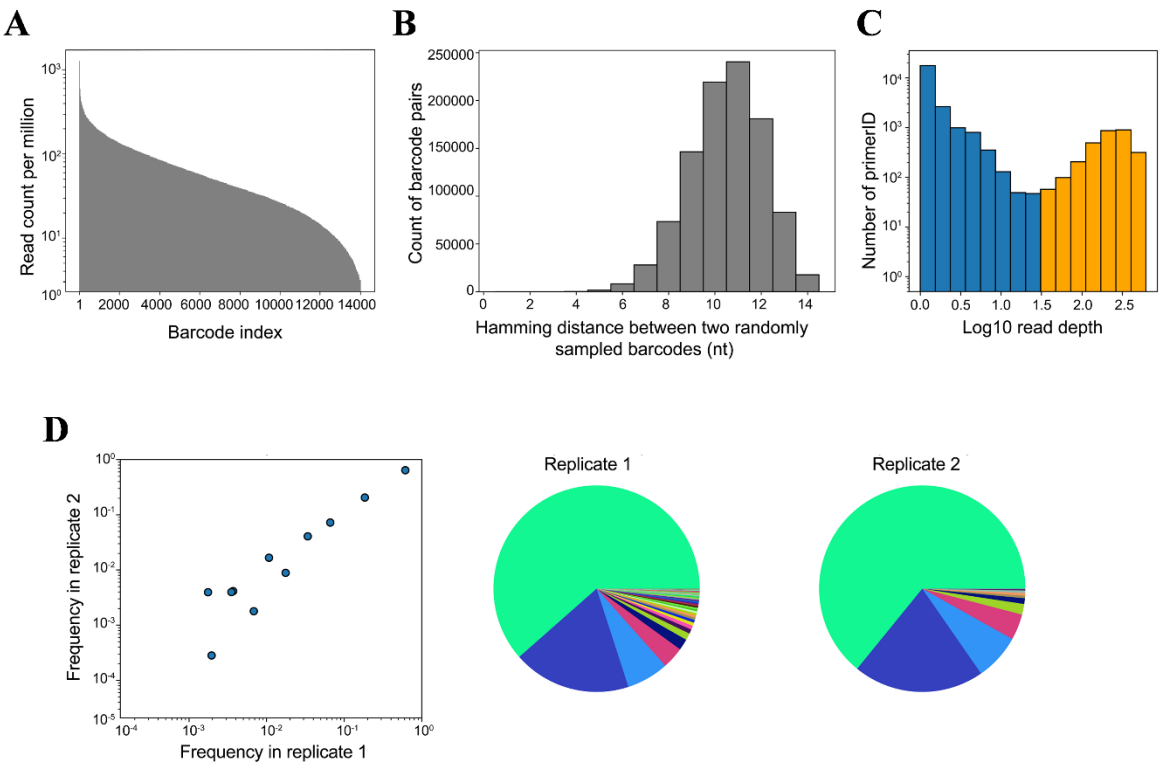

Supplemental Figure 2-10. Analysis of barcoded NL-HABC. A) Histogram demonstrates ~14,000 viral barcodes with relatively equal distribution as quantified by Hiseq sequencing derived from virion-associated viral RNA of the virus supernatant collected from HIV-producing transfected 293T cells. **B)** Histogram shows the pair-wise distance between barcodes is 11 bp. **C)** Representative histogram shows the frequency of Primer ID following a bi-modal distribution of authentic barcodes (orange) versus barcodes containing PCR error (blue). d, RNA molecules from the same population were sampled at two different times to quantify the starting number of RNA molecules in each replicate and thereby assess the reproducibility of the results. Scatterdot plot of the two replicates **(C)**. r =0.92, Spearman coefficient. P=6.7 x 10^{-5}. Pie chart depicting the absolute diversity of clones obtained from the same sample for each replicate **(D)**.

Percentage human CD45+ cells in peripheral blood	p value
Before LRA administration: Control group vs LRA group	0.786108
After LRA administration: Control group vs LRA group	0.923628
Control group before vs after Control group after LRA administration	0.896905
LRA group before vs after LRA administration	0.949451

Supplemental Table 2-1. *In vivo* humanization levels are not significantly affected by LRA administration. Related to Figs 2-3 and 2-4. P values for comparisons between the closest timepoint before and after LRA administration are shown (2-sided equal variance unpaired t test).

Experiment	Treatment	Mouse ID	Time to rebound (wk)	Number of viral barcodes per mouse
4	DMSO	4_1	1.57	3
		4_2	10.3	6
		4_3	2.71	10
		4_4	3	3
		Mean ± s.e.m	4.9 ± 2.7	6.3 ± 2.0
	DMSO+NK	4_5	4.71	4
		4_6	7.71	2
		4_7	3.71	2
		4_8	2	4
		4_9	2	3
		Mean ± s.e.m	4.0 ± 1.1	3.0 ± 0.5
	SUW133+NK	4_10	0.71	4
		4_11	NR	0
		4_12	NR	0
		4_13	NR	0
		4_14	NR	0
		Mean ± s.e.m	8.4 ± 2.8	0.8 ± 0.8
5	DMSO	5_1	1.71	3
		5_2	2.71	3
		5_3	2.71	9
		5_4	2.71	6
		5_5	1.71	4
		5_6	0.71	4
		5_7	0.71	1
		Mean ± s.e.m	1.9 ± 0.3	4.3 ± 1.0
	SUW133	5_8	1.71	11
		5_9	3.71	3
		5_10	0.71	3
		5_11	4.71	3
		5_12	2.71	4
		5_13	0.71	2
		5_14	1.71	4
		5_15	1.71	3
		Mean ± s.e.m	2.2 ± 0.5	4.1 ± 1.0
	SUW133+NK	5_16	5.71	2
		5_17	4.71	3
		5_18	2.71	1
		5_19	2.71	1
		5_20	7.86	1
		Mean ± s.e.m	4.7 ± 1.0	1.6 ± 0.4

Supplemental Table 2-2. Time to rebound and number of unique barcodes in mice that received SUW133 plus NK cells. Mice from Fig. 2-5 were tabulated based on their experiment number, treatment group, mouse ID, time to rebound after ART interruption, and number of viral barcodes per mouse. No significant differences in the time to rebound between the DMSO groups in Experiments 4 and 5 (P=0.19, DMSO Exp4 vs DMSO Exp5) or number of barcodes (P=0.66, DMSO Exp4 vs DMSO Exp5). No significant differences in the time to rebound among rebounding animals in the SUW133 plus NK groups in Experiments 4 and 5 based (P=0.39, SUW133 plus NK Exp4 vs SUW133 plus NK Exp5) or number of barcodes (P= 0.14, SUW133 plus NK Exp4 vs SUW133 plus NK Exp5). NR = no rebound. s.e.m = standard error of mean. P values were calculated using unpaired two-tailed Mann Whitney t-test.

				p24 ng/ml			
Treatment	Mouse ID	Rebound viremia?	HIV DNA Spleen?	Day 3	Day 7	Day 10	Day 14
LRA+NK	4_11	No	No	ND	ND	ND	ND
LRA+NK	4_12	No	No	ND	ND	ND	ND
LRA+NK	4_13	No	No	ND	ND	ND	ND
LRA+NK	4_14	No	No	ND	ND	ND	ND

Supplemental Table 2-3. *Ex vivo* viral outgrowth assay of mice that did or did not rebound after receiving SUW133 plus NK cells. Mice from Fig. 2-5 that received SUW133 plus NK cells and did not demonstrate presence of rebound viremia after ART interruption and cell-associated HIV DNA in the spleens, were tabulated based on levels of HIV p24 antigen by ELISA detected in the cell-free supernatant from the *ex vivo* viral outgrowth splenocyte cocultures at 7, 10 and 14 days after coculture. ND = not detected. Lower limit of detection was 0.25 ng of p24 per mL.

Oligonucleotide sequence	Name
agagcttctagagagtcgcgNNTNNTNNTNNTNNTNNTNNT**ATG**ggcagagcgatggtg	Primer 1
cgcctattctgctatgtcgacaccc	Primer 2
gaagcagagctagaactggcaga	Primer 3
ggactggttttatagacatcactatg	Primer 4
cgcctattctgctatgtcgacaccc	Primer 5
ccccagaagaccaagggc	Primer 6
ctgcgtgggtaggagcag	Primer 7
gccttgccagcacgctcacagnnnnnnnnnnnntaggagcagtgccagaagc	Primer 8
ctgacagaggacaggtggaacaagc	Primer 9
gccttgccagcacgctcacag	Primer 10
aagggccacagagggagc	Primer 11
gccttgccagcacgctcacag	Primer 12

Supplemental Table 2-4. Oligonucleotide Primer Sequences. Related to methods.

REFERENCES

Ali, A., & Yang, O. O. (2006). A novel small reporter gene and HIV-1 fitness assay. *J Virol Methods*, *133*(1), 41-47. https://doi.org/10.1016/j.jviromet.2005.10.016

Archin, N. M., Liberty, A. L., Kashuba, A. D., Choudhary, S. K., Kuruc, J. D., Crooks, A. M., Parker, D. C., Anderson, E. M., Kearney, M. F., Strain, M. C., Richman, D. D., Hudgens, M. G., Bosch, R. J., Coffin, J. M., Eron, J. J., Hazuda, D. J., & Margolis, D. M. (2012). Administration of vorinostat disrupts HIV-1 latency in patients on antiretroviral therapy. *Nature*, *487*(7408), 482-485. https://doi.org/10.1038/nature11286

Beans, E. J., Fournogerakis, D., Gauntlett, C., Heumann, L. V., Kramer, R., Marsden, M. D., Murray, D., Chun, T. W., Zack, J. A., & Wender, P. A. (2013). Highly potent, synthetically accessible prostratin analogs induce latent HIV expression in vitro and ex vivo. *Proc Natl Acad Sci U S A*, *110*(29), 11698-11703. https://doi.org/10.1073/pnas.1302634110

Borducchi, E. N., Cabral, C., Stephenson, K. E., Liu, J., Abbink, P., Ng'ang'a, D., Nkolola, J. P., Brinkman, A. L., Peter, L., Lee, B. C., Jimenez, J., Jetton, D., Mondesir, J., Mojta, S., Chandrashekar, A., Molloy, K., Alter, G., Gerold, J. M., Hill, A. L., . . . Barouch, D. H. (2016). Ad26/MVA therapeutic vaccination with TLR7 stimulation in SIV-infected rhesus monkeys. *Nature*, *540*(7632), 284-287. https://doi.org/10.1038/nature20583

Borducchi, E. N., Liu, J., Nkolola, J. P., Cadena, A. M., Yu, W. H., Fischinger, S., Broge, T., Abbink, P., Mercado, N. B., Chandrashekar, A., Jetton, D., Peter, L., McMahan, K., Moseley, E. T., Bekerman, E., Hesselgesser, J., Li, W., Lewis, M. G., Alter, G., . . . Barouch, D. H. (2018). Antibody and TLR7 agonist delay viral rebound in SHIV-infected monkeys. *Nature*, *563*(7731), 360-364. https://doi.org/10.1038/s41586-018-0600-6

Bristol, G. C., Gao, L. Y., & Zack, J. A. (1997). Preparation and maintenance of SCID-hu mice for HIV research. . *Methods*, *12*(4), 343-347. https://doi.org/10.1006/meth.1997.0488.

Brooks, D. G., Hamer, D. H., Arlen, P. A., Gao, L., Bristol, G., Kitchen, C. M., Berger, E. A., & Zack, J. A. (2003). Molecular Characterization, Reactivation, and Depletion of Latent HIV. *Immunity*, *19*(3), 413-423. https://doi.org/10.1016/s1074-7613(03)00236-x

Chen, H. C., Martinez, J. P., Zorita, E., Meyerhans, A., & Filion, G. J. (2017). Position effects influence HIV latency reversal. *Nat Struct Mol Biol*, *24*(1), 47-54. https://doi.org/10.1038/nsmb.3328

Chun, T. W., Davey, R. T. J., Ostrowski, M., Shawn Justement, J., Engel, D., Mullins, J. I., & Fauci, A. S. (2000). Relationship between pre-existing viral reservoirs and the re-emergence of plasma viremia after discontinuation of highly active anti-retroviral therapy. *Nat Med*, *6*(7), 757–761. https://doi.org/10.1038/77481

Chun, T. W., Engel, D., Mizell, S. B., Hallahan, C. W., Fischette, M., Park, S., Davey, R. T., Dybul, M., Kovacs, J. A., Metcalf, J. A., Mican, J. M., Berrey, M. M., Corey, L., Lane, H. C., & Fauci, A. S. (1999). Effect of interleukin-2 on the pool of latently infected, resting CD4+ T cells in HIV-1-infected patients receiving highly active anti-retroviral therapy. *Nat Med*, *5*(6), 651-655. https://doi.org/10.1038/9498

Chun, T. W., Stuyver, L., Mizell, S. B., Ehler, L. A., Mican, J. A., Baseler, M., Lloyd, A. L., Nowak, M. A., & Fauci, A. S. (1997). Presence of an inducible HIV-1 latent reservoir during highly active antiretroviral therapy. *Proc Natl Acad Sci U S A 94*, 13193-13197. https://doi.org/10.1073/pnas.94.24.13193

Davey, R. T., Jr, Bhat, N., Yoder, C., Chun, T. W., Metcalf, J. A., Dewar, R., Natarajan, V., Lempicki, R. A., Adelsberger, J. W., Miller, K. D., Kovacs, J. A., Polis, M. A., Walker, R. E., Falloon, J., Masur, H., Gee, D., Baseler, M., Dimitrov, D. S., Fauci, A. S., & Lane, H. C. (1999). HIV-1 and T cell dynamics after interruption of highlyactive antiretroviral therapy (HAART) in patients witha history of sustained viral suppression. *Proc Natl Acad Sci U S A*, *96*(26), 15109–15114. https://doi.org/10.1073/pnas.96.26.15109.

Davis, Z. B., Felices, M., Verneris, M. R., & Miller, J. S. (2015). Natural Killer Cell Adoptive Transfer Therapy: Exploiting the First Line of Defense Against Cancer. *Cancer J*, *21*(6), 486-491. https://doi.org/10.1097/PPO.0000000000000156

DeChristopher, B. A., Loy, B. A., Marsden, M. D., Schrier, A. J., Zack, J. A., & Wender, P. A. (2012). Designed, synthetically accessible bryostatin analogues potently induce activation of latent HIV reservoirs in vitro. *Nat Chem*, *4*(9), 705-710. https://doi.org/10.1038/nchem.1395

Denton, P. W., Olesen, R., Choudhary, S. K., Archin, N. M., Wahl, A., Swanson, M. D., Chateau, M., Nochi, T., Krisko, J. F., Spagnuolo, R. A., Margolis, D. M., & Garcia, J. V. (2012). Generation of HIV latency in humanized BLT mice. *J Virol*, *86*(1), 630-634. https://doi.org/10.1128/JVI.06120-11

Fennessey, C. M., Pinkevych, M., Immonen, T. T., Reynaldi, A., Venturi, V., Nadella, P., Reid, C., Newman, L., Lipkey, L., Oswald, K., Bosche, W. J., Trivett, M. T., Ohlen, C., Ott, D. E., Estes, J. D., Del Prete, G. Q., Lifson, J. D., Davenport, M. P., & Keele, B. F. (2017). Genetically-barcoded SIV facilitates enumeration of rebound variants and estimation of reactivation rates in nonhuman primates following interruption of suppressive antiretroviral therapy. *PLoS Pathog*, *13*(5), e1006359. https://doi.org/10.1371/journal.ppat.1006359

Finzi, D., Hermankova, M., Pierson, T., Carruth, L. M., Buck, C., Chaisson, R. E., Quinn, T. C., Chadwick, K., Margolick, J., Brookmeyer, R., Gallant, J., Markowitz, M., Ho, D. D., Richman, D. D., & Siliciano, R. F. (1997). Identification of a Reservoir for HIV-1 in Patients on Highly Active Antiretroviral Therapy. *Science*, *278*, 1295-1300. https://doi.org/10.1126/science.278.5341.1295

Halper-Stromberg, A., Lu, C. L., Klein, F., Horwitz, J. A., Bournazos, S., Nogueira, L., Eisenreich, T. R., Liu, C., Gazumyan, A., Schaefer, U., Furze, R. C., Seaman, M. S., Prinjha, R., Tarakhovsky, A., Ravetch, J. V., & Nussenzweig, M. C. (2014). Broadly neutralizing antibodies and viral inducers decrease rebound from HIV-1 latent reservoirs in humanized mice. *Cell*, *158*(5), 989-999. https://doi.org/10.1016/j.cell.2014.07.043

Huntington, N. D., Legrand, N., Alves, N. L., Jaron, B., Weijer, K., Plet, A., Corcuff, E., Mortier, E., Jacques, Y., Spits, H., & Di Santo, J. P. (2009). IL-15 trans-presentation promotes human NK cell development and differentiation in vivo. *J Exp Med*, *206*(1), 25-34. https://doi.org/10.1084/jem.20082013

Jabara, C. B., Jones, C. D., Roach, J., Anderson, J. A., & Swanstrom, R. (2011). Accurate sampling and deep sequencing of the HIV-1 protease gene using a Primer ID. *Proc Natl Acad Sci U S A*, *108*(50), 20166-20171. https://doi.org/10.1073/pnas.1110064108

Jennes, W., Verheyden, S., Mertens, J. W., Camara, M., Seydi, M., Dieye, T. N., Mboup, S., Demanet, C., & Kestens, L. (2013). Inhibitory KIR/HLA incompatibility between sexual partners confers protection against HIV-1 transmission. *Blood*, *121*(7), 1157-1164. https://doi.org/10.1182/blood-2012-09-455352

Jeyaraman, M., Muthu, S., Bapat, A., Jain, R., Sushmitha, E. S., Gulati, A., Channaiah Anudeep, T., Dilip, S. J., Jha, N. K., Kumar, D., Kesari, K. K., Ojha, S., Dholpuria, S., Gupta, G., Dureja, H., Chellappan, D. K., Singh, S. K., Dua, K., & Jha, S. K. (2021). Bracing NK cell based therapy to relegate pulmonary inflammation in COVID-19. *Heliyon*, *7*(7), e07635. https://doi.org/10.1016/j.heliyon.2021.e07635

Jiang, G., Mendes, E. A., Kaiser, P., Wong, D. P., Tang, Y., Cai, I., Fenton, A., Melcher, G. P., Hildreth, J. E., Thompson, G. R., Wong, J. K., & Dandekar, S. (2015). Synergistic Reactivation of Latent HIV Expression by Ingenol-3-Angelate, PEP005, Targeted NF-kB Signaling in Combination with JQ1 Induced p-TEFb Activation. *PLoS Pathog*, *11*(7), e1005066. https://doi.org/10.1371/journal.ppat.1005066

Kulkosky, J., Culnan, D. M., Roman, J., Dornadula, G., Schnell, M., Boyd, M. R., & Pomerantz, R. J. (2001). Prostratin: activation of latent HIV-1 expression suggests a potential inductive adjuvant therapy for HAART. *Blood*, *98*(10), 3006-3015. https://doi.org/10.1182/blood.v98.10.3006

Laird, G. M., Bullen, C. K., Rosenbloom, D. I., Martin, A. R., Hill, A. L., Durand, C. M., Siliciano, J. D., & Siliciano, R. F. (2015). Ex vivo analysis identifies effective HIV-1 latency-reversing drug combinations. *J Clin Invest*, *125*(5), 1901-1912. https://doi.org/10.1172/JCI80142

Lavender, K. J., Pace, C., Sutter, K., Messer, R. J., Pouncey, D. L., Cummins, N. W., Natesampillai, S., Zheng, J., Goldsmith, J., Widera, M., Van Dis, E. S., Phillips, K., Race, B., Dittmer, U., Kukolj, G., & Hasenkrug, K. J. (2018). An advanced BLT-humanized

mouse model for extended HIV-1 cure studies. *AIDS*, *32*(1), 1-10. https://doi.org/10.1097/QAD.0000000000001674

Lavender, K. J., Pang, W. W., Messer, R. J., Duley, A. K., Race, B., Phillips, K., Scott, D., Peterson, K. E., Chan, C. K., Dittmer, U., Dudek, T., Allen, T. M., Weissman, I. L., & Hasenkrug, K. J. (2013). BLT-humanized C57BL/6 Rag2-/-gammac-/-CD47-/- mice are resistant to GVHD and develop B- and T-cell immunity to HIV infection. *Blood*, *122*(25), 4013-4020. https://doi.org/10.1182/blood-2013-06-506949

Llewellyn, G. N., Seclen, E., Wietgrefe, S., Liu, S., Chateau, M., Pei, H., Perkey, K., Marsden, M. D., Hinkley, S. J., Paschon, D. E., Holmes, M. C., Zack, J. A., Louie, S. G., Haase, A. T., & Cannon, P. M. (2019). Humanized Mouse Model of HIV-1 Latency with Enrichment of Latent Virus in PD-1(+) and TIGIT(+) CD4 T Cells. *J Virol*, *93*(10). https://doi.org/10.1128/JVI.02086-18

Marsden, M. D. (2020). Benefits and limitations of humanized mice in HIV persistence studies. *Retrovirology*, *17*(1), 7. https://doi.org/10.1186/s12977-020-00516-2

Marsden, M. D., Kovochich, M., Suree, N., Shimizu, S., Mehta, R., Cortado, R., Bristol, G., An, D. S., & Zack, J. A. (2012). HIV latency in the humanized BLT mouse. *J Virol*, *86*(1), 339-347. https://doi.org/10.1128/JVI.06366-11

Marsden, M. D., Loy, B. A., Wu, X., Ramirez, C. M., Schrier, A. J., Murray, D., Shimizu, A., Ryckbosch, S. M., Near, K. E., Chun, T. W., Wender, P. A., & Zack, J. A. (2017). In vivo activation of latent HIV with a synthetic bryostatin analog effects both latent cell "kick" and "kill" in strategy for virus eradication. *PLoS Pathog*, *13*(9), e1006575. https://doi.org/10.1371/journal.ppat.1006575

Marsden, M. D., Wu, X., Navab, S. M., Loy, B. A., Schrier, A. J., DeChristopher, B. A., Shimizu, A. J., Hardman, C. T., Ho, S., Ramirez, C. M., Wender, P. A., & Zack, J. A. (2018). Characterization of designed, synthetically accessible bryostatin analog HIV latency reversing agents. *Virology*, *520*, 83-93. https://doi.org/10.1016/j.virol.2018.05.006

Marsden, M. D., & Zack, J. A. (2013). HIV/AIDS eradication. *Bioorg Med Chem Lett*, *23*(14), 4003-4010. https://doi.org/10.1016/j.bmcl.2013.05.032

Marsden, M. D., & Zack, J. A. (2017). Humanized Mouse Models for Human Immunodeficiency Virus Infection. *Annu Rev Virol*, *4*(1), 393-412. https://doi.org/10.1146/annurev-virology-101416-041703

Marsden, M. D., Zhang, T. H., Du, Y., Dimapasoc, M., Soliman, M. S. A., Wu, X., Kim, J. T., Shimizu, A., Schrier, A., Wender, P. A., Sun, R., & Zack, J. A. (2020). Tracking HIV Rebound following Latency Reversal Using Barcoded HIV. *Cell Rep Med*, *1*(9), 100162. https://doi.org/10.1016/j.xcrm.2020.100162

McCune, J. M., Namikawa, R., Kaneshima, H., Shultz, L. D., Lieberman, M., & Weissman, I. L. (1988). The SCID-hu mouse: murine model for the analysis of human hematolymphoid differentiation and function. *Science*, *241*(4873), 1632–1639. https://doi.org/10.1126/science.241.4873.1632

Melkus, M. W., Estes, J. D., Padgett-Thomas, A., Gatlin, J., Denton, P. W., Othieno, F. A., Wege, A. K., Haase, A. T., & Garcia, J. V. (2006). Humanized mice mount specific adaptive and innate immune responses to EBV and TSST-1. *Nat Med*, *12*(11), 1316-1322. https://doi.org/10.1038/nm1431

Ni, Z., Knorr, D. A., Bendzick, L., Allred, J., & Kaufman, D. S. (2014). Expression of chimeric receptor CD4zeta by natural killer cells derived from human pluripotent stem cells improves in vitro activity but does not enhance suppression of HIV infection in vivo. *Stem Cells*, *32*(4), 1021-1031. https://doi.org/10.1002/stem.1611

Pache, L., Marsden, M. D., Teriete, P., Portillo, A. J., Heimann, D., Kim, J. T., Soliman, M. S. A., Dimapasoc, M., Carmona, C., Celeridad, M., Spivak, A. M., Planelles, V., Cosford, N. D. P., Zack, J. A., & Chanda, S. K. (2020). Pharmacological Activation of Non-canonical NF-kappaB Signaling Activates Latent HIV-1 Reservoirs In Vivo. *Cell Rep Med*, *1*(3), 100037. https://doi.org/10.1016/j.xcrm.2020.100037

Persaud, D., Gay, H., Ziemniak, C., Chen, Y. H., Piatak, M., Jr., Chun, T. W., Strain, M., Richman, D., & Luzuriaga, K. (2013). Absence of detectable HIV-1 viremia after treatment cessation in an infant. *N Engl J Med*, *369*(19), 1828-1835. https://doi.org/10.1056/NEJMoa1302976

Richard, J., Sindhu, S., Pham, T. N., Belzile, J. P., & Cohen, E. A. (2010). HIV-1 Vpr up-regulates expression of ligands for the activating NKG2D receptor and promotes NK cell-mediated killing. *Blood*, *115*(7), 1354-1363. https://doi.org/10.1182/blood-2009-08-237370

Shimizu, S., Ringpis, G. E., Marsden, M. D., Cortado, R. V., Wilhalme, H. M., Elashoff, D., Zack, J. A., Chen, I. S., & An, D. S. (2015). RNAi-Mediated CCR5 Knockdown Provides HIV-1 Resistance to Memory T Cells in Humanized BLT Mice. *Mol Ther Nucleic Acids*, *4*(2), e227. https://doi.org/10.1038/mtna.2015.3

Spivak, A. M., Nell, R. A., Petersen, M., Martins, L., Sebahar, P., Looper, R. E., & Planelles, V. (2018). Synthetic Ingenols Maximize Protein Kinase C-Induced HIV-1 Latency Reversal. *Antimicrob Agents Chemother*, *62*(11). https://doi.org/10.1128/AAC.01361-18

Thorlund, K., Horwitz, M. S., Fife, B. T., Lester, R., & Cameron, D. W. (2017). Landscape review of current HIV 'kick and kill' cure research - some kicking, not enough killing. *BMC Infect Dis*, *17*(1), 595. https://doi.org/10.1186/s12879-017-2683-3

Tsai, P., Wu, G., Baker, C. E., Thayer, W. O., Spagnuolo, R. A., Sanchez, R., Barrett, S., Howell, B., Margolis, D., Hazuda, D. J., Archin, N. M., & Garcia, J. V. (2016). In vivo

analysis of the effect of panobinostat on cell-associated HIV RNA and DNA levels and latent HIV infection. *Retrovirology*, *13*(1), 36. https://doi.org/10.1186/s12977-016-0268-7

UNAIDS. (2023). *Global HIV & AIDS statistics — Fact sheet*. https://www.unaids.org/en/resources/fact-sheet

Ward, J., Davis, Z., DeHart, J., Zimmerman, E., Bosque, A., Brunetta, E., Mavilio, D., Planelles, V., & Barker, E. (2009). HIV-1 Vpr triggers natural killer cell-mediated lysis of infected cells through activation of the ATR-mediated DNA damage response. *PLoS Pathog*, *5*(10), e1000613. https://doi.org/10.1371/journal.ppat.1000613

Zhou, S., Jones, C., Mieczkowski, P., & Swanstrom, R. (2015). Primer ID Validates Template Sampling Depth and Greatly Reduces the Error Rate of Next-Generation Sequencing of HIV-1 Genomic RNA Populations. *J Virol*, *89*(16), 8540-8555. https://doi.org/10.1128/JVI.00522-15

Zhu, J., Gaiha, G. D., John, S. P., Pertel, T., Chin, C. R., Gao, G., Qu, H., Walker, B. D., Elledge, S. J., & Brass, A. L. (2012). Reactivation of latent HIV-1 by inhibition of BRD4. *Cell Rep*, *2*(4), 807-816. https://doi.org/10.1016/j.celrep.2012.09.008

CHAPTER 3

Defining the effects of PKC modulator HIV latency reversing agents on natural killer cells

ABSTRACT

The persistence of a long-lived reservoir of latently-infected cells remains a major obstacle to achieving a sterilizing HIV cure. Eradication of latent virus by a "kick and kill" strategy aims to reactivate proviral gene expression in latently infected cells and cause host cell death by HIV-induced killing or immune-mediated clearance. Previous studies have shown that administration of latency reversing agents (LRAs), such as protein kinase C (PKC) modulators, results in reduction of the rebound-competent HIV reservoir in small animal models of HIV persistence. Furthermore, administration of natural killer (NK) cells following LRA treatment improves this reservoir reduction. While the effect of PKC modulators on $CD4^+$ T cells has been well-characterized, their effect on NK cells remains unclear. Hence, it is currently unknown exactly why the combination of PKC modulator and NK cells is so potent, and whether exposure to PKC modulators may augment NK cell function in some way. In this study, we treated primary human NK cells with the PKC modulators bryostatin-1, prostratin, or the designed, synthesized bryostatin-1 analog SUW133, and characterized their effects compared to untreated cells. PKC modulators increased expression of proteins involved in NK cell activation. Transcriptomic profiles from PKC-treated NK cells displayed signatures of cellular activation and enrichment of genes associated with the NFκB pathway. Cytotoxicity was unaffected by prostratin, but significantly decreased by bryostatin and SUW133. Cytokines from PKC-stimulated NK cells did not induce latency reversal in J-Lat cell lines. These findings suggest that although PKC modulators have some significant effects on NK cells, their contribution in kick and kill strategies is likely due to upregulating HIV-expression in $CD4^+$ T cells, not enhancing the effector functions of NK cells. Hence, PKC modulators are primarily augmenting the "kick" rather than the "kill" arm of this HIV cure approach.

INTRODUCTION

Since the start of the HIV epidemic, more than 85 million people have been infected with HIV, and nearly half have died of AIDS-related illnesses (WHO, 2023b). Despite advances in the development of antiretroviral therapy (ART), HIV remains a significant cause of worldwide morbidity and mortality. ART often suppresses HIV to undetectable levels in the plasma; however, a subset of long-lived, latent memory $CD4^+$ T cells harboring integrated replication-competent provirus persists and can produce virus upon interruption of therapy, leading to viral rebound (Chun et al., 1995; Chun, Stuyver, et al., 1997; Finzi et al., 1997; Wong et al., 1997). Moreover, there are several limitations to lifelong ART, including cost, compliance, the development of drug-resistant viruses (Hirsch et al., 1998), and inadequate access to treatment, especially in more resource-limited countries (Orrell, 2005), which underscores the need to develop more effective therapeutic approaches beyond lifelong ART.

Significant progress has been made in the development of various cure strategies that target HIV. These approaches include bone marrow transplantation using CCR5-deficient cells (Allers et al., 2011; Hütter et al., 2009), gene-editing strategies that excise (Aubert et al., 2011; Ebina et al., 2013; Qu et al., 2013; Sarkar et al., 2007) or permanently inactivate latent provirus (Kessing et al., 2017), improvement of immune responses (Kumar et al., 2018; Macedo et al., 2019; Roberts et al., 1994; Stephenson, 2018; Stephenson & Barouch, 2016; Wykes & Lewin, 2018; Yang et al., 1997), and elimination of infected cells through other mechanisms (Campbell et al., 2018; Cummins et al., 2017; Lucas et al., 2010). One approach, known as the “kick and kill” strategy, focuses on eliminating or reducing the size of the latent reservoir through induction of, or “kicking,” latently infected cells with latency-reversing agents (LRAs) that stimulate expression of viral proteins, thereby allowing them to be targeted or “killed” by virus-induced cytopathic effects, immune

clearance, apoptosis, or antiviral therapies (Marsden & Zack, 2015, 2019). This treatment would be performed in the presence of ART to prevent HIV replication and further spread of infection. Several structural classes of LRAs belonging to distinct functional categories have been reported and have shown efficacy in reversing latency *in vitro*, *ex vivo,* and in animal models (Kim et al., 2018; Sadowski & Hashemi, 2019; Spivak & Planelles, 2018). One of the most promising classes of LRAs is the protein kinase C (PKC) modulators (Baxter et al., 2016; Beans et al., 2013; Bullen et al., 2014; Darcis et al., 2015; DeChristopher et al., 2012; Jiang et al., 2015; Kinter et al., 1990; Marsden et al., 2017; Pérez et al., 2010; Qatsha et al., 1993). PKC modulators activate and recruit the transcription factor NF-kappa B (NFκB), which binds to the HIV LTR to promote transcription (Williams et al., 2004). Previous reports have also shown that PKC modulators can affect NK cell functions, including activation, cytotoxicity, antibody-dependent cellular cytotoxicity (ADCC), and secretion of interferon-gamma (IFNγ), an important pro-inflammatory cytokine involved in the pathogenesis of HIV/AIDS (Chuang et al., 2003; Ito et al., 1988; Tassi et al., 2008). The PKC modulator prostratin (Supplemental Figure 3-1A), a non-tumorigenic phorbol ester derived from the bark of the Samoan medicinal plant *Homalanthus nutans*, has been shown to promote transcriptional activation of latent HIV provirus, as well as inhibit viral replication by down-regulating the HIV entry receptors CD4 and CXCR4 (Gulakowski et al., 1997; Korin et al., 2002; Kulkosky et al., 2001; Marsden et al., 2018). Purified NK cells showed enhanced killing of autologous $CD4^+$ T cells harboring reactivated HIV *in vitro* when both cell types were stimulated with prostratin (Desimio et al., 2018). Another PKC modulator, bryostatin-1 (Supplemental Figure 3-1B), a naturally occurring macrocyclic lactone derived from the marine invertebrate *Bugula neritina*, has also shown potency in reversing HIV latency and is the only PKC modulator that has been tested in clinical trials in ART-treated individuals (Gutierrez et al., 2016). However, results

from this study demonstrated that single administration of bryostatin-1 at the low doses tested induced neither PKC activation nor HIV transcription *in vivo*. Moreover, bryostatin-1 inhibited target cell lysis and ADCC function of NK cells (Desimio et al., 2018). These findings, combined with the issues of a narrow therapeutic window and limitations associated with natural sourcing (Schaufelberger et al., 1991), highlight the need for better latency-reversing compounds.

Recent practical syntheses of the natural PKC modulators prostratin and bryostatin-1 have enabled the creation of designed and synthetic PKC modulator analogs that exhibit superior efficacy and tolerability when compared to their parent compounds (Beans et al., 2013; Marsden et al., 2018; Sloane et al., 2020; Wender, Donnelly, et al., 2015; Wender et al., 2017; Wender et al., 2008; Wender, Quiroz, & Stevens, 2015). One notable bryostatin-1 analog, SUW133 (Supplemental Figure 3-1C), was shown to reverse HIV latency in cell lines and patient-derived cells (Marsden et al., 2018). Moreover, *in vivo* treatment with SUW133 prior to cessation of ART reduced barcoded HIV diversity, caused a delay in viral rebound, and reduced the number of rebounding viral lineages in a humanized mouse model of HIV latency, suggesting a reduction in the latent reservoir (Marsden et al., 2020). Significantly, a greater reduction in the rebound-competent HIV reservoir was observed in similar experiments in which NK cells were also injected into ART-suppressed animals following the administration of SUW133 (Kim et al., 2022). While SUW133 resulted in upregulation of several cytokines during *in vitro* stimulation of primary human peripheral blood mononuclear cells (PBMCs), these secreted factors did not directly induce HIV latency reversal (Moran et al., 2023), suggesting SUW133's effects in reversing latency are primarily mediated by a direct cellular response to the compound rather than indirect stimulation of latently infected cells via secreted factors and cytokines. These results demonstrate SUW133's potential as a compelling candidate in the pursuit of HIV eradication and that it warrants further

characterization of the molecular mechanisms underpinning its effects on kick and kill strategies.

Here, we sought to characterize the effects of PKC modulators, particularly SUW133, on human peripheral NK cells to identify why combining PKC modulators and NK cells is more potent in depleting latently infected cells than a single treatment alone and whether PKC modulators have a direct effect on NK cell function, which may explain this observation. We showed that while PKC modulators activate NK cells and modify their gene expression profile and phenotype, exposure to SUW133 did not enhance NK cell cytotoxic function. Additionally, consistent with previous findings in PBMCs, SUW133 led to increased secretion of cytokines by NK cells, but these secreted factors did not independently induce HIV latency reversal. Most importantly, through transcriptomic analysis, we report that the effects of PKC modulators were more robust in $CD4^+$ T cells than in NK cells. Together, these data suggest that the primary impact of PKC modulators, when used in combination with NK cells, lies in stimulating the induction of HIV expression (the kick arm) rather than enhancing the elimination of reactivated cells by improving NK cell cytotoxic activity (the kill arm) of this proposed approach.

RESULTS

NK Cells are Activated by PKC Modulators

To assess the effect of SUW133 on NK cell viability and degranulation, primary NK cells were isolated from healthy human donors and cultured for 24 hours in various concentrations of SUW133 (Supplemental Figure 3-2). In all conditions, the viability of NK cells was not significantly affected (Supplemental Figure 3-2A), thus we decided to use the 10nM concentration of SUW133, which was sufficient to show effects on degranulation (Supplemental Figure 3-2B) and has been previously shown to reverse HIV-1 latency *in vitro* (DeChristopher et al., 2012;

Marsden et al., 2017). For bryostatin-1 and prostratin, concentrations previously shown to reverse HIV-1 latency *in vitro* (Beans et al., 2013; Biancotto et al., 2004; Darcis et al., 2015; DeChristopher et al., 2012; Marsden et al., 2017; Trushin et al., 2005; Williams et al., 2004) were used. Primary NK cells were isolated from healthy human donors and cultured for 24 hours in the presence of PKC modulators. After 24 hours of culture, we evaluated NK cell viability, using the cell-surface expression of CD69 and NKG2D to assess the effects of PKC modulators on NK cell activation, and the cell-surface expression of CD107a to assess their effects on NK cell degranulation (Figure 3-1, Supplemental Figure 3-3). There was no significant difference in NK cell viability between the different LRA treatment groups and the control (Figure 3-1A). Consistent with prior work (Desimio et al., 2018), bryostatin-1 and prostratin increased the expression of CD69, NKG2D, and CD107a on NK cells compared to no treatment (DMSO only; Figure 3-1B-D). Similarly, treatment with SUW133 resulted in increased expression of all 3 markers (Figure 3-1B-D). Moreover, while there was variation between donors, there was no statistically significant difference in the level of expression of all 3 markers among the 3 PKC modulators. Overall, these results indicate that bryostatin-1, prostratin, and SUW133 induce activation and degranulation in NK cells.

PKC Modulators Induce Increased Secretion of IFNγ, MIP-1α, MIP-1β, and TNFα by NK Cells

Cytokine composition was analyzed in the supernatant from NK cells treated for 24 hours with PKC modulating LRAs. Consistent with previous studies in PBMCs (Marsden et al., 2018; Sloane et al., 2020), we observed variations in cytokine concentrations between the 3 conditions, with many cytokines displaying elevated levels compared to the control (Figure 3-2A). Of the 38 cytokines measured, pro-inflammatory cytokines IFNγ, MIP-1α, MIP-1β, and TNFα showed a

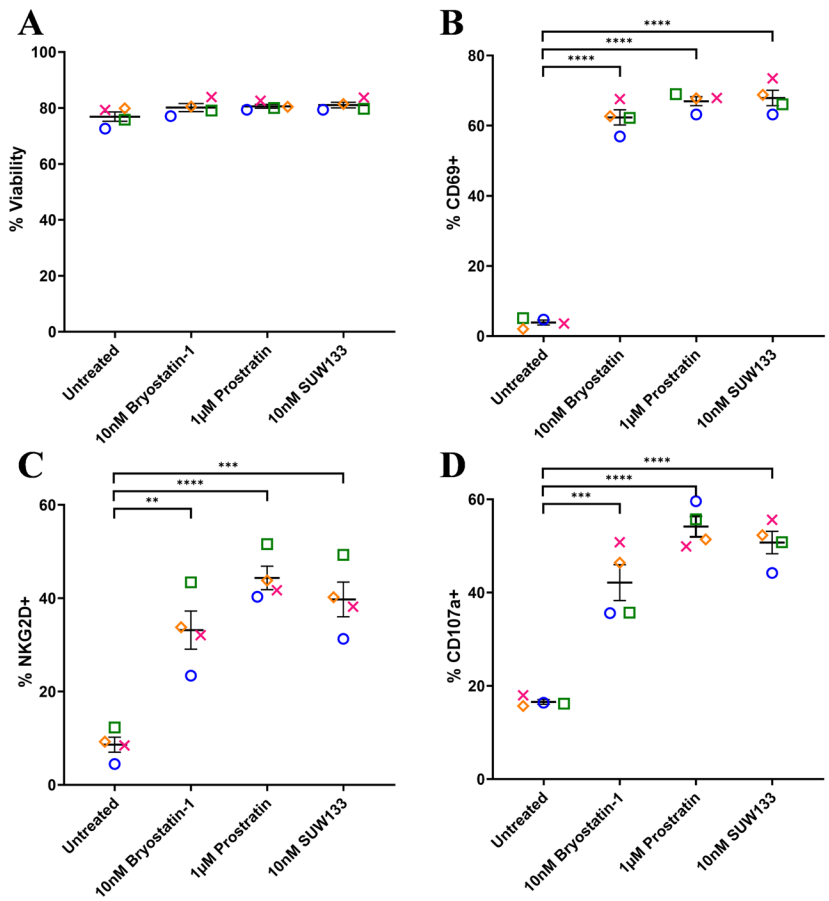

Figure 3-1. Viability and cell-surface expression of activation and degranulation markers on NK cells treated with PKC modulators. NK cells were cultured for 24 hours untreated (DMSO only), with 10nM bryostatin-1, 1μM prostratin, or 10nM SUW133 and analyzed for viability **(A)**, CD69 **(B)**, NKG2D **(C)**, and CD107a **(D)** via flow cytometry. Data from 4 healthy human donors are shown, with each color and shape representing results from a different donor. Horizontal lines indicate the mean. Error bars indicate the standard error of the mean (SEM). An unpaired, unequal variance Student's *t*-test was performed, with (***) indicating $p < 0.001$ and (****) indicating $p < 0.0001$.

significant increase in concentration compared to untreated cells (Figure 3-2B). IFNγ plays an important role in immune regulation and antiviral response by activating and recruiting cells and inhibiting viral replication (Boehm et al., 1997; Cobos Jimenez et al., 2012; Frucht et al., 2001; Harris et al., 2005; Koirala et al., 2008; Spellberg & Edwards, 2001). MIP-1α and MIP-1β are involved in the development and recruitment of T_H1 cells (Aliberti et al., 2000; Karpus et al., 1997; Zou et al., 2000). These cytokines can also suppress HIV infection by blocking and downregulating cell-surface expression of CCR5 (Alkhatib et al., 1997; Berger et al., 1999; Cocchi et al., 1995;

Pierson & Doms, 2003), which is used as a co-receptor for entry by R5 tropic strains of HIV-1 (Choe et al., 1996; Deng et al., 1996; Doranz et al., 1996; Dragic et al., 1996). TNFα is a pleiotropic cytokine that can both stimulate and inhibit HIV replication. It has been shown to activate NFκB and induce HIV transcription (Duh et al., 1989; Folks et al., 1989; Griffin et al., 1989; Mellors et al., 1991; Michihiko et al., 1989; Osborn et al., 1989). However, it can also stimulate the secretion of cytokines that suppress HIV (Cocchi et al., 1995; Coffey et al., 1997; McManus et al., 1998; Simmons et al., 1997). Thus, the secretion of these cytokines by NK cells may play an important role in the immune response against HIV following latency reversal.

NK and CD4$^+$ T Cells Treated with PKC Modulators Show Distinct Gene Expression Profiles

To define the molecular mechanisms underlying the effects of PKC modulators on NK and CD4$^+$

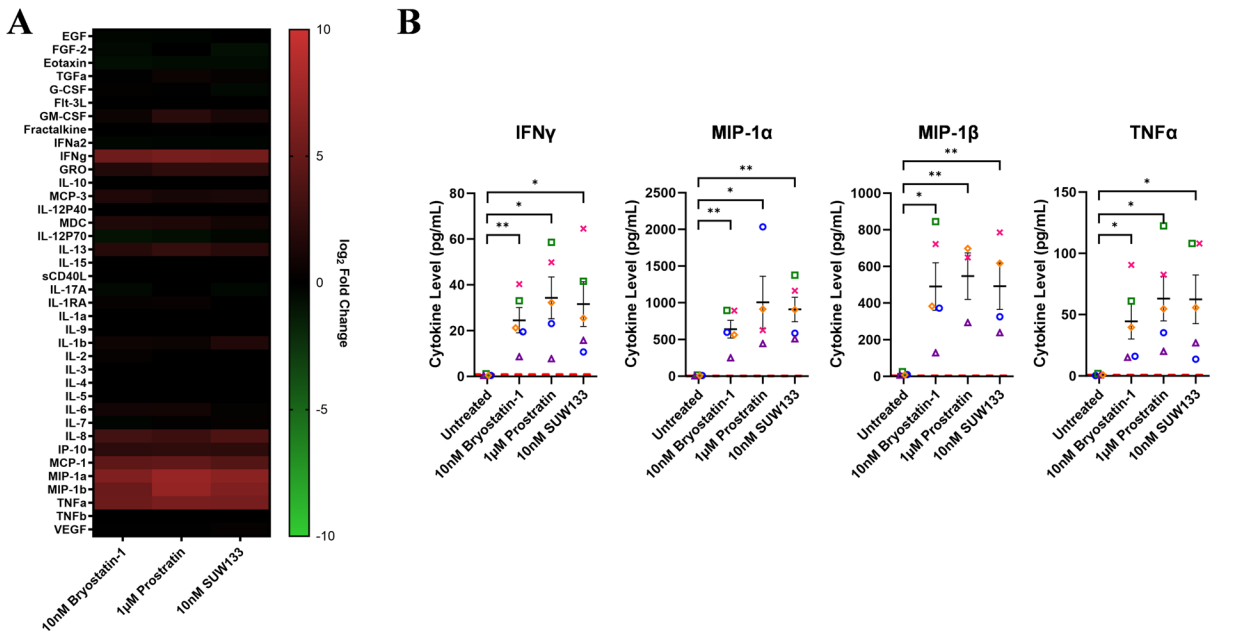

Figure 3-2. Cytokine induction in NK cells by PKC modulators. Supernatant from NK cells treated with 10nM bryostatin-1, 1μM prostratin, or 10nM SUW133 was filtered and analyzed using a Luminex 38-plex human cytokine immunoassay for cytokine composition. **(A)** Heatmap showing the mean fold change relative to the untreated (DMSO only) control from 5 different biological donors. **(B)** Example cytokine profiles from data shown in panel A, with each color and shape representing results from a different human donor (n=5). Horizontal lines indicate the mean. Error bars indicate the standard error of the mean (SEM). Dashed red lines indicate the lower limit of detection for the assay, which varies between different cytokines. A 2-tailed, unpaired, unequal variance Student's *t*-test was performed, with (*) indicating $p < 0.05$ and (**) indicating $p < 0.01$.

T cells, we performed RNA sequencing (RNA-seq) on LRA-stimulated and untreated cells. The transcriptomic profiles revealed distinct clustering by principal component analysis (PCA) between each condition within both cell types (Figure 3-3A), indicating unique gene changes induced by bryostatin-1, prostratin, SUW133, and the unstimulated control. Moreover, based on PCA clustering, all conditions for NK cells are more similar to each other than to $CD4^+$ T cells and vice versa. Based on the relative distance to the controls, each cell type exhibited the same hierarchy in magnitude of transcriptomic changes between conditions, with prostratin having the greatest effect, followed by SUW133, then bryostatin-1. This was confirmed by comparing the number of differentially expressed genes (DEGs) induced by each PKC modulator (Figure 3-3B).

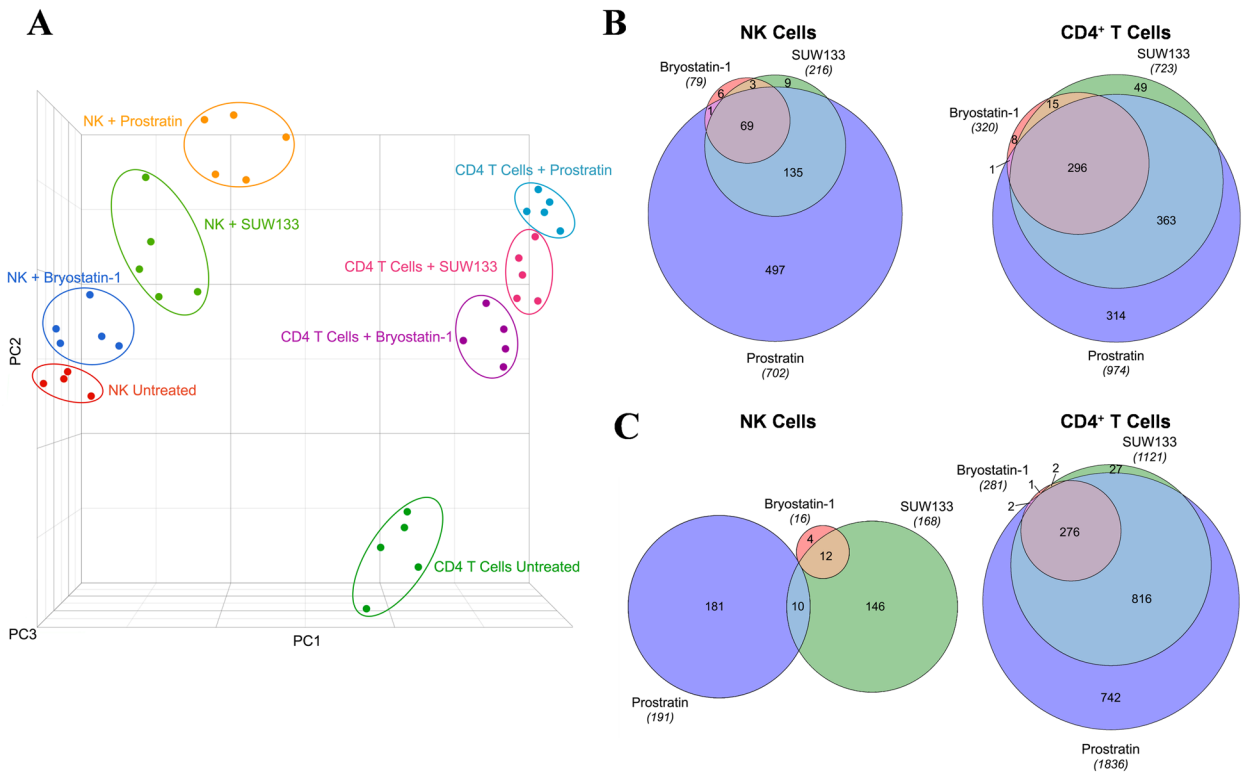

Figure 3-3. Transcriptomic profiles of NK and $CD4^+$ T cells treated with PKC modulators. RNA-seq was performed on NK and $CD4^+$ T cells cultured for 24 hours untreated (DMSO only), with 10nM bryostatin-1, 1μM prostratin, or 10nM SUW133. **(A)** Principal component analysis (PCA) plot of data from 5 healthy human donors is shown, with each point representing results from a different donor and each color representing a different treatment group. Venn diagram illustrating the overlap of upregulated **(B)** and downregulated **(C)** genes between the 3 different PKC modulators in NK and $CD4^+$ T cells. Areas shown are proportional to the numbers of genes within each category.

DEGs were defined as having false discovery rate (FDR) corrected *p*-values (*q*-values) < 0.01 and $|\log_2 FC| > 2$. Prostratin had the greatest number of both up- and down-regulated genes, followed by SUW133, and then bryostatin-1.

Volcano plots were generated (Figure 3-4A and C, Supplemental Figure 3-4A and C, Supplemental Figure 3-5A and C), and based on these data, we identified the top 15 DEGs for each PKC modulator in both NK (Figure 3-4B, Supplemental Figure 3-4B, Supplemental Figure 3-5B) and $CD4^+$ T cells (Figure 3-4D, Supplemental Figure 3-4D, Supplemental Figure 3-5D), the majority of which were upregulated. Amongst the top 15 DEGs, only 2 (*RSG1* and *RSG16*) were shared between all 3 PKC modulators in NK cells, while 10 (*DUSP4, EGR1, EGR2, NPBWR1, NR4A1, PHLDA1, RGS16, SPRED2, SPRY4, ZBED2*) were common to all 3 conditions in $CD4^+$ T cells, suggesting that the effects of these drugs are more conserved in $CD4^+$ T cells than in NK cells. *RSG16* was the only transcript upregulated by all PKC modulators in both cell types. *RSG16* inhibits G protein-coupled receptor signaling as well as cancer and inflammatory diseases through various other signaling pathways (Berthebaud et al., 2005; Johnson et al., 2003; Liang et al., 2009). The magnitude of fold change for the top DEGs in all PKC treatment groups was lower in NK cells compared to $CD4^+$ T cells, implying that treatment with PKC modulators more robustly perturbs the transcriptome of $CD4^+$ T cells than NK cells. Additionally, similar to the ordinal ranking between each PKC treatment group in the number of DEGs, we saw that cells treated with prostratin had the highest magnitude fold change for gene expression, followed by SUW133, then bryostatin-1. Enrichment analysis of transcription factors using the transcriptional regulatory relationships unraveled by the sentence-based text-mining (TRRUST) database revealed several transcription factors responsible for the regulation of the observed phenotype (Supplemental Figure 3-6). PKC agonists are believed

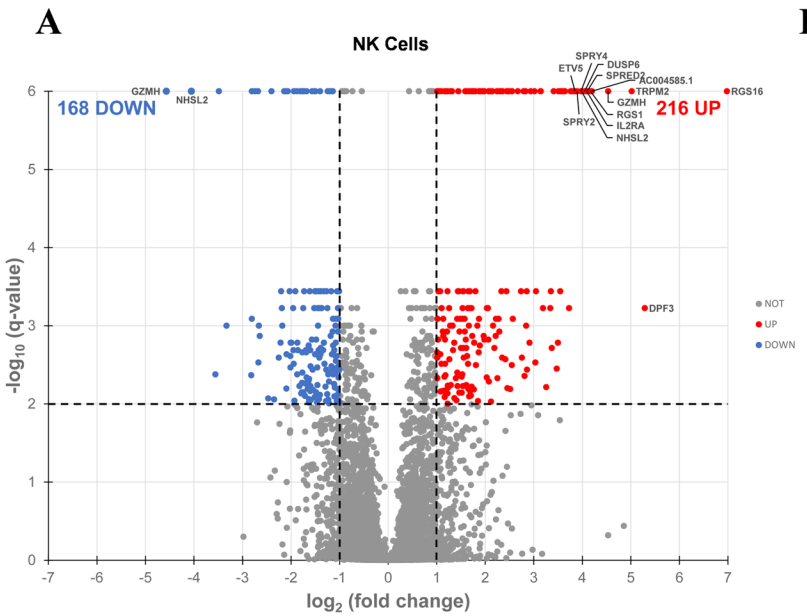

B

NK Cells

Gene	Fold change	Log_2 (FC)	Log_{10} (q-value)	Change trend
RGS16	126.098	6.9784	6.0000	UP
DPF3	39.038	5.2868	3.2255	UP
TRPM2	32.373	5.0167	6.0000	UP
GZMH	0.042	-4.5713	6.0000	DOWN
AC004585.1	23.156	4.5333	6.0000	UP
RGS1	18.342	4.1971	6.0000	UP
SPRED2	17.975	4.1679	6.0000	UP
IL2RA	17.164	4.1013	6.0000	UP
DUSP6	17.003	4.0877	6.0000	UP
NHSL2	0.06	-4.0562	6.0000	DOWN
SPRY4	16.539	4.0478	6.0000	UP
SPRY2	15.825	3.9841	6.0000	UP
ETV5	15.718	3.9743	6.0000	UP
DUSP5	14.844	3.8918	6.0000	UP
KIR3DX1	14.427	3.8507	6.0000	UP

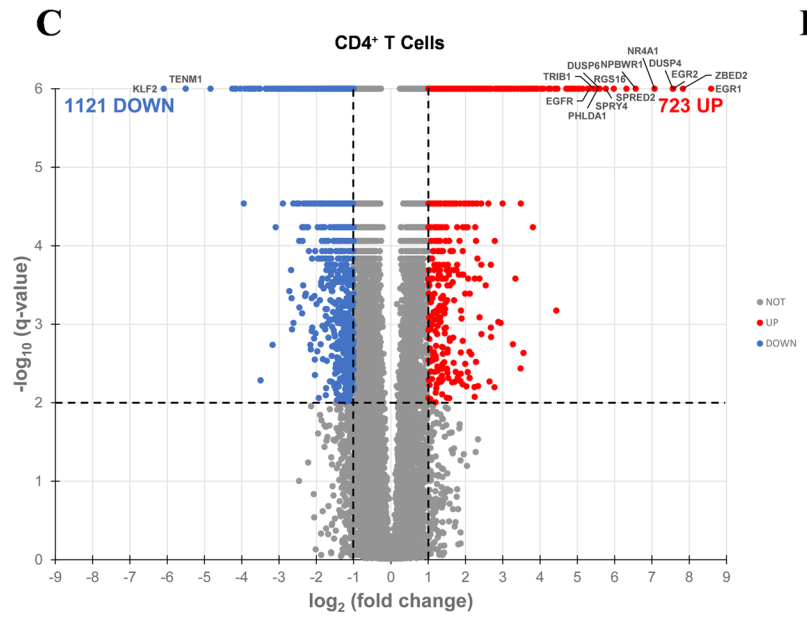

D

CD4⁺ T Cells

Gene	Fold change	Log_2 (FC)	Log_{10} (q-value)	Change trend
EGR1	384.543	8.587	6.0000	UP
ZBED2	227.433	7.8293	6.0000	UP
EGR2	190.085	7.5705	6.0000	UP
DUSP4	188.55	7.5588	6.0000	UP
NR4A1	134.364	7.07	6.0000	UP
NPBWR1	94.563	6.5632	6.0000	UP
SPRED2	79.694	6.3164	6.0000	UP
KLF2	0.015	-6.0913	6.0000	DOWN
RGS16	63.084	5.9792	6.0000	UP
SPRY4	54.395	5.7654	6.0000	UP
DUSP6	48.412	5.5973	6.0000	UP
PHLDA1	46.844	5.5498	6.0000	UP
TENM1	0.022	-5.5063	6.0000	DOWN
TRIB1	43.565	5.4451	6.0000	UP
EGFR	40.105	5.3257	6.0000	UP

Figure 3-4. Differentially expressed genes induced by SUW133 in NK and CD4$^+$ T cells. RNA-seq was performed on NK and CD4$^+$ T cells cultured for 24 hours untreated (DMSO only) or with 10nM SUW133. Volcano plot of the distribution of all differentially expressed genes in NK cells **(A)** and CD4$^+$ T cells **(C)**. The red and blue dots represent the upregulated and downregulated genes (q-value < 0.01 and $|\log_2 FC| > 2$), respectively. The 15 most differentially expressed genes are labeled on each plot and shown in tables **(B)** & **(D)**.

to induce latent HIV expression through NFκB signaling (Kinter et al., 1990; Laurence et al., 1990; Pätzold et al., 1993; Steffan et al., 1995; Tong-Starkesen et al., 1989). Consistent with this, NFκB family transcription factors *NFKB1* and *RELA* were within the top 3 enriched transcription factors

for all 3 PKC modulators in both NK and $CD4^+$ T cells. Other transcription factors known to bind to the HIV-1 LTR promotor, such as *ETS1* and *SP1,* were also enriched.

Bryostatin-1 Inhibits NK Cell Cytotoxic Activity

Previous research examining the impact of PKC modulators on NK cell cytotoxicity suggested that exposure to prostratin increased NK cell-mediated killing, whereas it was diminished following exposure to bryostatin-1 (Desimio et al., 2018; Garrido et al., 2016). To further explore the functional effect of PKC modulators on NK cells and compare them with the effects of SUW133, we cultured NK cells for 24 hours in either bryostatin-1, prostratin, or SUW133 in parallel with untreated cells, then incubated in a 4-hour lysis assay with K562 cells, a human leukemia cell line that lacks HLA-antigen expression (Robertson et al., 1996), at various effector-to-target (E:T) ratios (Figure 3-5). Confirming and extending the previously published findings, our results showed that pre-treatment of NK cells with bryostatin-1 consistently inhibited NK cell cytotoxicity while prostratin tended to enhance NK cell cytotoxic function, though the effects of prostratin were not statistically significant. SUW133, like bryostatin-1, decreased NK cell cytotoxicity, but this finding was only statistically significant at the highest tested E:T ratio (Figure

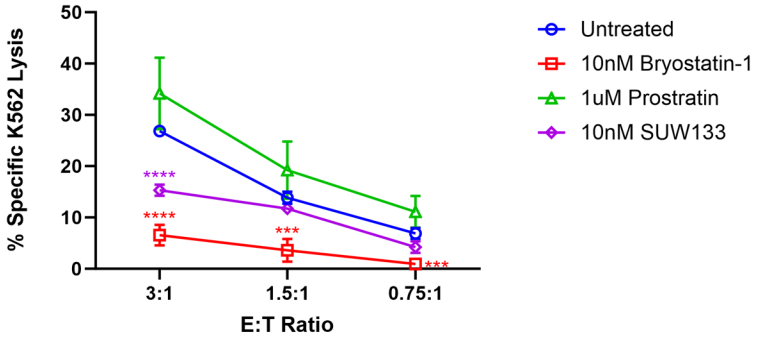

Figure 3-5. Impact of PKC modulators on NK cell cytotoxicity. NK cells were cultured for 24 hours untreated (DMSO only), with 10nM bryostatin-1, 1μM prostratin, or 10nM SUW133 and tested for cytotoxicity against K562 cells at the indicated effector-to target (E:T) ratios. The mean percentage specific lysis from 5 independent biological replicates was measured. Error bars indicate the standard error of the mean (SEM). An unpaired, unequal variance Student's *t*-test was performed, with (***) indicating $p < 0.001$ and (****) indicating $p < 0.0001$.

3-5). Because HIV infection results in changes that NK cells can recognize (Desimio et al., 2018; Garrido et al., 2016), a similar experiment was conducted using HIV-infected $CD4^+$ T cells, wherein NK cells were pre-treated for 24 hours in either bryostatin-1, prostratin, or SUW133 in parallel with untreated cells, then incubated in a 4-hour lysis assay with HIV-infected $CD4^+$ T cells at an E:T ratio of 1:1 (Supplemental Figure 3-7). We observed statistically indistinguishable frequencies of total HIV-expressing (HA^+) cells (Supplemental Figure 3-7A) and no difference in NK cell cytotoxicity between the untreated control and any of the PKC modulators (Supplemental Figure 3-7B). These data suggest that, although treatment of NK cells with PKC modulators resulted in increased expression of activation and degranulation markers, this did not result in increased killing by NK cells.

Cytokines Released by NK Cells Treated with SUW133 Do Not Independently Reverse Latency in J-Lat Cell Lines

Cytokines such as IL-2, IL-7, and TNFα, as well as certain combinations of cytokines, have been shown to induce HIV latency reversal (Chun et al., 1998; Chun, Engel, et al., 1999; Rabbi et al., 1998; Scripture-Adams et al., 2002). To assess whether cytokines produced by SUW133-stimulated NK cells could independently induce the expression of HIV in the absence of LRAs, NK cells were treated for 5 hours with SUW133, after which the LRA was removed, then the cells were washed and cultured in fresh media for an additional 24 hours to allow for the accumulation of cytokines. After 24 hours, LRA-free, cell-free supernatant, or conditioned media (CM), from stimulated cells was collected and analyzed for cytokine composition. Again, we observed higher levels of several cytokines compared to the control (Figure 3-6A), including MIP-1α and MIP-1β, though the measured concentrations (Figure 3-6B) were much lower than those seen with direct stimulation (Figure 3-2B), likely due to early removal of the compound.

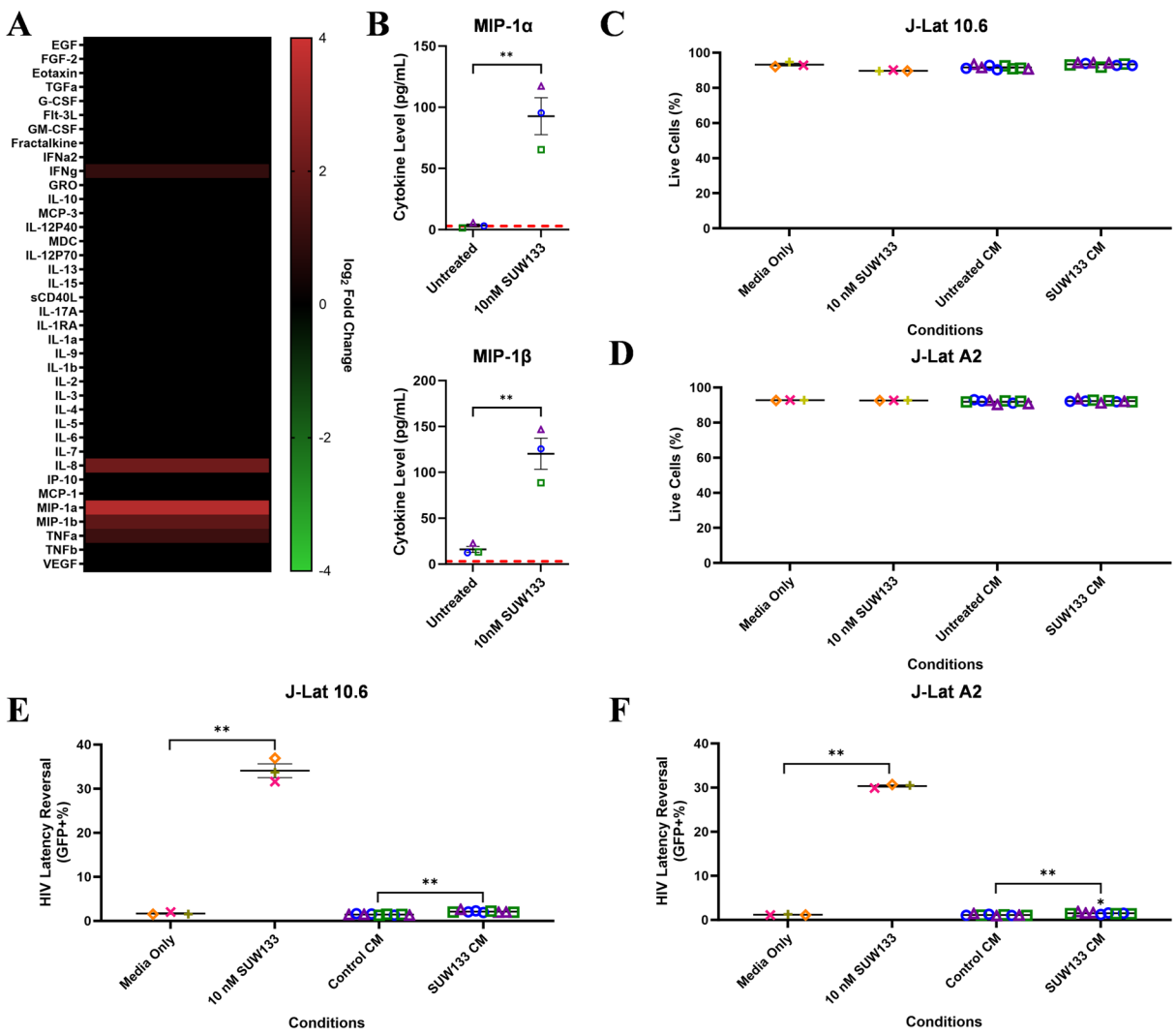

Figure 3-6. Evaluation of secreted factors from NK cells treated with SUW133 and their effect on latency reversal in select J-Lat clones. Conditioned media (CM) generated with NK cells from 3 different healthy human donors were analyzed using a Luminex 38-plex human cytokine immunoassay. **(A)** Heatmap showing the mean fold change relative to the untreated (DMSO only) control**. (B)** Example cytokine profiles from data shown in panel A, with each color and shape representing results from a different human donor. **(C - F)** Jurkat-Latency (J-Lat) clones (10.6 and A2) were treated with direct LRA or CM for 48 hours and assessed for viability **(C, D)** and GFP+ expression **(E, F)**. All control conditions (media only and direct stimulations) were technical singlets in 3 independent biological replicates, resulting in an n = 3; For CM samples, technical triplicates in 3 independent biological replicates per donor (3 donors each) resulted in n = 9. A 2-tailed, unpaired, unequal variance Student's *t*-test was performed, with (*) indicating $p < 0.01$ and (**) indicating $p < 0.001$. The single asterisk above the 10nM SUW133 CM condition in panel D corresponds to a comparison with direct stimulation with media only.

Indirect latency reversal by CM was measured *in vitro* as previously described (Moran et al., 2023). Briefly, select J-Lat clones were stimulated either directly with an LRA or with CM for 48 hours, then evaluated for viability and the expression of HIV via flow cytometry. J-Lat 10.6 cells contain

a near-full-length HIV genome, while J-Lat A2 cells lack most HIV genes except the regulatory protein Tat, which enhances viral transcription (Jordan et al., 2003; Jordan et al., 2001). Both J-Lat clones contain a GFP reporter gene, which allows for the measurement of HIV expression. There was no significant difference in viability for either J-Lat clone between the different treatment groups and the control (Figure 3-6C and D). Consistent with previous studies (Darcis et al., 2015; Marsden et al., 2018; Mehla et al., 2010; Sloane et al., 2020), we observed an increase in latency reversal when cells were directly stimulated with SUW133 compared to control (Figures 3-6E and F). Additionally, similar to what was observed with CM from LRA-stimulated PBMCs (Marsden et al., 2018), there was little to no observed latency reversal by any of the CM samples in either latently infected cell line. However, there was a small (less than 1%) but statistically significant increase in GFP expression between the SUW133-treated CM compared to media only in J-Lat A2 cells, as well as between SUW133-treated CM and untreated CM in both J-Lat cell lines. This small (<1%) difference is unlikely to be biologically relevant and does not account for the robust LRA activity observed upon direct compound stimulation. Together, our findings suggest that the cytokines generated by NK cells stimulated with SUW133 do not independently stimulate latency reversal.

DISCUSSION

Natural PKC modulators, such as bryostatin-1 and prostratin, can induce HIV transcription in latently infected cells (Gutierrez et al., 2016; Korin et al., 2002; Kulkosky et al., 2001; Mehla et al., 2010; Pérez et al., 2010; Williams et al., 2004) and are under investigation as therapeutic agents against other diseases, including cancer (He et al., 2022; Kortmansky & Schwartz, 2003), Alzheimer's disease (Sun & Alkon, 2012; Talman et al., 2016; Tian et al., 2023), and multiple

sclerosis (Abramson et al., 2021). The scaled laboratory synthesis of bryostatin-1, now converted to a GMP synthesis, led to the production of synthetic bryostatin-1 analogs, some of which are more potent and less toxic than the parent compound (Beans et al., 2013; Marsden et al., 2018; Sloane et al., 2020; Wender, Donnelly, et al., 2015; Wender et al., 2017; Wender et al., 2008; Wender, Quiroz, & Stevens, 2015). One notable bryostatin-1 analog, SUW133, has been shown to successfully deplete latently infected cells and delay viral rebound in humanized mouse models (Marsden et al., 2018). Additionally and significantly, when combined with a kill agent (NK cells), SUW133 resulted in an even greater reduction in reservoir size and further delay in viral rebound (Kim et al., 2022). While its direct effect on $CD4^+$ T cells has been studied, it was not known whether SUW133 has any effect on NK cells.

In this study, we characterized the effect of SUW133 on primary human NK cells, in comparison to the classic PKC modulators bryostatin-1 and prostratin to determine whether it would result in increased NK function that may explain the previously observed results. We found that SUW133 induced increased CD69 and NKG2D expression, as well as increased CD107a expression, on NK cells, suggesting increased cellular activation and degranulation, respectively (Figure 3-1). Furthermore, the observed level of induction of these markers by SUW133 was similar to that induced by bryostatin-1 and prostratin, and there was no observed difference in viability between the different PKC treatment groups (Figure 3-1). Similarly, treatment of NK cells with SUW133 resulted in increased secretion of several pro-inflammatory cytokines, including IFNγ, MIP-1α, MIP-1β, and TNFα, at levels comparable to that of bryostatin-1 and prostratin (Figure 3-2). When comparing global transcriptomic changes induced by these PKC modulators on NK cells and $CD4^+$ T cells, we observed distinct gene expression profiles (Figure 3-3A). All treatment groups had a greater effect in $CD4^+$ T cells compared to NK cells, as evidenced by the quantity and magnitude

of differentially expressed genes (Figure 3-3B, Figure 3-4, Supplemental Figure 3-4 and Supplemental Figure 3-5). The top 15 most differentially expressed genes in $CD4^+$ T cells were more consistent amongst the 3 PKC modulators compared to NK cells, indicating a more conserved effect (Figure 3-4B and D, Supplemental Figure 3-4B and D, Supplemental Figure 3-5B and D). Consistent with prior studies (Kinter et al., 1990; Laurence et al., 1990; Pätzold et al., 1993; Steffan et al., 1995; Tong-Starkesen et al., 1989), transcription factor enrichment analysis showed that all PKC modulators resulted in responses consistent with enrichment for NFκB activity in both NK cells and $CD4^+$ T cells (Supplemental Figure 3-6). When pre-treated with PKC modulators, then co-cultured with K562 target cells, NK cells exhibited different levels of cytotoxicity. At the tested concentrations and effector-to-target ratios, SUW133 and prostratin had fairly modest effects on NK cell cytotoxicity, while bryostatin-1 consistently inhibited killing (Figure 3-5). Moreover, when PKC modulator-treated NK cells were co-cultured with acutely infected HIV-infected $CD4^+$ T cells, there was no observed difference in cytotoxicity (Supplemental Figure 3-7), further underscoring the fact that PKC modulators have limited effects on NK cell killing ability. To test whether NK cells had an indirect effect on latency reversal after PKC modulator stimulation, NK cells were exposed to SUW133, then the LRA was removed, and after further incubation, the conditioned media was harvested, profiled for cytokine composition, and tested for its capacity to induce latency reversal in cell lines. Although the CM containing secreted factors from SUW133-stimulated NK cells had elevated concentrations of various cytokines, little-to-no latency reversal was observed in both J-Lat 10.6 and A2 cells (Figure 3-6). It is important to note that although this study examines the direct effect of PKC modulators on NK cell cytotoxic function, we did not examine the effect that PKC modulators may have on other immune cells, such as dendritic cells, macrophages, and $CD8^+$ T cells, which may affect NK cells

indirectly. However, it has been shown previously that PBMCs stimulated with PKC modulators do not indirectly cause HIV latency reversal via cytokine expression (Moran et al., 2023). Overall, our results, combined with our previous findings (Kim et al., 2022; Marsden et al., 2017; Marsden et al., 2020), suggest that the effects of PKC modulators on the eradication of the viral reservoir in the kick and kill approach is primarily due to increased provirus expression by $CD4^+$ T cells, rather than an enhancement of NK cell effector function.

We suspect that the duration of NK cell exposure to the LRAs plays an important role in their cytotoxic function. In the previous *in vivo* humanized mouse study (Kim et al., 2022), we observed NK cells helped to decrease the viral reservoir when the initial injection of NK cells occurred 8 hours and 5 days after SUW133 exposure. Due to the short blood half-life and rapid absorption of PKC modulators *in vivo* (Kraft et al., 1996; Zhang et al., 1996), it is likely that the NK cells had limited exposure to the LRA. All experiments performed in the current study were performed under prolonged exposure to LRAs (5-24 hours), yet only minor effects on NK function were observed, further supporting the interpretation that PKC modulators primarily augment the "kick" rather than the NK-mediated "kill" arm of this therapeutic approach.

An additional consideration is that the majority of experiments described here were performed in the absence of HIV infection and thus do not account for the possible contribution of the virus in augmenting the relationship between LRA-stimulated $CD4^+$ T cells and NK cells in kick and kill approaches. For example, previous work has shown that the HIV accessory protein Vpr synergizes with prostratin to improve NK cell-mediated clearance of recently reactivated HIV-infected cells (Desimio et al., 2018). Expression of ULBP2, an NKG2D ligand, was increased on $CD4^+$ T cells by both prostratin and HIV alone and further enhanced in combination, leading to sensitization of

these cells to NK cell cytotoxicity (Desimio et al., 2018). While our transcriptomics data on uninfected cells also showed a modest increase in *ULBP2* by all PKC modulators (fold change = 1.294 for bryostatin-1, 1.335 for prostratin, and 1.486 by SUW133), this effect likely did not contribute to the observed enhancement of viral clearance by SUW133 + NK cells *in vivo*, as the virus used for infection, NL-HABC, lacks a functional Vpr protein (Marsden et al., 2020). Consistent with this hypothesis, we did not observe any difference in NK cell cytotoxicity when NK cells were pre-treated with PKC modulators and co-cultured with NL-HABC-infected $CD4^+$ T cells (Supplemental Figure 3-7). Understanding the dynamics of other activating and inhibitory receptors induced by PKC modulators on both NK cells and Vpr-encoding HIV-infected $CD4^+$ T cells requires further investigation. Furthermore, the effects observed in this study are based on *in vitro* assays, which may not accurately recapitulate what occurs in a clinical setting. Further *in vitro* evaluation of the efficacy of this kick and kill approach as a potential therapeutic strategy would involve related studies on cells from HIV-positive individuals.

Overall, this study improves our understanding of how PKC modulators affect NK cells in kick and kill strategies, indicating that their primary effects are related to augmenting the kick rather than kill arm of this therapeutic approach. Results from this study can be used to inform and optimize future HIV cure strategies as well as treatments for other diseases in which PKC modulators are employed.

METHODS

Isolation of NK and $CD4^+$ T Cells

De-identified PBMCs from healthy, HIV seronegative human donors were obtained with informed consent from the UCLA AIDS Institute Virology Core Laboratory under IRB approval. Prior to

cell isolation, adherent macrophages were removed from PBMCs by culturing in flasks overnight in R10 media (RPMI 1640 medium supplemented with 10% vol/vol fetal bovine serum [FBS, Omega Scientific] and 1% penicillin/streptomycin [Invitrogen]). Primary NK and resting $CD4^+$ T cells were isolated from PBMCs by negative selection using the NK Isolation Kit (Miltenyi Biotec) and EasySep Human Resting $CD4^+$ T Cell Isolation Kit (STEMCELL Technologies), respectively, according to the manufacturers' protocols. Purity of isolated NK cells was evaluated by staining with Ghost Violet 510 (Tonbo Biosciences); CD3-Alexa Fluor 700 (A700, clone HIT3a, BioLegend); CD4-Allophycocyanin-Cyanine7 (APC-Cy7, clone OKT4, BioLegend); CD8-Peridinin-Chlorophyll-Protein-Cyanine5.5 (PerCP-Cy5.5, clone RPA-T8, BioLegend); CD14-Phycoerythrin (PE, clone M5E2, BioLegend); CD19-PE-Cy7 (clone HIB19, BioLegend); CD45-Pacific Blue (PB, clone HI30, BioLegend); CD56-APC (clone 5.1H11, BioLegend); and CD69-Fluorescein (FITC, clone FN50, BioLegend). Resting $CD4^+$ T cells were assessed for purity by staining with Ghost Violet 510 (Tonbo Biosciences); CD3-A700 (clone HIT3a, BioLegend); CD4-APC-Cy7 (clone OKT4, BioLegend); CD8-PerCP-Cy5.5 (clone RPA-T8, BioLegend); CD14-PE (clone M5E2, BioLegend); CD25-APC (clone M-A251, BioLegend); CD45-PB (clone HI30, BioLegend); CD69-FITC (clone FN50, BioLegend); and HLA-DR-PE-Cy7 (clone LN3, BioLegend). Data was collected on an LSR Fortessa flow cytometer (BD Biosciences) and analyzed with FlowJo software (version 10.8.1 or later). Purified NK and resting $CD4^+$ T cells were frozen at a concentration of $5x10^6$ cells/mL in Bambanker (GC Lymphotec) and stored in liquid nitrogen prior to use.

Assessment of NK Cell Activation by Flow Cytometry

NK cells were thawed and cultured overnight in C10 media consisting of RPMI 1640 media supplemented with 10% vol/vol FBS (Omega Scientific), 1% L-glutamine, 1%

penicillin/streptomycin (Invitrogen), 500mM 2-mercaptoethanol (Sigma), 1mM sodium pyruvate (Gibco), 0.1mM MEM non-essential amino acids (Gibco), and 10mM HEPES (Gibco). NK cells were then cultured in C10 media containing 10nM bryostatin-1, 1μM prostratin, or 10nM SUW133 for 24 hours at 37°C and 5% CO_2. Unstimulated cells (DMSO only) were cultured in parallel throughout LRA stimulations in C10 medium. To stain for CD107a (LAMP-1), cell cultures were supplemented with CD107a-APC mAb (clone H4A3, BioLegend) 1 hour after the addition of the compound, then 1X Protein Transport Inhibitor Cocktail (eBioscience) was added and cells were cultured for an additional 23 hours. Cells were then washed twice with phosphate buffered saline (PBS) and resuspended in a 1:1000 dilution of Ghost Violet 510 (Tonbo Biosciences) in PBS at 4°C for 30 minutes. Cells were washed with PBS + 2% FBS and then resuspended in a 1:1 dilution of PBS:Human AB serum (Sigma). To label cell-surface molecules, the following fluorescent conjugated antibodies were then added: CD3-A700 (clone HIT3a, BioLegend); CD4-APC-Cy7 (clone OKT4, BioLegend); CD56-PB (clone 5.1H11, BioLegend); CD69-FITC (clone FN50, BioLegend); and NKG2D-PECy7 (clone 1D11, BioLegend). During staining, cells were incubated at 4°C for 30 minutes, then washed with PBS + 2% FBS. Cells were fixed in 1% paraformaldehyde at room temperature for 20 minutes, then washed and resuspended in PBS + 2% FBS and stored at 4°C until collection. Data was collected on an LSR Fortessa flow cytometer (BD Biosciences) and analyzed with FlowJo software (version 10.8.1 or later). Statistical analyses were performed using GraphPad Prism (version 9.4.1 or later).

Quantification of Secreted Cytokines

Supernatant samples from LRA-stimulated cells were analyzed by the UCLA Immune Assessment Core using the Luminex 38-plex Human Cytokine/Chemokine panel. For the purpose of statistical analysis, undetectable values were reported as the mean between 0 and the quantification limit,

which varies by cytokine. Statistical analyses were performed using GraphPad Prism (version 9.4.1 or later).

RNA Isolation and Sequencing

Frozen NK and $CD4^+$ T cell pellets were submitted to the UCLA Technology Center for Genomics and Bioinformatics (TCGB) for RNA extraction and sequencing. RNA was extracted using an RNeasy mini kit (QIAGEN). Libraries for RNA-seq were prepared with a KAPA mRNA HyperPrep Kit. The workflow consists of the depletion of rRNA by hybridization of complementary DNA oligonucleotides, followed by treatment with RNase H and DNase. The next steps include mRNA enrichment and fragmentation, first-strand cDNA synthesis using random priming followed by second-strand synthesis converting cDNA:RNA hybrid to double-stranded cDNA (dscDNA), and incorporating dUTP into the second cDNA strand. Next, cDNA generation is followed by end repair to generate blunt ends, A-tailing, adaptor ligation, and PCR amplification. Different adaptors were used for multiplexing samples in one lane. Sequencing was performed on Illumina NovaSeq6000 for a paired-end 2x50 run. A data quality check was done on Illumina SAV. Demultiplexing was performed with Illumina Bcl2fastq v2.19.1.403 software. The reads were mapped by STAR 2.7.9a (Dobin et al., 2013), and read counts per gene were quantified using the human genome GRCh38.104. In Partek Flow (*Partek® Flow® software*, 2019), read counts were normalized by CPM +1.0E-4 to generate PCA plots. For transcriptomic analysis, gene expression data were quantified as gene transcripts per million mapped reads (TPM), with values floored at 1 TPM (to suppress spurious variability) and $\log_2$ transformed (to stabilize variance) for statistical analysis of differential expression using a standard linear statistical model (base R lm procedure) to quantify the magnitude of differential gene expression across conditions. Venn diagrams were generated using BioVenn (Hulsen et al., 2008). Transcription factor enrichment

analysis was performed using Metascape (Zhou et al., 2019).

NK Cell Cytotoxicity Assays

For the K562 co-culture assays, previously frozen NK cells were thawed and cultured overnight in C10 media, then stimulated with C10 media containing LRA for 24 hours at 37°C and 5% CO_2. Unstimulated cells (DMSO only) were cultured in parallel in C10 medium. Wells containing only NK cells, only K562 cells, or K562 cells treated with 0.1% Tween 20 served as assay controls. NK cells were labeled with 200nM 5,6-carboxyfluroscein diacetatesuccinimidyl ester (CFSE, eBioscience) for 15 minutes at 37°C, washed twice, then seeded with 25,000 K562 cells at different effect-to-target (E:T) ratios for 4 hours at 37°C and 5% CO_2. The co-cultured cells were then labeled with 20 µg/mL 7-aminoactinomycin D (7-AAD, Invitrogen) for 20 minutes at room temperature, washed and fixed in 1% paraformaldehyde at room temperature for 20 minutes, then washed and resuspended in PBS + 2% FBS and stored at 4°C until collection. Data was collected on an LSR Fortessa flow cytometer (BD Biosciences) and analyzed with FlowJo software (version 10.8.1 or later). For each E:T ratio, 10,000 target cells (gated as $CFSE^-$) were acquired by FACS. The percentage of specific lysis was calculated as follows: 100 x (%$7AAD^+$ target cells in sample – basal %$7AAD^+$ target cell death, from K562 only control) ÷ (maximum %$7AAD^+$ target cell death, from 0.1% Tween 20 treated K562 cells – basal %$7AAD^+$ target cell death, from K562 only control). K562 cells (cat# CCL-243) were obtained through the American Type Culture Collection (ATCC). Statistical analyses were performed using GraphPad Prism (version 9.4.1 or later).

For the HIV-infected $CD4^+$ T cell co-culture assays, previously frozen NK^- cells were thawed and stimulated for 4 days using Dynabeads Human T-Activator CD3/CD28 for T-Cell Expansion and Activation (Gibco) in C10 medium with IL-2. $CD4^+$ T cells were isolated from the NK^- cells by

positive selection using $CD4^+$ microbeads (Miltenyi Biotec) according to the manufacturer's protocol. Purity of isolated $CD4^+$ T cells was evaluated as described above. $CD4^+$ T cells were then infected with barcoded NL-HABC virus (600 ng/10^6 cells) by spinoculating 1.5x10^6 cells/mL in virus containing 5 mg/mL of polybrene in a 24-well plate. Plates were centrifuged at 1200*g* for 2 hours at 25°C. After infection, cells were incubated overnight at 37°C and 5% CO_2. Previously frozen, donor-matched NK cells were thawed and cultured overnight in C10 media, then stimulated with C10 media containing LRA for 24 hours at 37°C and 5% CO_2. Unstimulated cells (DMSO only) were cultured in parallel in C10 medium. Wells containing only NK cells, only $CD4^+$ T cells, or $CD4^+$ T cells treated with 1X Cell Activation Cocktail (without Brefeldin A; BioLegend) served as assay controls. NK and $CD4^+$ T cells were washed twice, then seeded at an effect-to-target (E:T) ratio of 1:1 (50,000 NK + 50,000 $CD4^+$ T cells) for 4 hours at 37°C and 5% CO_2. The co-cultured cells were labeled with CD3-A700 (clone HIT3a, BioLegend); CD4-APC-Cy7 (clone OKT4, BioLegend); CD56-PB (clone 5.1H11, BioLegend); and Ghost Violet 510 (Tonbo Biosciences), as described above. To detect surface HA expression, cells were first stained with high affinity anti-HA-Biotin (Sigma) at 4°C for 30 minutes, washed, then stained with streptavidin (R-PE conjugate, Invitrogen). After staining, cells were washed and fixed in 1% paraformaldehyde at room temperature for 20 minutes, then washed and resuspended in PBS + 2% FBS and stored at 4°C until collection. Data was collected on an LSR Fortessa flow cytometer (BD Biosciences) and analyzed with FlowJo software (version 10.8.1 or later). For each sample, 10,000 target cells (gated as $CD3^+CD4^+$) were acquired by FACS. The percentage of specific lysis was calculated as follows: 100 x (%HA^+ target cells in sample – basal %HA^+ target cell death, from $CD4^+$ T cell only control) ÷ (maximum %HA^+ target cell death, from 1X CAC treated $CD4^+$ T cells – basal %HA^+ target cell death, from $CD4^+$ T cell only control). Statistical analyses were performed using

GraphPad Prism (version 9.4.1 or later).

Conditioned Media Synthesis in NK Cells

Previously frozen NK cells were thawed and cultured overnight in C10 media (RPMI 1640 media supplemented with 10% vol/vol FBS (Omega Scientific), 1% L-glutamine, 1% penicillin/streptomycin (Invitrogen), 500mM 2-mercaptoethanol (Sigma), 1 mM sodium pyruvate (Gibco), 0.1mM MEM non-essential amino acids (Gibco), and 10 mM HEPES (Gibco)). NK cells were then plated in C10 media containing 10nM SUW133 or untreated (DMSO only) for 5 hours at 37°C and 5% CO_2. Five hours post-stimulation, NK cells were washed twice with C10 to remove LRA, then resuspended in fresh C10 and incubated for an additional 24 hours to allow for the accumulation of cytokines and secreted factors. Culture supernatant (or conditioned media, CM) was collected, filtered using a 0.22-µm filter, and stored at -80°C prior to use.

HIV Latency Reversal Assay

J-Lat A2 and 10.6 cells were cultured in CM and assessed for HIV expression as described previously (Moran et al., 2023). J-Lat A2 (cat# 9854) and 10.6 (cat# 9849) were obtained through the NIH HIV Reagent Program, Division of AIDS, NIAID, NIH from Dr. Eric Verdin.

ACKNOWLEDGEMENTS

Equipment used for this project was provided by the James B. Pendleton Charitable Trust and the McCarthy Family Foundation.

FUNDING SOURCES

This work was supported by the National Institutes of Health [AI172727 to M.D.M., AI172410 to

P.A.W. and J.A.Z., AI161803 to J.A.Z., AI55232 to J.T.K. and CA031845 to P.A.W.] and the UCLA-CDU CFAR [AI152501 to J.TK.]. J.A.M. is a predoctoral trainee supported by US Public Health Service training grant T32 AI007319 from the NIH.

CONFLICTS OF INTEREST

Stanford University has filed patent applications on SUW133 and related technology, which has been licensed by Neurotrope BioScience (Synaptogenix, Inc.) for the treatment of neurological disorders and by BryoLogyx, Inc. for use in HIV/AIDS eradication and cancer immunotherapy. P.A.W. is an adviser to both companies and a cofounder of the latter. J.A.Z. is on the scientific advisory board for BryoLogyx, Inc. and is a cofounder of CDR3 Therapeutics. The remaining authors declare no competing interests.

SUPPLEMENTAL FIGURES

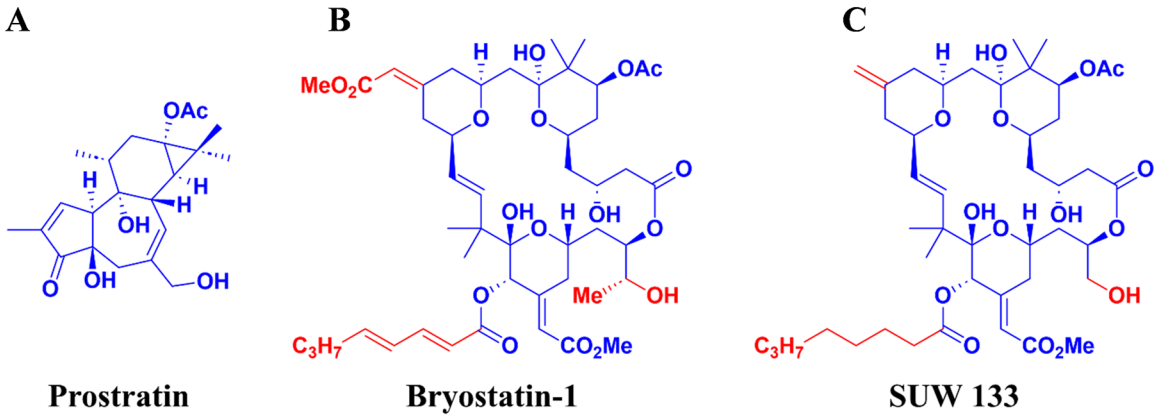

Supplemental Figure 3-1. Chemical structure of select PKC modulators. Chemical structures of prostratin **(A)**, bryostatin-1 **(B)** and SUW133 **(C)**. Moieties highlighted in red show the differences between bryostatin-1 and SUW133.

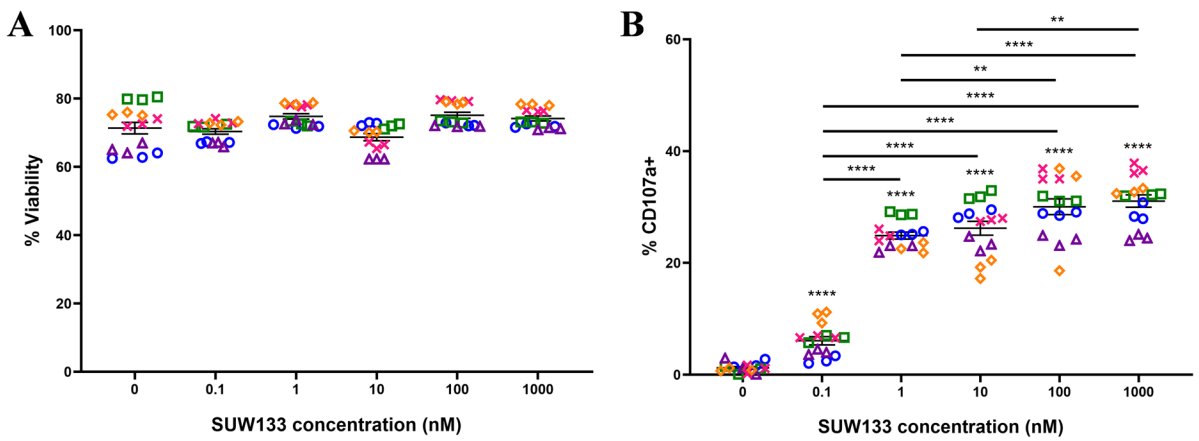

Supplemental Figure 3-2. Effect of SUW133 concentration on NK cell viability and degranulation. NK cells were cultured for 24 hours untreated (DMSO only) or with various concentrations of SUW133 and analyzed for viability **(A)** and degranulation, as measured by CD107a **(B)**, via flow cytometry. All conditions were conducted in technical triplicates in 5 independent biological replicates (5 donors per condition) resulting in n = 15. Each bar graph depicts the mean with error bars indicating the standard error of the mean (SEM). A two-tailed, unpaired, unequal variance Student's *t*-Test was performed, with (**) indicating $p < 0.01$ and (****) indicating $p < 0.0001$. The asterisks above each bar graph in panel B corresponds to a comparison with the untreated control.

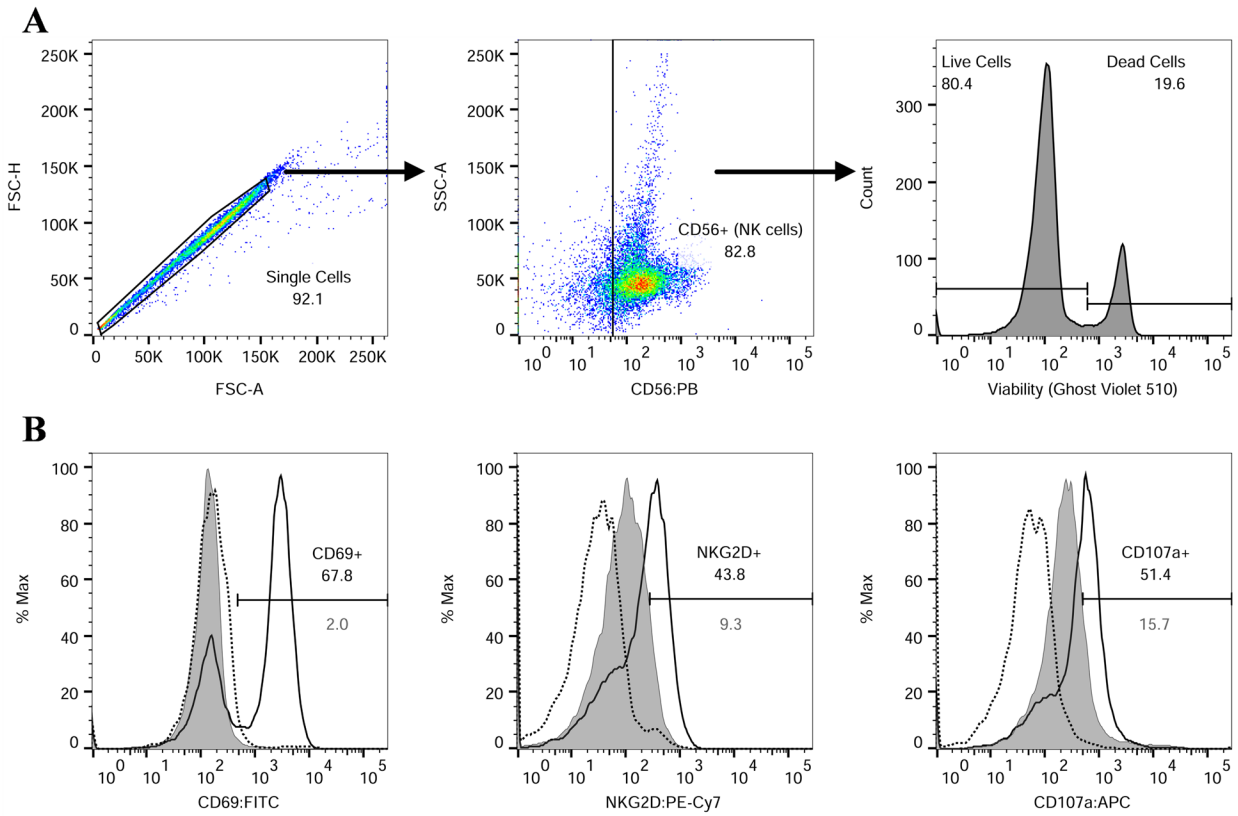

Supplemental Figure 3-3. Example flow cytometry profile/gating strategy. Related to Fig 3-1. NK cells were cultured for 24 hours untreated (DMSO only), with 10nM bryostatin-1, 1μM prostratin or 10nM SUW133 and analyzed for viability, CD69, NKG2D and CD107a via flow cytometry. **A)** Representative scatter plots and histograms with percentages of gated cells shown. Positive gates were determined using an isotype control. **B)** Population comparison of the frequency of $CD69^{+}$, $NKG2D^{+}$ $CD107a^{+}$ NK cells among untreated (DMSO only; filled gray histograms, gray percentages) and treated cells (black lines, black percentages) along with the isotype control (dotted line) for a representative donor.

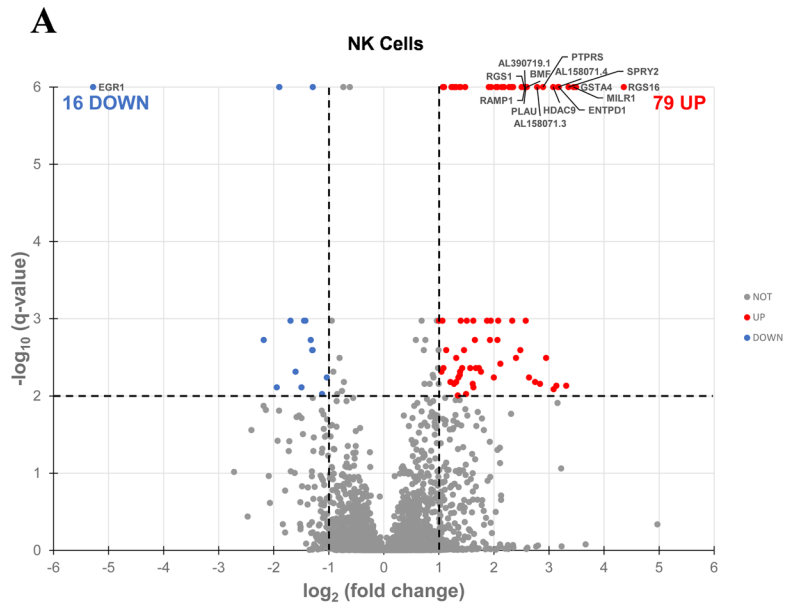

B

NK Cells

Gene	Fold change	Log_2 (FC)	Log_{10} (q-value)	Change trend
EGR1	0.026	-5.2815	6.0000	DOWN
RGS16	20.525	4.3593	6.0000	UP
GSTA4	11.25	3.4919	6.0000	UP
MILR1	10.906	3.4471	6.0000	UP
SPRY2	10.227	3.3543	6.0000	UP
ENTPD1	9.947	3.3143	2.1329	UP
AL158071.4	9.05	3.1779	6.0000	UP
HDAC9	8.955	3.1627	6.0000	UP
PTPRS	8.781	3.1344	2.1329	UP
AL158071.3	8.479	3.0839	2.0868	UP
BMF	8.433	3.076	6.0000	UP
PLAU	7.721	2.9487	2.4925	UP
AL390719.1	7.423	2.892	6.0000	UP
RAMP1	7.145	2.837	2.1574	UP
RGS1	6.895	2.7856	6.0000	UP

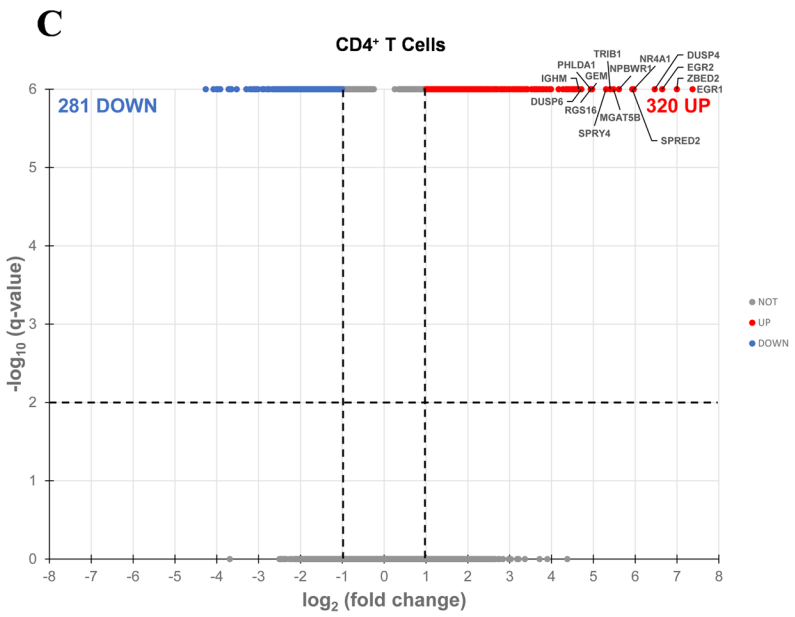

D

CD4⁺ T Cells

Gene	Fold change	Log_2 (FC)	Log_{10} (q-value)	Change trend
EGR1	165.524	7.3709	1.00e-06	UP
ZBED2	127.566	6.9951	1.00e-06	UP
EGR2	100.024	6.6442	1.00e-06	UP
DUSP4	88.365	6.4654	1.00e-06	UP
NR4A1	62.475	5.9652	1.00e-06	UP
SPRED2	60.99	5.9305	1.00e-06	UP
NPBWR1	48.881	5.6112	1.00e-06	UP
MGAT5B	44.734	5.4833	1.00e-06	UP
TRIB1	42.242	5.4006	1.00e-06	UP
SPRY4	39.429	5.3012	1.00e-06	UP
GEM	31.333	4.9696	1.00e-06	UP
RGS16	30.762	4.9431	1.00e-06	UP
PHLDA1	30.631	4.9369	1.00e-06	UP
DUSP6	26.256	4.7146	1.00e-06	UP
IGHM	25.136	4.6517	1.00e-06	UP

Supplemental Figure 3-4. Differentially expressed genes induced by bryostatin-1 in NK and CD4⁺ T cells. Volcano plot of the distribution of all differentially expressed genes in NK cells **(A)** and CD4⁺ T cells **(C)** treated for 24 hours with 10nM bryostatin-1 compared to the untreated (DMSO only) control. The red and blue dots represent the upregulated and downregulated genes (q-value < 0.01 and $|\log_2 FC| > 2$), respectively. The 15 most differentially expressed genes are labeled on each plot and shown in tables **(B)** & **(D)**.

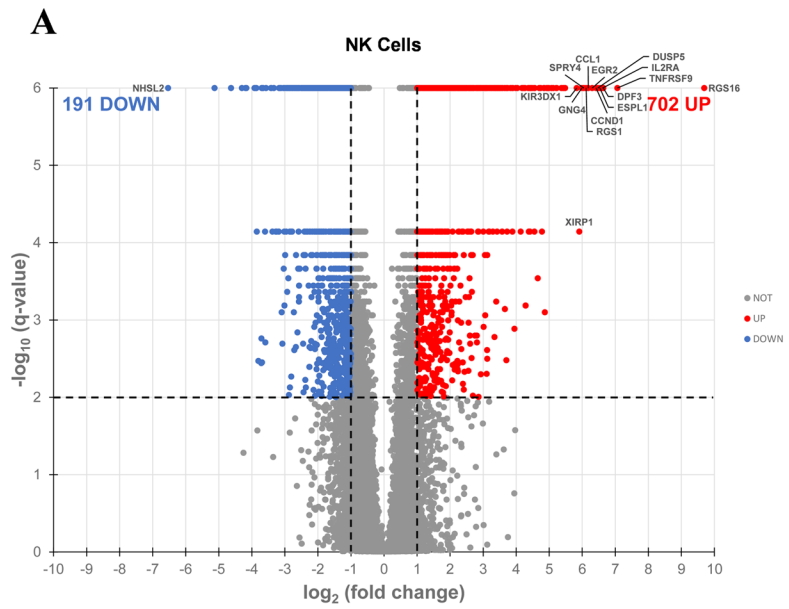

B

NK Cells

Gene	Fold change	Log_2 (FC)	Log_{10} (q-value)	Change trend
RGS16	827.204	9.6921	6.0000	UP
TNFRSF9	133.621	7.062	6.0000	UP
DPF3	99.685	6.6393	6.0000	UP
IL2RA	98.115	6.6164	6.0000	UP
ESPL1	92.732	6.535	6.0000	UP
NHSL2	0.011	-6.5344	6.0000	DOWN
DUSP5	88.641	6.4699	6.0000	UP
CCND1	85.568	6.419	6.0000	UP
EGR2	78.728	6.2988	6.0000	UP
CCL1	72.585	6.1816	6.0000	UP
RGS1	69.402	6.1169	6.0000	UP
SPRY4	66.019	6.0448	6.0000	UP
GNG4	63.589	5.9907	6.0000	UP
XIRP1	60.23	5.9124	4.1427	UP
KIR3DX1	56.965	5.832	6.0000	UP

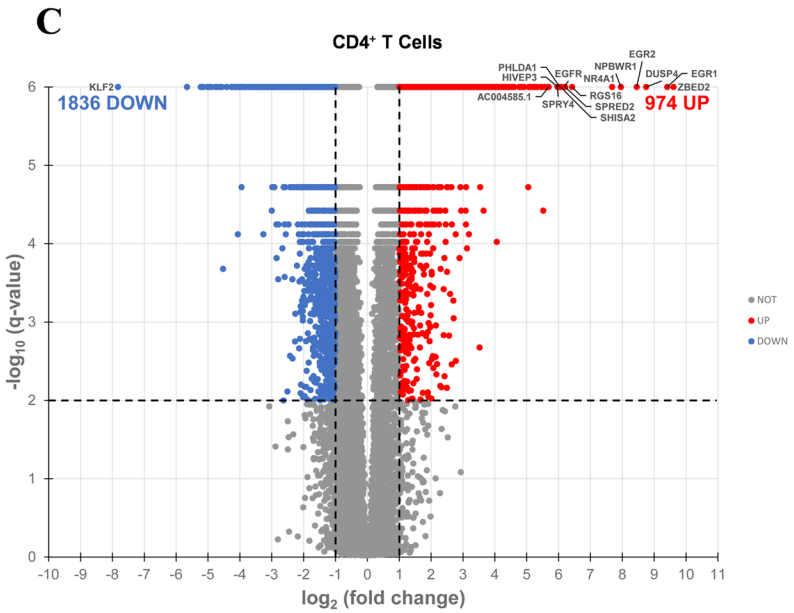

D

CD4⁺ T Cells

Gene	Fold change	Log_2 (FC)	Log_{10} (q-value)	Change trend
ZBED2	779.767	9.6069	6.0000	UP
EGR1	680.334	9.4101	6.0000	UP
DUSP4	429.794	8.7475	6.0000	UP
EGR2	350.216	8.4521	6.0000	UP
NPBWR1	247.949	7.9539	6.0000	UP
KLF2	0.004	-7.8244	6.0000	DOWN
NR4A1	204.804	7.6781	6.0000	UP
RGS16	85.812	6.4231	6.0000	UP
SPRED2	73.874	6.207	6.0000	UP
EGFR	71.999	6.1699	6.0000	UP
SHISA2	66.741	6.0605	6.0000	UP
PHLDA1	65.676	6.0373	6.0000	UP
HIVEP3	62.866	5.9742	6.0000	UP
SPRY4	62.41	5.9637	6.0000	UP
AC004585.1	51.468	5.6856	6.0000	UP

Supplemental Figure 3-5. Differentially expressed genes induced by prostratin in NK and CD4⁺ T cells. Volcano plot of the distribution of all differentially expressed genes in NK cells **(A)** and CD4⁺ T cells **(C)** treated for 24 hours with 1μM prostratin compared to the untreated (DMSO only) control. The red and blue dots represent the upregulated and downregulated genes (q-value < 0.01 and $|\log_2 FC| > 2$), respectively. The 15 most differentially expressed genes are labeled on each plot and shown in tables **(B)** & **(D)**.

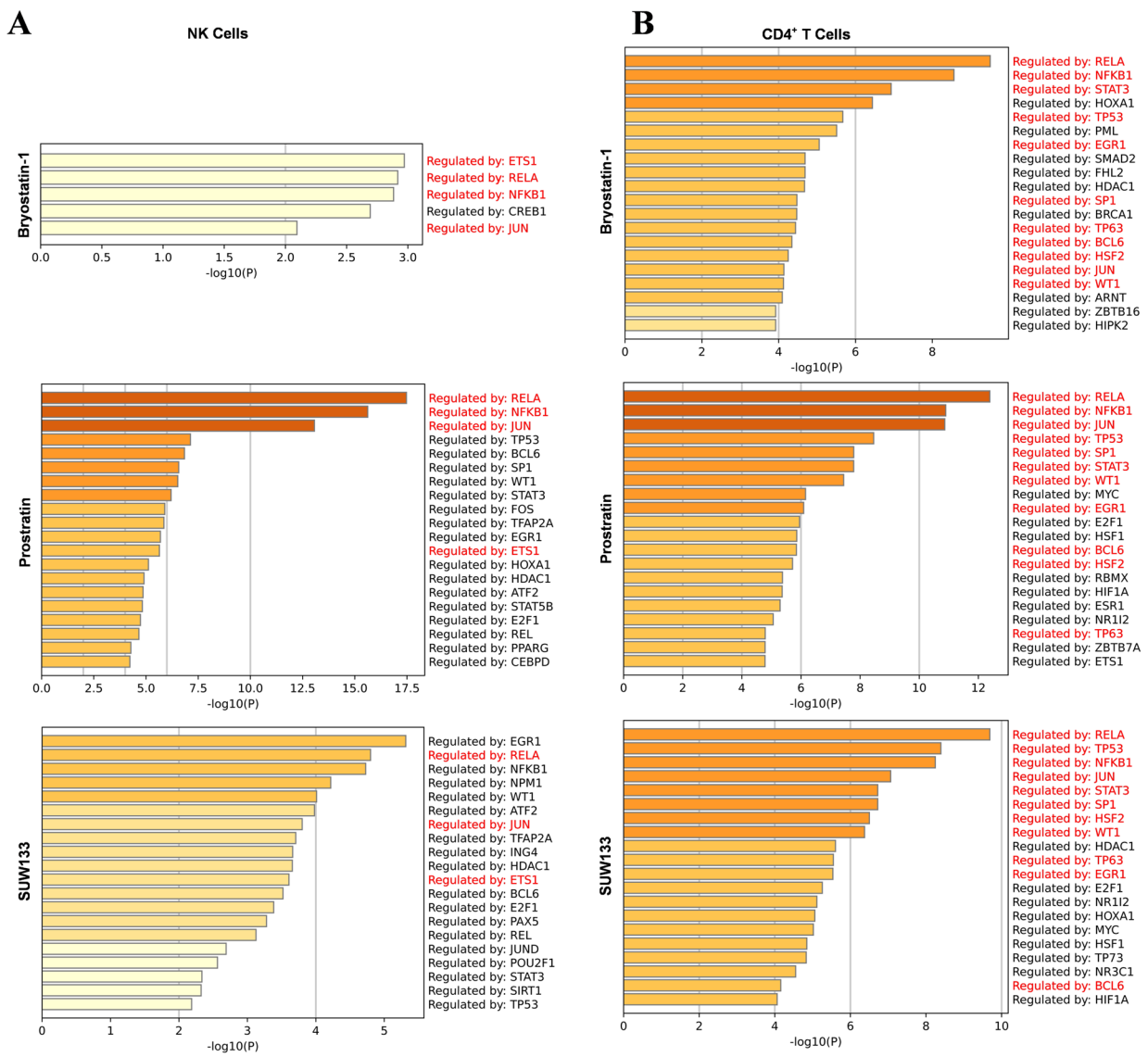

Supplemental Figure 3-6. Summary of enrichment of transcription factors for upregulated genes in NK and CD4$^+$ T cells treated with PKC modulators. Metascape gene set enrichment analysis was performed on the lists of upregulated genes for NK cells **(A)** and CD4$^+$ T cells **(B)** treated for 24 hours with 10nM bryostatin-1, 1μM prostratin or 10nM SUW133 using the transcriptional regulatory relationships unraveled by sentence-based text-mining (TRRUST) database. Terms with a $p < 0.01$, a minimum count of 3 and an enrichment factor >1.5 were collected and grouped into clusters based on their membership similarities. The p values were calculated based on the hypergeometric distribution. The data shown is ranked by statistical significance. Terms highlighted in red are shared between all PKC treatment groups.

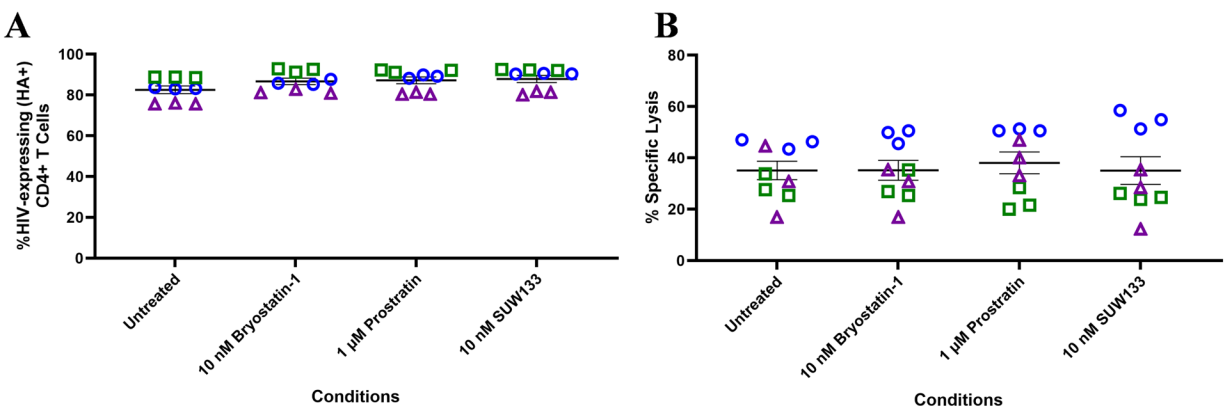

Supplemental Figure 3-7. Impact of PKC modulators on NK cell killing of HIV-infected CD4$^+$ T cells. NK cells were pre-treated for 24 hours in vehicle control (DMSO only), with 10nM bryostatin-1, 1μM prostratin or10 nM SUW133 and co-cultured for 4 hours with HIV-infected CD4$^+$ T cells at a 1:1 effector-to-target (E:T) ratio. All conditions were conducted in technical triplicates in 3 independent biological replicates (3 donors per condition) resulting in n = 9. The percent HIV-expressing target cells **(A)** and specific lysis **(B)** was measured, with each color and shape representing results from a different human donor.

REFERENCES

Abramson, E., Hardman, C., Shimizu, A. J., Hwang, S., Hester, L. D., Snyder, S. H., Wender, P. A., Kim, P. M., & Kornberg, M. D. (2021). Designed PKC-targeting bryostatin analogs modulate innate immunity and neuroinflammation. *Cell Chem Biol*, *28*(4), 537-545 e534. https://doi.org/10.1016/j.chembiol.2020.12.015

Aliberti, J., Reis e Sousa, C., Schito, M., Hieny, S., Wells, T., Huffnagle, G. B., & Sher, A. (2000). CCR5 provides a signal for microbial induced production of IL-12 by CD8 alpha+ dendritic cells. *Nat Immunol*, *1*(1), 83-87. https://doi.org/10.1038/76957

Alkhatib, G., Locati, M., Kennedy, P. E., Murphy, P. M., & Berger, E. A. (1997). HIV-1 coreceptor activity of CCR5 and its inhibition by chemokines: independence from G protein signaling and importance of coreceptor downmodulation. *Virology*, *234*(2), 340-348. https://doi.org/10.1006/viro.1997.8673

Aubert, M., Ryu, B. Y., Banks, L., Rawlings, D. J., Scharenberg, A. M., & Jerome, K. R. (2011). Successful targeting and disruption of an integrated reporter lentivirus using the engineered homing endonuclease Y2 I-AniI. *PLoS One*, *6*(2), e16825. https://doi.org/10.1371/journal.pone.0016825

Baxter, A. E., Niessl, J., Fromentin, R., Richard, J., Porichis, F., Charlebois, R., Massanella, M., Brassard, N., Alsahafi, N., Delgado, G. G., Routy, J. P., Walker, B. D., Finzi, A., Chomont, N., & Kaufmann, D. E. (2016). Single-Cell Characterization of Viral Translation-Competent Reservoirs in HIV-Infected Individuals. *Cell Host Microbe*, *20*(3), 368-380. https://doi.org/10.1016/j.chom.2016.07.015

Beans, E. J., Fournogerakis, D., Gauntlett, C., Heumann, L. V., Kramer, R., Marsden, M. D., Murray, D., Chun, T. W., Zack, J. A., & Wender, P. A. (2013). Highly potent, synthetically accessible prostratin analogs induce latent HIV expression in vitro and ex vivo. *Proc Natl Acad Sci U S A*, *110*(29), 11698-11703. https://doi.org/10.1073/pnas.1302634110

Berger, E. A., Murphy, P. M., & Farber, J. M. (1999). Chemokine receptors as HIV-1 coreceptors: roles in viral entry, tropism, and disease. *Annu Rev Immunol*, *17*, 657-700. https://doi.org/10.1146/annurev.immunol.17.1.657

Berthebaud, M., Riviere, C., Jarrier, P., Foudi, A., Zhang, Y., Compagno, D., Galy, A., Vainchenker, W., & Louache, F. (2005). RGS16 is a negative regulator of SDF-1-CXCR4 signaling in megakaryocytes. *Blood*, *106*(9), 2962-2968. https://doi.org/10.1182/blood-2005-02-0526

Biancotto, A., Grivel, J. C., Gondois-Rey, F., Bettendroffer, L., Vigne, R., Brown, S., Margolis, L. B., & Hirsch, I. (2004). Dual role of prostratin in inhibition of infection and reactivation of human immunodeficiency virus from latency in primary blood

lymphocytes and lymphoid tissue. *J Virol*, *78*(19), 10507-10515. https://doi.org/10.1128/JVI.78.19.10507-10515.2004

Boehm, U., Klamp, T., Groot, M., & Howard, J. C. (1997). Cellular responses to interferon-gamma. *Annu Rev Immunol*, *15*, 749-795. https://doi.org/10.1146/annurev.immunol.15.1.749

Bullen, C. K., Laird, G. M., Durand, C. M., Siliciano, J. D., & Siliciano, R. F. (2014). New ex vivo approaches distinguish effective and ineffective single agents for reversing HIV-1 latency in vivo. *Nat Med*, *20*(4), 425-429. https://doi.org/10.1038/nm.3489

Campbell, G. R., Bruckman, R. S., Chu, Y. L., Trout, R. N., & Spector, S. A. (2018). SMAC Mimetics Induce Autophagy-Dependent Apoptosis of HIV-1-Infected Resting Memory CD4+ T Cells. *Cell Host Microbe*, *24*(5), 689-702 e687. https://doi.org/10.1016/j.chom.2018.09.007

Choe, H., Farzan, M., Sun, Y., Sullivan, N., Rollins, B., Ponath, P. D., Wu, L., Mackay, C. R., LaRosa, G., Newman, W., Gerard, N., Gerard, C., & Sodroski, J. (1996). The beta-chemokine receptors CCR3 and CCR5 facilitate infection by primary HIV-1 isolates. *Cell*, *85*(7), 1135-1148. https://doi.org/10.1016/s0092-8674(00)81313-6

Chuang, S. S., Lee, J. K., & Mathew, P. A. (2003). Protein kinase C is involved in 2B4 (CD244)-mediated cytotoxicity and AP-1 activation in natural killer cells. *Immunology*, *109*(3), 432-439. https://doi.org/10.1046/j.1365-2567.2003.01662.x

Chun, T. W., Engel, D., Mizell, S. B., Ehler, L. A., & Fauci, A. S. (1998). Induction of HIV-1 replication in latently infected CD4+ T cells using a combination of cytokines. *J Exp Med*, *188*(1), 83-91. https://doi.org/10.1084/jem.188.1.83

Chun, T. W., Engel, D., Mizell, S. B., Hallahan, C. W., Fischette, M., Park, S., Davey, R. T., Dybul, M., Kovacs, J. A., Metcalf, J. A., Mican, J. M., Berrey, M. M., Corey, L., Lane, H. C., & Fauci, A. S. (1999). Effect of interleukin-2 on the pool of latently infected, resting CD4+ T cells in HIV-1-infected patients receiving highly active anti-retroviral therapy. *Nat Med*, *5*(6), 651-655. https://doi.org/10.1038/9498

Chun, T. W., Finzi, D., Margolick, J., Chadwick, K., Schwartz, D., & Siliciano, R. F. (1995). In vivo fate of HIV-1-infected T cells: Quantitative analysis of the transition to stable latency. *Nat Med*, *1*, 1284-1290. https://doi.org/10.1038/nm1295-1284

Chun, T. W., Stuyver, L., Mizell, S. B., Ehler, L. A., Mican, J. A., Baseler, M., Lloyd, A. L., Nowak, M. A., & Fauci, A. S. (1997). Presence of an inducible HIV-1 latent reservoir during highly active antiretroviral therapy. *Proc Natl Acad Sci U S A 94*, 13193-13197. https://doi.org/10.1073/pnas.94.24.13193

Cobos Jimenez, V., Booiman, T., de Taeye, S. W., van Dort, K. A., Rits, M. A., Hamann, J., & Kootstra, N. A. (2012). Differential expression of HIV-1 interfering factors in monocyte-

derived macrophages stimulated with polarizing cytokines or interferons. *Sci Rep*, *2*, 763. https://doi.org/10.1038/srep00763

Cocchi, F., DeVico, A. L., Garzino-Demo, A., Arya, S. K., Gallo, R. C., & Lusso, P. (1995). Identification of RANTES, MIP-1 alpha, and MIP-1 beta as the major HIV-suppressive factors produced by CD8+ T cells. *Science*, *270*(5243), 1811-1815. https://doi.org/10.1126/science.270.5243.1811

Coffey, M. J., Woffendin, C., Phare, S. M., Strieter, R. M., & Markovitz, D. M. (1997). RANTES inhibits HIV-1 replication in human peripheral blood monocytes and alveolar macrophages. *Am J Physiol*, *252*(5), L1025-L1029. https://doi.org/10.1152/ajplung.1997.272.5.L1025

Cummins, N. W., Sainski-Nguyen, A. M., Natesampillai, S., Aboulnasr, F., Kaufmann, S., & Badley, A. D. (2017). Maintenance of the HIV Reservoir Is Antagonized by Selective BCL2 Inhibition. *J Virol*, *91*(11). https://doi.org/10.1128/JVI.00012-17

Darcis, G., Kula, A., Bouchat, S., Fujinaga, K., Corazza, F., Ait-Ammar, A., Delacourt, N., Melard, A., Kabeya, K., Vanhulle, C., Van Driessche, B., Gatot, J. S., Cherrier, T., Pianowski, L. F., Gama, L., Schwartz, C., Vila, J., Burny, A., Clumeck, N., . . . Van Lint, C. (2015). An In-Depth Comparison of Latency-Reversing Agent Combinations in Various In Vitro and Ex Vivo HIV-1 Latency Models Identified Bryostatin-1+JQ1 and Ingenol-B+JQ1 to Potently Reactivate Viral Gene Expression. *PLoS Pathog*, *11*(7), e1005063. https://doi.org/10.1371/journal.ppat.1005063

DeChristopher, B. A., Loy, B. A., Marsden, M. D., Schrier, A. J., Zack, J. A., & Wender, P. A. (2012). Designed, synthetically accessible bryostatin analogues potently induce activation of latent HIV reservoirs in vitro. *Nat Chem*, *4*(9), 705-710. https://doi.org/10.1038/nchem.1395

Deng, H., Liu, R., Ellmeier, W., Choe, S., Unutmaz, D., Burkhart, M., Di Marzio, P., Marmon, S., E., S. R., Hill, C. M., Davis, C. B., Peiper, S. C., Schall, T. J., Littman, D. R., & Landau, N. R. (1996). Identification of a major co-receptor for primary isolates of HIV-1. *Nature*, *381*(6584), 661-666. https://doi.org/10.1038/381661a0

Desimio, M. G., Giuliani, E., Ferraro, A. S., Adorno, G., & Doria, M. (2018). In Vitro Exposure to Prostratin but Not Bryostatin-1 Improves Natural Killer Cell Functions Including Killing of CD4(+) T Cells Harboring Reactivated Human Immunodeficiency Virus. *Front Immunol*, *9*, 1514. https://doi.org/10.3389/fimmu.2018.01514

Dobin, A., Davis, C. A., Schlesinger, F., Drenkow, J., Zaleski, C., Jha, S., Batut, P., Chaisson, M., & Gingeras, T. R. (2013). STAR: ultrafast universal RNA-seq aligner. *Bioinformatics*, *29*(1), 15-21. https://doi.org/10.1093/bioinformatics/bts635

Doranz, B. J., Rucker, J., Yi, Y., Smyth, R. J., Samson, M., Peiper, S. C., Parmentier, M., Collman, R. G., & Doms, R. W. (1996). A dual-tropic primary HIV-1 isolate that uses

fusin and the beta-chemokine receptors CKR-5, CKR-3, and CKR-2b as fusion cofactors. *Cell*, *85*(7), 1149-1158. https://doi.org/10.1016/s0092-8674(00)81314-8

Dragic, T., Litwin, V., Allaway, G. P., Martin, S. R., Huang, Y., Nagashima, K. A., Cayanan, C., Maddon, P. J., Koup, R. A., Moore, J. P., & Paxton, W. A. (1996). HIV-1 entry into CD4+ cells is mediated by the chemokine receptor CC-CKR-5. *Nature*, *381*(6584), 667-673. https://doi.org/10.1038/381667a0

Duh, E. J., Maury, W. J., Folks, T. M., Fauci, A. S., & Rabson, A. B. (1989). Tumor necrosis factor alpha activates human immunodeficiency virus type 1 through induction of nuclear factor binding to the NF-kappa B sites in the long terminal repeat. *Proc Natl Acad Sci U S A*, *86*(15), 5974-5978. https://doi.org/10.1073/pnas.86.15.5974

Ebina, H., Misawa, N., Kanemura, Y., & Koyanagi, Y. (2013). Harnessing the CRISPR/Cas9 system to disrupt latent HIV-1 provirus. *Sci Rep*, *3*, 2510. https://doi.org/10.1038/srep02510

Finzi, D., Hermankova, M., Pierson, T., Carruth, L. M., Buck, C., Chaisson, R. E., Quinn, T. C., Chadwick, K., Margolick, J., Brookmeyer, R., Gallant, J., Markowitz, M., Ho, D. D., Richman, D. D., & Siliciano, R. F. (1997). Identification of a Reservoir for HIV-1 in Patients on Highly Active Antiretroviral Therapy. *Science*, *278*, 1295-1300. https://doi.org/10.1126/science.278.5341.1295

Folks, T. M., Clouse, K. A., Justement, J., Rabson, A., Duh, E., Kehrl, J. H., & Fauci, A. S. (1989). Tumor necrosis factor alpha induces expression of human immunodeficiency virus in a chronically infected T-cell clone. *Proc Natl Acad Sci U S A*, *86*(7), 2365-2368. https://doi.org/10.1073/pnas.86.7.2365

Frucht, D. M., Fukao, T., Bogdan, C., Schindler, H., O'Shea, J. J., & Koyasu, S. (2001). IFN-gamma production by antigen-presenting cells: mechanisms emerge. *Trends Immunol 22*(10), 556-560. https://doi.org/10.1016/s1471-4906(01)02005-1

Garrido, C., Spivak, A. M., Soriano-Sarabia, N., Checkley, M. A., Barker, E., Karn, J., Planelles, V., & Margolis, D. M. (2016). HIV Latency-Reversing Agents Have Diverse Effects on Natural Killer Cell Function. *Front Immunol*, *7*, 356. https://doi.org/10.3389/fimmu.2016.00356

Griffin, G. E., Leung, K., Folks, T. M., Kunkel, S., & Nabel, G. J. (1989). Activation of HIV gene expression during monocyte differentiation by induction of NF-kappa B. *Nature*, *339*(6219), 70-73. https://doi.org/10.1038/339070a0

Gulakowski, R. J., McMahon, J. B., Buckheit, R. W. J., Gustafson, K. R., & Boyd, M. R. (1997). Antireplicative and anticytopathic activities of prostratin, a non-tumor-promoting phorbol ester, against human immunodeficiency virus (HIV). *Antiviral Res*, *33*(2), 87-97. https://doi.org/10.1016/s0166-3542(96)01004-2

Gutierrez, C., Serrano-Villar, S., Madrid-Elena, N., Perez-Elias, M. J., Martin, M. E., Barbas, C., Ruiperez, J., Munoz, E., Munoz-Fernandez, M. A., Castor, T., & Moreno, S. (2016). Bryostatin-1 for latent virus reactivation in HIV-infected patients on antiretroviral therapy. *AIDS*, *30*(9), 1385-1392. https://doi.org/10.1097/QAD.0000000000001064

Harris, D. P., Goodrich, S., Gerth, A. J., Peng, S. L., & Lund, F. E. (2005). Regulation of IFN-gamma production by B effector 1 cells: essential roles for T-bet and the IFN-gamma receptor. *J Immunol*, *174*(11), 6781-6790. https://doi.org/10.4049/jimmunol.174.11.6781

He, S., Li, Q., Huang, Q., & Cheng, J. (2022). Targeting Protein Kinase C for Cancer Therapy. *Cancers (Basel)*, *14*(5). https://doi.org/10.3390/cancers14051104

Hirsch, M. S., Conway, B., D'Aquila, R. T., Johnson, V. A., Brun-Vézinet, F., Clotet, B., Demeter, L. M., Hammer, S. M., Jacobsen, D. M., Kuritzkes, D. R., Loveday, C., Mellors, J. W., Vella, S., & Richman, D. D. (1998). Antiretroviral Drug Resistance Testing in Adults With HIV Infection. *JAMA*, *279*, 1984-1991. https://doi.org/10.1001/jama.279.24.1984

Hulsen, T., de Vlieg, J., & Alkema, W. (2008). BioVenn - a web application for the comparison and visualization of biological lists using area-proportional Venn diagrams. *BMC Genomics*, *9*, 488. https://doi.org/10.1186/1471-2164-9-488

Ito, M., Tanabe, F., Sato, A., Takami, Y., & Shigeta, S. (1988). A potent inhibitor of protein kinase C inhibits natural killer activity. *Int J Immunopharmacol 10*, 211-216. https://doi.org/10.1016/0192-0561(88)90051-3

Jiang, G., Mendes, E. A., Kaiser, P., Wong, D. P., Tang, Y., Cai, I., Fenton, A., Melcher, G. P., Hildreth, J. E., Thompson, G. R., Wong, J. K., & Dandekar, S. (2015). Synergistic Reactivation of Latent HIV Expression by Ingenol-3-Angelate, PEP005, Targeted NF-kB Signaling in Combination with JQ1 Induced p-TEFb Activation. *PLoS Pathog*, *11*(7), e1005066. https://doi.org/10.1371/journal.ppat.1005066

Johnson, E. N., Seasholtz, T. M., Waheed, A. A., Kreutz, B., Suzuki, N., Kozasa, T., Jones, T. L., Brown, J. H., & Druey, K. M. (2003). RGS16 inhibits signalling through the G alpha 13-Rho axis. *Nat Cell Biol*, *5*(12), 1095-1103. https://doi.org/10.1038/ncb1065

Jordan, A., Bisgrove, D., & Verdin, E. (2003). HIV reproducibly establishes a latent infection after acute infection of T cells in vitro. *EMBO J*, *22*(8), 1868-1877. https://doi.org/10.1093/emboj/cdg188

Jordan, A., Defechereux, P., & Verdin, E. (2001). The site of HIV-1 integration in the human genome determines basal transcriptional activity and response to Tat transactivation. *EMBO J*, *20*(7), 1726-1738. https://doi.org/10.1093/emboj/20.7.1726

Karpus, W. J., Lukacs, N. W., Kennedy, K. J., Smith, W. S., Hurst, S. D., & Barrett, T. A. (1997). Differential CC chemokine-induced enhancement of T helper cell cytokine production. *J Immunol*, *158*(9), 4129-4136. https://doi.org/10.4049/jimmunol.158.9.4129

Kessing, C. F., Nixon, C. C., Li, C., Tsai, P., Takata, H., Mousseau, G., Ho, P. T., Honeycutt, J. B., Fallahi, M., Trautmann, L., Garcia, J. V., & Valente, S. T. (2017). In Vivo Suppression of HIV Rebound by Didehydro-Cortistatin A, a "Block-and-Lock" Strategy for HIV-1 Treatment. *Cell Rep*, *21*(3), 600-611. https://doi.org/10.1016/j.celrep.2017.09.080

Kim, J. T., Zhang, T. H., Carmona, C., Lee, B., Seet, C. S., Kostelny, M., Shah, N., Chen, H., Farrell, K., Soliman, M. S. A., Dimapasoc, M., Sinani, M., Blanco, K. Y. R., Bojorquez, D., Jiang, H., Shi, Y., Du, Y., Komarova, N. L., Wodarz, D., . . . Zack, J. A. (2022). Latency reversal plus natural killer cells diminish HIV reservoir in vivo. *Nat Commun*, *13*(1), 121. https://doi.org/10.1038/s41467-021-27647-0

Kim, Y., Anderson, J. L., & Lewin, S. R. (2018). Getting the "Kill" into "Shock and Kill": Strategies to Eliminate Latent HIV. *Cell Host Microbe*, *23*(1), 14-26. https://doi.org/10.1016/j.chom.2017.12.004

Kinter, A. L., Poli, G., Maury, W., Folks, T. M., & Fauci, A. S. (1990). Direct and cytokine-mediated activation of protein kinase C induces human immunodeficiency virus expression in chronically infected promonocytic cells. *J Virol 64*(9), 4306-4312. https://doi.org/10.1128/JVI.64.9.4306-4312.1990

Koirala, J., Adamski, A., Koch, L., Stueber, D., El-Azizi, M., Khardori, N. M., Ghassemi, M., & Novak, R. M. (2008). Interferon-gamma receptors in HIV-1 infection. *AIDS Res Hum Retroviruses*, *24*(8), 1097-1102. https://doi.org/10.1089/aid.2007.0261

Korin, Y. D., Brooks, D. G., Brown, S., Korotzer, A., & Zack, J. A. (2002). Effects of prostratin on T-cell activation and human immunodeficiency virus latency. *J Virol*, *76*(16), 8118-8123. https://doi.org/10.1128/jvi.76.16.8118-8123.2002

Kortmansky, J., & Schwartz, G. K. (2003). Bryostatin-1: a novel PKC inhibitor in clinical development. *Cancer Invest*, *21*(6), 924-936. https://doi.org/10.1081/cnv-120025095

Kraft, A. S., Woodley, S. P., G. R., & Gao, F., J. C. Wagner, F. (1996). Comparison of the antitumor activity of bryostatins 1, 5, and 8. *Cancer Chemother Pharmacol*, *37*, 271-278. https://doi.org/10.1007/BF00688328

Kulkosky, J., Culnan, D. M., Roman, J., Dornadula, G., Schnell, M., Boyd, M. R., & Pomerantz, R. J. (2001). Prostratin: activation of latent HIV-1 expression suggests a potential inductive adjuvant therapy for HAART. *Blood*, *98*(10), 3006-3015. https://doi.org/10.1182/blood.v98.10.3006

Kumar, R., Qureshi, H., Deshpande, S., & Bhattacharya, J. (2018). Broadly neutralizing antibodies in HIV-1 treatment and prevention. *Ther Adv Vaccines Immunother*, *6*(4), 61-68. https://doi.org/10.1177/2515135518800689

Laurence, J., Sikder, S. K., Jhaveri, S., & Salmon, J. E. (1990). Phorbol ester-mediated induction of HIV-1 from a chronically infected promonocyte clone: blockade by protein kinase inhibitors and relationship to tat-directed trans-activation. *Biochem Biophys Res Commun*, *166*(1), 349-357. https://doi.org/10.1016/0006-291X(90)91952-O

Liang, G., Bansal, G., Xie, Z., & Druey, K. M. (2009). RGS16 inhibits breast cancer cell growth by mitigating phosphatidylinositol 3-kinase signaling. *J Biol Chem*, *284*(32), 21719-21727. https://doi.org/10.1074/jbc.M109.028407

Lucas, A., Kim, Y., Rivera-Pabon, O., Chae, S., Kim, D. H., & Kim, B. (2010). Targeting the PI3K/Akt cell survival pathway to induce cell death of HIV-1 infected macrophages with alkylphospholipid compounds. *PLoS One*, *5*(9). https://doi.org/10.1371/journal.pone.0013121

Macedo, A. B., Novis, C. L., & Bosque, A. (2019). Targeting Cellular and Tissue HIV Reservoirs With Toll-Like Receptor Agonists. *Front Immunol*, *10*, 2450. https://doi.org/10.3389/fimmu.2019.02450

Marsden, M. D., Loy, B. A., Wu, X., Ramirez, C. M., Schrier, A. J., Murray, D., Shimizu, A., Ryckbosch, S. M., Near, K. E., Chun, T. W., Wender, P. A., & Zack, J. A. (2017). In vivo activation of latent HIV with a synthetic bryostatin analog effects both latent cell "kick" and "kill" in strategy for virus eradication. *PLoS Pathog*, *13*(9), e1006575. https://doi.org/10.1371/journal.ppat.1006575

Marsden, M. D., Wu, X., Navab, S. M., Loy, B. A., Schrier, A. J., DeChristopher, B. A., Shimizu, A. J., Hardman, C. T., Ho, S., Ramirez, C. M., Wender, P. A., & Zack, J. A. (2018). Characterization of designed, synthetically accessible bryostatin analog HIV latency reversing agents. *Virology*, *520*, 83-93. https://doi.org/10.1016/j.virol.2018.05.006

Marsden, M. D., & Zack, J. A. (2015). Experimental Approaches for Eliminating Latent HIV. *For Immunopathol Dis Therap*, *6*(1-2), 91-99. https://doi.org/10.1615/forumimmundisther.2016015242

Marsden, M. D., & Zack, J. A. (2019). HIV cure strategies: a complex approach for a complicated viral reservoir? *Future Virology*, *14*(1), 5-8. https://doi.org/10.2217/fvl-2018-0205

Marsden, M. D., Zhang, T. H., Du, Y., Dimapasoc, M., Soliman, M. S. A., Wu, X., Kim, J. T., Shimizu, A., Schrier, A., Wender, P. A., Sun, R., & Zack, J. A. (2020). Tracking HIV Rebound following Latency Reversal Using Barcoded HIV. *Cell Rep Med*, *1*(9), 100162. https://doi.org/10.1016/j.xcrm.2020.100162

McManus, C. M., Brosnan, C. F., & Berman, J. W. (1998). Cytokine Induction of MIP-1α and MIP-1β in Human Fetal Microglia. *J Immunol*, *160*(3), 1449-1455. https://doi.org/10.4049/jimmunol.160.3.1449

Mehla, R., Bivalkar-Mehla, S., Zhang, R., Handy, I., Albrecht, H., Giri, S., Nagarkatti, P., Nagarkatti, M., & Chauhan, A. (2010). Bryostatin modulates latent HIV-1 infection via PKC and AMPK signaling but inhibits acute infection in a receptor independent manner. *PLoS One*, *5*(6), e11160. https://doi.org/10.1371/journal.pone.0011160

Mellors, J. W., Griffith, B. P., Ortiz, M. A., Landry, M. L., & Ryan, J. L. (1991). Tumor necrosis factor-alpha/cachectin enhances human immunodeficiency virus type 1 replication in primary macrophages. *J Infect Dis 163*(1), 78-82. https://doi.org/10.1093/infdis/163.1.78

Michihiko, S., Yamamoto, N., Shinozaki, F., Shimada, K., Soma, G., & Kobayashi, N. (1989). Augmentation of in-vitro HIV replication in peripheral blood mononuclear cells of AIDS and ARC patients by tumour necrosis factor. *Lancet*, *1*(8648), 1206-1207. https://doi.org/10.1016/s0140-6736(89)92788-8

Moran, J. A., Ranjan, A., Hourani, R., Kim, J. T., Wender, P. A., Zack, J. A., & Marsden, M. D. (2023). Secreted factors induced by PKC modulators do not indirectly cause HIV latency reversal. *Virology*, *581*, 8-14. https://doi.org/10.1016/j.virol.2023.02.009

Orrell, C. (2005). Antiretroviral Adherence in a Resource-poor Setting. *Curr HIV/AIDS Rep*, *2*, 171-176. https://doi.org/10.1007/s11904-005-0012-8

Osborn, L., Kunkel, S., & Nabel, G. J. (1989). Tumor necrosis factor alpha and interleukin 1 stimulate the human immunodeficiency virus enhancer by activation of the nuclear factor kappa B. *Proc Natl Acad Sci U S A*, *86*(7), 2365-2368. https://doi.org/10.1073/pnas.86.7.2365

Partek® Flow® software. In. (2019). (Version 7.0) Partek Inc.

Pätzold, S., Schneider, J., Rudolph, C., Marmé, D., & Schächtele, C. (1993). Novel indolocarbazole protein kinase C inhibitors prevent reactivation of HIV-1 in latently infected cells. *Antiviral Res 1993*, *22*(4), 273-283. https://doi.org/10.1016/0166-3542(93)90037-j

Pérez, M., de Vinuesa, A. G., Sanchez-Duffhues, G., Marquez, N., Bellido, M. L., Muñoz-Fernandez, M. A., Moreno, S., Castor, T. P., Calzado, M. A., & Muñoz, E. (2010). Bryostatin-1 Synergizes with Histone Deacetylase Inhibitors to Reactivate HIV-1 from Latency. *Curr HIV Res*, *8*(6), 418-419. https://doi.org/10.2174/157016210793499312

Pierson, T. C., & Doms, R. W. (2003). HIV-1 Entry and Its Inhibition. In J. A. T. Young (Ed.), *Cellular Factors Involved in Early Steps of Retroviral Replication* (Vol. 281, pp. 1-27). Springer Berlin, Heidelberg. https://doi.org/10.1007/978-3-642-19012-4

Qatsha, K. A., Rudolph, C., Marmé, D., Schächtele, C., & May, W. S. (1993). Gö 6976, a selective inhibitor of protein kinase C, is a potent antagonist of human immunodeficiency virus 1 induction from latent/low-level-producing reservoir cells in vitro. *Proc Natl Acad Sci U S A 90*(10), 4674-4678. https://doi.org/10.1073/pnas.90.10.4674

Qu, X., Wang, P., Ding, D., Li, L., Wang, H., Ma, L., Zhou, X., Liu, S., Lin, S., Wang, X., Zhang, G., Liu, S., Liu, L., Wang, J., Zhang, F., Lu, D., & Zhu, H. (2013). Zinc-finger-nucleases mediate specific and efficient excision of HIV-1 proviral DNA from infected and latently infected human T cells. *Nucleic Acids Res*, *41*(16), 7771-7782. https://doi.org/10.1093/nar/gkt571

Rabbi, M. F., Finnegan, A., Al-Harthi, L., Song, S., & Roebuck, K. A. (1998). Interleukin-10 enhances tumor necrosis factor-alpha activation of HIV-1 transcription in latently infected T cells. *J Acquir Immune Defic Syndr Hum Retrovirol*, *19*(4), 321-331. https://doi.org/10.1097/00042560-199812010-00002

Roberts, M. R., Qin, L., Zhang, D., Smith, D. H., Tran, A. C., Dull, T. J., Groopman, J. E., Capon, D. J., Byrn, R. A., & Finer, M. H. (1994). Targeting of human immunodeficiency virus-infected cells by CD8+ T lymphocytes armed with universal T-cell receptors. *Blood*, *84*(9), 2878-2889. https://doi.org/10.1182/blood.V84.9.2878.2878

Robertson, M. J., Cameron, C., Lazo, S., Cochran, K. J., Voss, S. D., & Ritz, J. (1996). Costimulation of human natural killer cell proliferation: role of accessory cytokines and cell contact-dependent signals. *Nat Immun 15*(5), 213-226.

Sadowski, I., & Hashemi, F. B. (2019). Strategies to eradicate HIV from infected patients: elimination of latent provirus reservoirs. *Cell Mol Life Sci*, *76*(18), 3583-3600. https://doi.org/10.1007/s00018-019-03156-8

Sarkar, I., Hauber, I., Hauber, J., & Buchholz, F. (2007). HIV-1 Proviral DNA Excision Using an Evolved Recombinase. *Science*, *316*(5833), 1912-1915. https://doi.org/10.1126/science.1141453

Schaufelberger, D. E., Koleck, M. P., Beutler, J. A., Vatakis, A. M., Alvarado, A. B., Andrews, P., Marzo, L. V., Muschik, G. M., Roach, J., & Ross, J. T. (1991). The large-scale isolation of bryostatin 1 from Bugula neritina following current good manufacturing practices. *J Nat Prod*, *54*(5), 1265-1270. https://doi.org/10.1021/np50077a004

Scripture-Adams, D. D., Brooks, D. G., Korin, Y. D., & Zack, J. A. (2002). Interleukin-7 induces expression of latent human immunodeficiency virus type 1 with minimal effects on T-cell phenotype. *J Virol*, *76*(24), 13077-13082. https://doi.org/10.1128/jvi.76.24.13077-13082.2002

Simmons, G., Clapham, P. R., Picard, L., Offord, R. E., Rosenkilde, M. M., Schwartz, T. W., Buser, R., Wells, T. N., & Proudfoot, A. E. (1997). Potent inhibition of HIV-1 infectivity

in macrophages and lymphocytes by a novel CCR5 antagonist. *Science*, *276*(5310), 276-279. https://doi.org/10.1126/science.276.5310.276

Sloane, J. L., Benner, N. L., Keenan, K. N., Zang, X., Soliman, M. S. A., Wu, X., Dimapasoc, M., Chun, T. W., Marsden, M. D., Zack, J. A., & Wender, P. A. (2020). Prodrugs of PKC modulators show enhanced HIV latency reversal and an expanded therapeutic window. *Proc Natl Acad Sci U S A*, *117*(20), 10688-10698. https://doi.org/10.1073/pnas.1919408117

Spellberg, B., & Edwards, J. E. J. (2001). Type 1/Type 2 immunity in infectious diseases. *Clin Infect Dis 32*(1), 76-102. https://doi.org/10.1086/317537

Spivak, A. M., & Planelles, V. (2018). Novel Latency Reversal Agents for HIV-1 Cure. *Annu Rev Med*, *69*, 421-436. https://doi.org/10.1146/annurev-med-052716-031710

Steffan, N. M., Bren, G. D., Frantz, B., Tocci, M. J., O'Neill, E. A., & Paya, C. V. (1995). Regulation of IkB alpha phosphorylation by PKC- and Ca(2+)-dependent signal transduction pathways. *J Immunol*, *155*(10), 4685-4691. https://doi.org/10.4049/jimmunol.155.10.4685

Stephenson, K. E. (2018). Therapeutic vaccination for HIV: hopes and challenges. *Curr Opin HIV AIDS*, *13*(5), 408-415. https://doi.org/10.1097/COH.0000000000000491

Stephenson, K. E., & Barouch, D. H. (2016). Broadly Neutralizing Antibodies for HIV Eradication. *Curr HIV/AIDS Rep*, *13*(1), 31-37. https://doi.org/10.1007/s11904-016-0299-7

Sun, M. K., & Alkon, D. L. (2012). Activation of protein kinase C isozymes for the treatment of dementias. *Adv Pharmacol*, *64*, 273-302. https://doi.org/10.1016/B978-0-12-394816-8.00008-8

Talman, V., Pascale, A., Jantti, M., Amadio, M., & Tuominen, R. K. (2016). Protein Kinase C Activation as a Potential Therapeutic Strategy in Alzheimer's Disease: Is there a Role for Embryonic Lethal Abnormal Vision-like Proteins? *Basic Clin Pharmacol Toxicol*, *119*(2), 149-160. https://doi.org/10.1111/bcpt.12581

Tassi, I., Cella, M., Presti, R., Colucci, A., Gilfillan, S., Littman, D. R., & Colonna, M. (2008). NK cell-activating receptors require PKC-theta for sustained signaling, transcriptional activation, and IFN-gamma secretion. *Blood*, *112*(10), 4109-4116. https://doi.org/10.1182/blood-2008-02-139527

Tian, Z., Lu, X. T., Jiang, X., & Tian, J. (2023). Bryostatin-1: a promising compound for neurological disorders. *Front Pharmacol*, *14*, 1187411. https://doi.org/10.3389/fphar.2023.1187411

Tong-Starkesen, S. E., Luciw, P. A., & Peterlin, B. M. (1989). Signaling through T lymphocyte surface proteins, TCR/CD3 and CD28, activates the HIV-1 long terminal repeat. *J Immunol*, *142*(2), 702-707. https://doi.org/10.4049/jimmunol.142.2.702

Trushin, S. A., Bren, G. D., Asin, S., Pennington, K. N., Paya, C. V., & Badley, A. D. (2005). Human immunodeficiency virus reactivation by phorbol esters or T-cell receptor ligation requires both PKCalpha and PKCtheta. *J Virol*, *79*(15), 9821-9830. https://doi.org/10.1128/JVI.79.15.9821-9830.2005

Wender, P. A., Donnelly, A. C., Loy, B. A., Near, K. E., & Staveness, D. (2015). Rethinking the role of natural products: Function-oriented synthesis, bryostatin, and bryologs. In S. Hanessian (Ed.), *Natural Products in Medicinal Chemistry* (pp. 473–544). Wiley-VCH. https://doi.org/10.1002/9783527676545.ch14

Wender, P. A., Hardman, C. T., Ho, S., Jeffreys, M. S., Maclaren, J. K., Quiroz, R. V., Ryckbosch, S. M., Shimizu, A. J., Sloane, J. L., & Stevens, M. C. (2017). Scalable synthesis of bryostatin 1 and analogs, adjuvant leads against latent HIV. *Science*, *358*, 218–223. https://doi.org/10.1126/science.aan7969

Wender, P. A., Kee, J. M., & Warrington, J. M. (2008). Practical synthesis of prostratin, DPP, and their analogs, adjuvant leads against latent HIV. *Science*, *320*(5876), 649-652. https://doi.org/10.1126/science.1154690

Wender, P. A., Quiroz, R. V., & Stevens, M. C. (2015). Function through synthesis-informed design. *Acc Chem Res*, *48*(3), 752-760. https://doi.org/10.1021/acs.accounts.5b00004

WHO | HIV & AIDS. https://www.who.int/news-room/fact-sheets/detail/hiv-aids

Williams, S. A., Chen, L. F., Kwon, H., Fenard, D., Bisgrove, D., Verdin, E., & Greene, W. C. (2004). Prostratin antagonizes HIV latency by activating NF-kappaB. *J Biol Chem*, *279*(40), 42008-42017. https://doi.org/10.1074/jbc.M402124200

Wong, J. K., Hezareh, M., Günthard, H. F., Havlir, D. V., Ignacio, C. C., Spina, C. A., & Richman, D. D. (1997). Recovery of Replication-Competent HIV Despite Prolonged Suppression of Plasma Viremia. *Science*, *278*, 1291-1295. https://doi.org/10.1126/science.278.5341.1291

Wykes, M. N., & Lewin, S. R. (2018). Immune checkpoint blockade in infectious diseases. *Nat Rev Immunol*, *18*(2), 91-104. https://doi.org/10.1038/nri.2017.112

Yang, O. O., Tran, A. C., Kalams, S. A., Johnson, R. P., Roberts, M. R., & Walker, B. D. (1997). Lysis of HIV-1-infected cells and inhibition of viral replication by universal receptor T cells. *Proc. Natl. Acad. Sci. USA*, *94*, 11478–11483. https://doi.org/10.1073/pnas.94.21.11478

Zhang, X., Zhang, R., Zhao, H., Cai, H., Gush, K. A., Kerr, R. G., Pettit, G. R., & Kraft, A. S. (1996). Preclinical Pharmacology of the Natural Product Anticancer Agent Bryostatin 1, an Activator of Protein Kinase C. *Cancer research*, *56*, 802-808.

Zhou, Y., Zhou, B., Pache, L., Chang, M., Khodabakhshi, A. H., Tanaseichuk, O., Benner, C., & Chanda, S. K. (2019). Metascape provides a biologist-oriented resource for the analysis of systems-level datasets. *Nat Commun*, *10*(1), 1523. https://doi.org/10.1038/s41467-019-09234-6

Zou, W., Borvak, J., Marches, F., Wei, S., Galanaud, P., Emilie, D., & Curiel, T. J. (2000). Macrophage-derived dendritic cells have strong Th1-polarizing potential mediated by beta-chemokines rather than IL-12. *J Immunol*, *165*(8), 4388-4396. https://doi.org/10.4049/jimmunol.165.8.4388

CHAPTER 4

Conclusions, Ongoing Experiments & Future Directions

SUMMARY

The work presented in this dissertation characterizes the effects of PKC modulator HIV latency reversing agents, particularly the novel bryostatin-1 analog (SUW133), on kick and kill strategies.

First, we infected humanized mice with a genetically barcoded HIV swarm, allowing us to quantify changes in viral diversity and compare these with more traditional metrics, such as viral load and time to rebound, to determine whether SUW133 reduces the latent reservoir. We showed that mice treated with SUW133 during ART exhibit a delay in rebound following ART interruption (Figure 2-5). Furthermore, we observed a reduction in the number of unique rebounding barcoded viruses in SUW133-treated animals compared to control-treated animals (Figure 2-6), suggesting that LRA treatment eliminated some reservoir cells that would have contributed to viral rebound. Additionally, we demonstrated that the addition of allogenic NK cells after LRA stimulation further deferred time to rebound and diminished barcode diversity compared to treatment with LRA or NK alone. Notably, 40% of the mice treated with SUW133 plus NK cells did not rebound during the 12.1 weeks following ART disruption (Figure 2-7B and cell-associated HIV DNA was not detected in the spleen or bone marrow of these non-rebounding mice (Figure 2-8). Furthermore, when splenocytes from these mice were cocultured with CEM cells to facilitate viral outgrowth, we did not detect any replication-competent virus (Supplemental Table 2-3), suggesting that the combination of SUW133 plus NK cells effectively eliminated the latent reservoir in these mice.

Next, to determine whether exposure to SUW133 may augment NK cell function in some way that may explain this improved reservoir reduction, we characterized the effects of PKC modulators on NK cells *in vitro*. We showed that PKC modulator-stimulated NK cells express increased expression of cellular markers involved in NK cell activation (Figure 3-1). Consistent with this

finding, transcriptomic profiles of NK cells treated with PKC modulators displayed signatures of cellular activation and enrichment of genes regulated by NFκB (Figure 3-4 and Supplemental Figures 3-4 to 3-6). Despite showing signs of activation, cytotoxicity against K562 target cells was unaffected by prostratin, but significantly decreased by bryostatin and SUW133 (Figure 3-5), and there was no effect on NK cell killing of HIV-infected $CD4^+$ T cells by any of the compounds (Supplemental Figure 3-7). Furthermore, while PKC-stimulated NK cells secreted increased levels of pro-inflammatory cytokines (Figures 3-2 & 3-6), this did not indirectly stimulate latency reversal in J-Lat cell lines (Figure 3-6). Together, these findings suggest that the effects of PKC modulators on the eradication of the viral reservoir in the kick and kill approach is primarily due to increased provirus expression by $CD4^+$ T cells, rather than an enhancement of NK cell effector function.

Altogether, this dissertation improves our understanding of the use of PKC modulating LRAs in the treatment of HIV latency and identifies SUW133 as a potential cure that warrants further investigation. Furthermore, it provides proof-of-concept for the use of NK cells for HIV immunotherapy and helps us better understand the effects of PKC modulators on different cell subtypes. My work adds to the growing body of knowledge of kick and kill strategies and can be used to guide future strategies for the treatment HIV and other diseases utilizing PKC modulators.

FUTURE DIRECTIONS

In the preceding chapters, I mentioned multiple prospective avenues of research, primarily aimed at addressing study limitations. In this chapter, I will briefly expand on the discussion of these proposed experiments, in addition to showcasing some preliminary data from ongoing studies that builds upon our findings and may address issues regarding the toxicity of SUW133.

Using cells from ART-suppressed HIV-infected individuals

Much of the work described in the previous chapters was performed *in vivo* in humanized mouse models, which do not recapitulate all aspects of the human immune system nor fully replicate the mechanisms that govern HIV latency in a clinical setting, especially in people living with HIV undergoing long-term ART treatment. Importantly, these mice have limited reconstitution of myeloid cells, which may comprise an important reservoir for HIV, and NK cells, which were studied here for their potential as killing agents for reactivated HIV. There are alternative mouse models aside from the NSG-BLT and TKO-BLT mice used in our studies that utilize genetic modifications to express cytokines or other immunomodulatory molecules to enhance differentiation and survival of these cells, which would allow for the examination of endogenous myeloid and NK cell function *in vivo* (Radtke et al., 2019; Rongvaux et al., 2014). However, this still does not address issues related to the short lifespan of humanized mice, which contributes to their limitation to accurately reflect changes in the HIV reservoir that may occur during chronic latency (Maldarelli et al., 2014; Wang et al., 2018). To more accurately assess the effects of our kick and kill strategy and its utility as a potential clinical therapeutic would require using cells from ART-treated HIV-positive individuals. Repeating the previously described experiments in this study using patient samples would provide a more robust assessment of the therapeutic value of PKC modulators plus NK cells.

Using full-length barcoded virus

Although our barcoded HIV infection strategy offers significant insight into clonal diversity and reservoir dynamics by quantifying changes in the number of viral barcodes elicited by our treatment strategy, the NL-HABC virus used during infection lacks a functional vpr gene. While

we have previously shown that this does not affect infectivity (Marsden et al., 2020), vpr has been is known to have various transcriptomics effects within the host cell (Bauby et al., 2021). Importantly, vpr can alter the cell-surface expression of ligands that can be recognized by NK cells, sensitizing them to killing (Desimio et al., 2018; Richard et al., 2010; Ward et al., 2009). Additionally, vpr alters the secretion of several pro-inflammatory cytokines, including MIP-1α, MIP-1β, RANTES and TNF, which can impact viral replication (Muthumani et al., 2000; Roesch et al., 2015). Similarly, vpr suppresses secretion of IL-12, which regulates the activity of NK and $CD8^+$ T cells, which are important in the clearance of infected cells (Mirani et al., 2002). Thus, in order to accurately assess how PKC modulators plus NK cells affect the viral reservoir, infection should be conducted using a full-length virus.

Performing in-depth transcriptomics analysis

The scope of the current study was not necessarily to determine a mechanism but rather to look at general effects induced by PKC modulator stimulation and or adoptive transfer of allogenic NK cells. Performing an in-depth transcriptomics analysis on our existing data or on data derived from the proposed experiments would help us better understand differences between each of the PKC modulators that may contribute to their distinct effects on latency reversal and/or their relative toxicity. Moreover, this may help us to identify and understand the dynamics of other activating and inhibitory receptors induced by PKC modulators on both NK and HIV-infected $CD4^+$ T cells aside from the ones assessed in this study.

Further exploration of the use of SUW133 in HIV kick and kill approaches

To further expand on the development of SUW133 in potent and novel kick and kill strategies, we

could combine it with HIV-specific cytotoxic cells, which should may lead to greater elimination of reactivated cells and therefore a more substantial reduction in the size of the latent reservoir.

Another potential modified kick and kill approach utilizing SUW133 would be to perform repeated dosing of LRA. Only a small fraction of latently infected cells is activated upon single-dose treatment with LRA (Battivelli et al., 2018). Thus, it may be necessary to perform sequential dosing to effectively eliminate the reservoir. Interval dosing using the histone deacetylase inhibitor (HDACi) vorinostat has been shown to improve reservoir reduction *in vivo* (Archin et al., 2017). Whether the same is true for SUW133 remains unknown.

An additional kick and kill strategy using SUW133 is to use combine it with other LRAs in synergistic combinations, thus improving tolerability via dose reduction (Laird et al., 2015). As with many LRAs, induction of HIV latency reversal by SUW133 and other PKC modulators is tied to generalized T cell activation, and results in cytokine secretion (Marsden et al., 2018; Sloane et al., 2020). Global immune activation results in hypercytokinemia, or a "cytokine storm," which can be toxic (Prins et al., 1999; van Praag et al., 2001). Combinations of functionally distinct LRAs may be more potent, as they can simultaneously combat multiple mechanisms governing HIV-1 latency (Burnett et al., 2010; Kauder et al., 2009; Mbonye & Karn, 2014; Reuse et al., 2009; Williams et al., 2006).

It has been previously shown that some combinations of PKC modulators and histone deacetylase inhibitors exhibit synergistic HIV latency reactivation (Albert et al., 2017; Pérez et al., 2010; Zaikos et al., 2018). Histone deacetylase inhibitors (HDACis) are a class of LRAs that work by blocking the deacetylation of histone proteins, therefore rendering chromatin more transcriptionally active. HDACis, such as vorinostat and panobinostat, have shown potent latency

reversal *in vivo* (Archin et al., 2014; Archin et al., 2017; Archin et al., 2012; Rasmussen et al., 2014). We previously showed that the combination of SUW133 plus another HDACi (entinostat), exhibits reactivation of HIV from latency in J-Lat cells (Marsden et al., 2018). In the next section, I briefly introduce our ongoing work evaluating the combination of SUW133 and histone deacetylase inhibitors as a synergistic treatment for HIV latency reversal.

ONGOING STUDIES

SUW133 plus HDACi exhibit synergistic cellular activation in PBMCs

Peripheral blood mononuclear cells (PBMCs) were treated with suboptimal concentration of SUW133 only, HDACis (vorinostat, panobinostat or entinostat) or the combination of the two alongside a vehicle control (DMSO) for 24 hours and evaluated for synergy using CD69 surface expression as a proxy for the efficacy of latency reversal. For SUW133, the previously tested suboptimal concentration was used (Marsden et al., 2018). To determine suboptimal dosing for

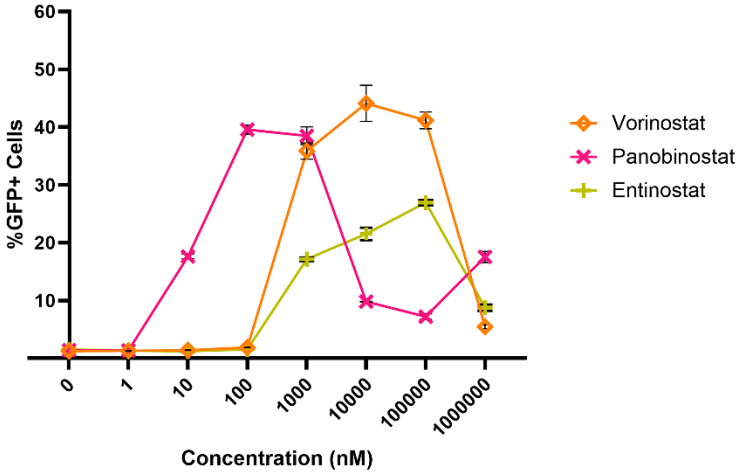

Figure 4-1. Titration of histone deacetylase inhibitors to determine suboptimal dosing. J-Lat 10.6 cells were cultured for 48 hours in various concentrations of vorinostat, panobinostat or entinostat and assessed for latency reversal. All concentrations were tested in triplicate resulting in n = 3. Each graph depicts the mean with error bars indicating the standard error of the mean (SEM).

each of the HDACis, J-Lat 10.6 cells were cultured for 48 hours in various concentrations of drugs (Figure 4-1). For this experiment, we define synergy using the Bliss independence principle (Bliss, 1956), wherein a drug combination is deemed synergistic if the combination effect is greater than the sum of the individual drug effects minus their product. We observed synergistic CD69 expression on $CD4^+$ T cells by all 3 combinations of SUW133 plus HDACi (Figure 4-2). Based on these results, we would expect that the combination of SUW133 plus HDACi would exhibit synergistic latency reactivation. While this was previously tested and confirmed for the combination of SUW133 plus entinostat in J-Lat 10.6 cells (Marsden et al., 2018), additional

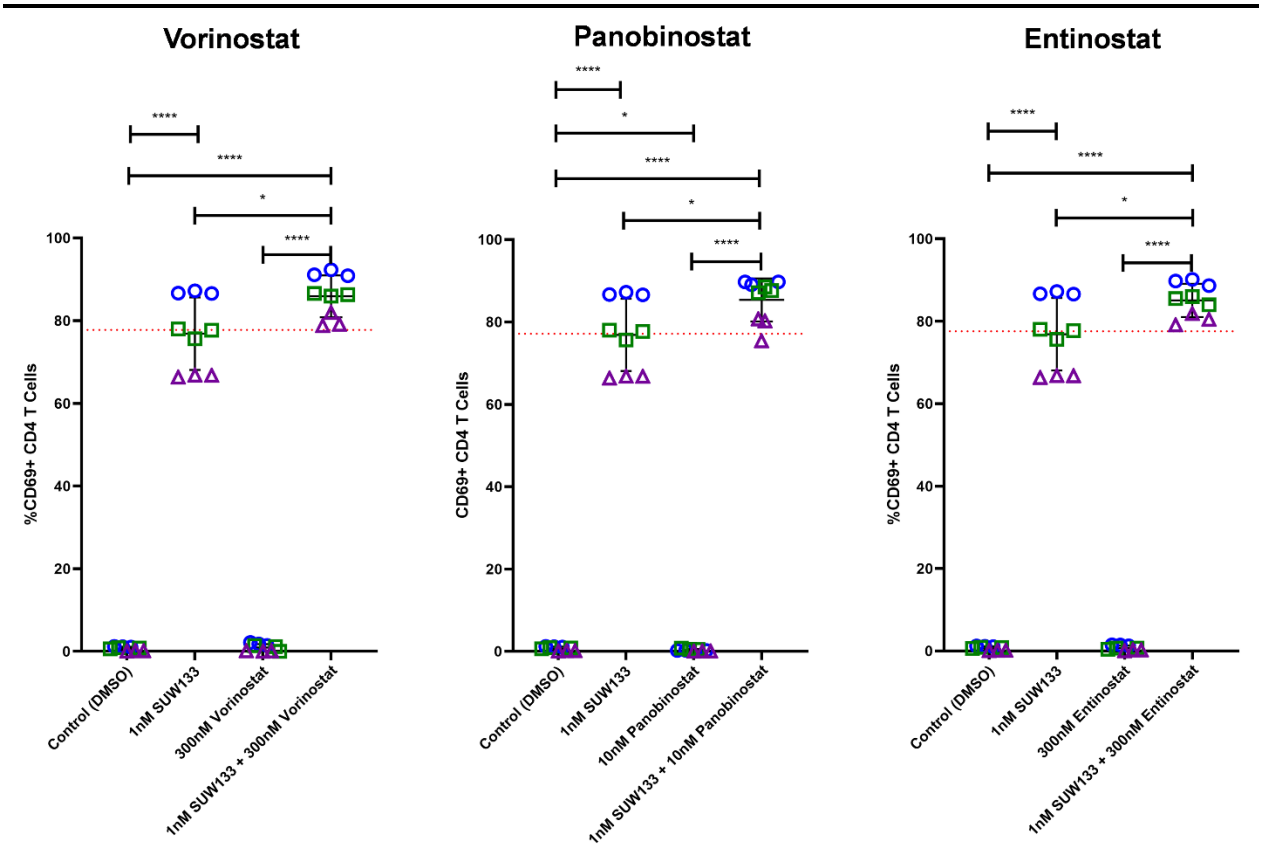

Figure 4-2. SUW133 plus histone deacetylase inhibitors (HDACi) exhibit synergistic cellular activation in PBMCs. PBMCs were cultured for 24 hours untreated (DMSO only), with 1nM SUW133 alone, with 300nM vorinostat alone, 10nM panobinostat alone, 300nM entinostat alone or the combination of SUW133 plus HDACi, and analyzed for CD69 expression on $CD4^+$ T cells (defined as $CD3^+CD4^+$) via flow cytometry. Data technical triplicates from 3 healthy human donors is shown (n=9), with each color and shape representing results from a different donor. Dashed red lines indicate the calculated threshold for synergy using the Bliss independence model. An unpaired, unequal variance Student's *t*-Test was performed, with (*) indicating $p < 0.05$ and (****) indicating $p < 0.0001$.

experiments are required to determine if this is true for the combination with vorinostat or panobinostat.

PBMCs treated with SUW133 ± HDACi show distinct gene expression profiles

To determine a potential mechanism underlying the synergistic effects of SUW133 plus HDACis, we performed RNA sequencing (RNA-seq) on LRA-stimulated and untreated cells. Principal component analysis (PCA) demonstrated well-defined clustering between the transcriptomic profiles of each treatment group (Figure 4-2A), indicating distinct genetic changes. Interestingly,

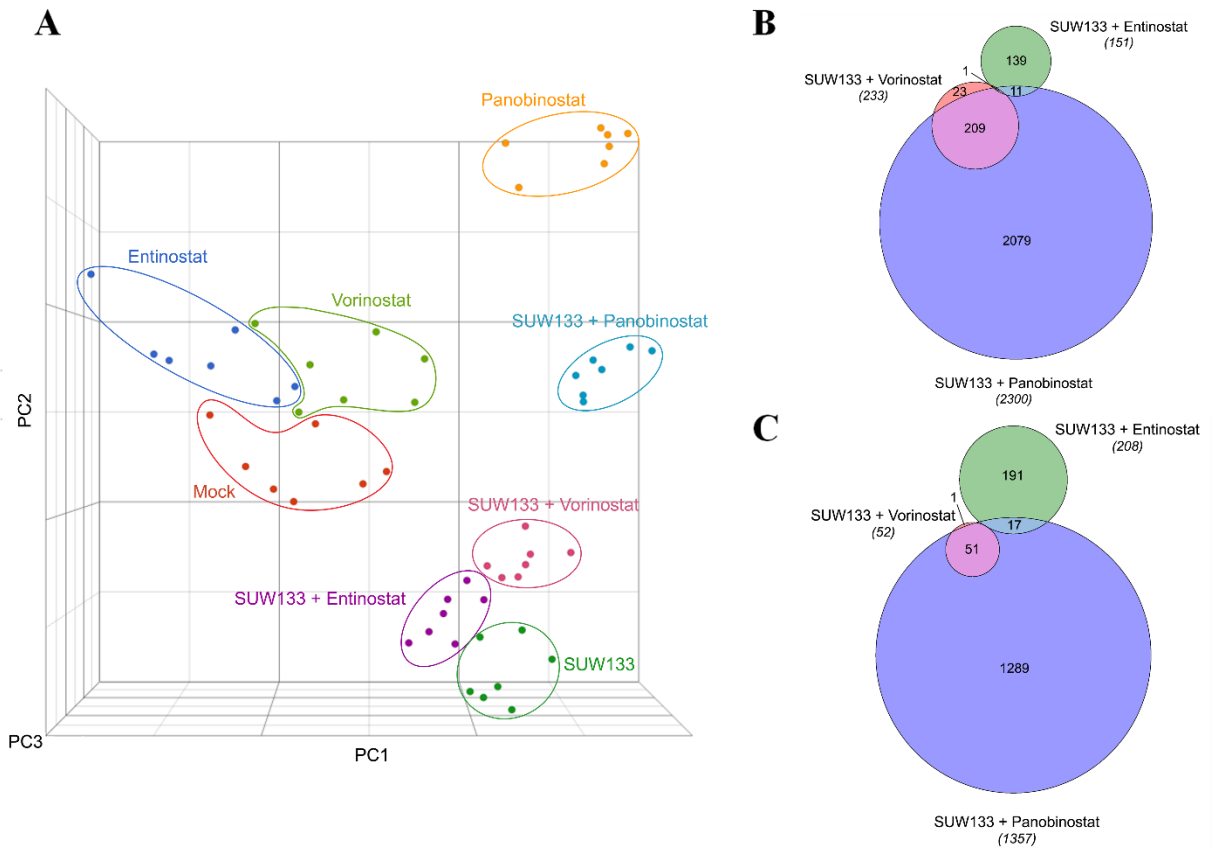

Figure 4-3. Transcriptomic profiles of PBMCs treated with PKC modulators. RNA-seq was performed on PBMCs cultured for 24 hours untreated (DMSO only), with 1nM SUW133 alone, with 300nM vorinostat alone, 10nM panobinostat alone, 300nM entinostat alone or the combination of SUW133 plus HDACi. **A)** Principal component analysis (PCA) plot of data from 7 healthy human donors is shown, with each point **representing results from a different donor and each color representing a different treatment group.** Venn diagram illustrating the overlap of upregulated **(B)** and downregulated **(C)** genes between the 3 different SUW133 + HDACi combinations. Areas shown are proportional to the numbers of genes within each category.

panobinostat showed the greatest effect amongst the 3 HDACis tested both alone or in combination with SUW133, based on relative distance to the controls (Figure 4-3A). This was consistent when comparing the relative number of differentially expressed genes (DEGs) that were upregulated Figure 4-3B) and downregulated (Figure 4-3C) induced by each treatment.

Synergistic latency reactivation by SUW133 + HDACi may be due to upregulation of *ARG2*

We generated volcano plots and identified the top 15 differentially expressed genes (DEGs) by each of the combinations of SUW133 plus HDACi (Figures 4-4, 4-5 & 4-6). Amongst the top 15 DEGs, there were no genes shared between all 3 combinations (Figures 4-4B, 4-5B & 4-6B). However, *ARG2* was modestly upregulated by each of the combinations (FC = 2.252 for SUW133 plus vorinostat, 4.416 for SUW133 plus panobinostat, and 2.972 for SUW133 plus entinostat). Increased *ARG2* expression may result in enhanced cell proliferation by catalyzing the hydrolysis of arginine to urea and ornithine, which can be metabolized to produce polyamines to promote cell cycle progression. Thus, it can be postulated that the mechanism of synergistic latency reactivation by the combination of SUW133 and HDACi is due to promotion of cell cycle progression by *ARG2*. Moreover, HIV Vpr, which is known to cause cell cycle arrest (Emerman, 1996), downregulates expression of *ARG2* (Zahoor et al., 2015), which aligns with this theory. Further experiments, including the knock-out of *ARG2*, are necessary to validate this hypothesis.

CLOSING STATEMENT

By thoroughly characterizing the effects of SUW133 on kick and kill strategies, this dissertation provides an in-depth understanding of how it affects both the “kick” and “kill” arm of this approach,

underscoring the promise for its use as in potential cure therapies, and provides insight into the optimization of future approaches aimed at eradicating the latent reservoir.

A

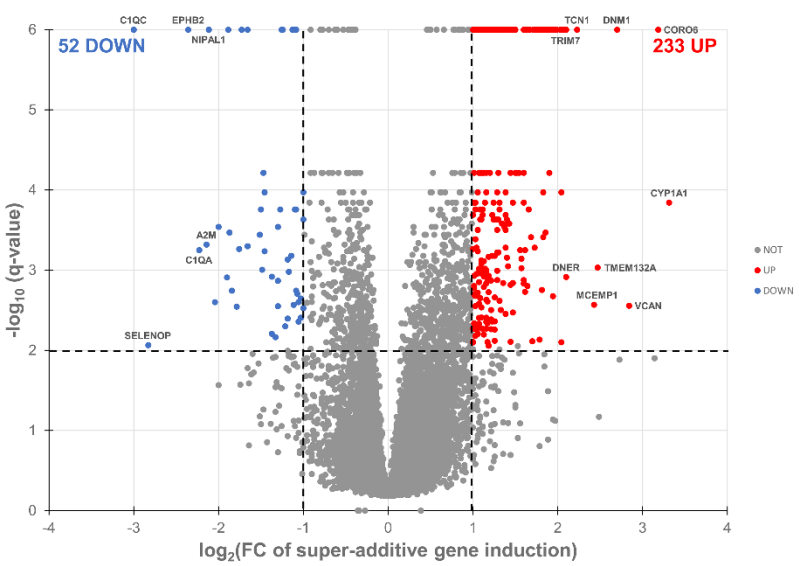

B

Gene	Fold change	Log_2 (FC)	Log_{10} (q-value)	Change trend
CYP1A1	9.947	3.3143	3.00E-06	UP
CORO6	9.099	3.1857	1.00E-06	UP
C1QC	0.125	-3.0000	1.00E-06	DOWN
VCAN	7.175	2.8429	1.92E-04	UP
SELENOP	0.141	-2.8286	9.65E-04	DOWN
DNM1	6.498	2.7000	1.00E-06	UP
TMEM132A	5.546	2.4714	4.00E-05	UP
MCEMP1	5.384	2.4286	1.84E-04	UP
EPHB2	0.195	-2.3571	1.00E-06	DOWN
TCN1	4.687	2.2286	1.00E-06	UP
C1QA	0.213	-2.2286	2.00E-05	DOWN
A2M	0.226	-2.1429	1.60E-05	DOWN
NIPAL1	0.231	-2.1143	1.00E-06	DOWN
TRIM7	4.287	2.1000	1.00E-06	UP
DNER	4.287	2.1000	6.00E-05	UP

Figure 4-4. Differentially expressed genes induced by SUW133 plus vorinostat in PBMCs. RNA-seq was performed on PBMCs cultured for 24 hours untreated (DMSO only), with 1nM SUW133 alone, with 300nM vorinostat alone, or the combination of SUW133 plus vorinostat. **A)** Volcano plot of the distribution of all differentially expressed genes. The red and blue dots represent the upregulated and downregulated genes (q-value < 0.01 and $|\log_2(\text{FC super-additive gene induction})| > 2$), respectively. B) Table listing the 15 most differentially expressed genes.

A

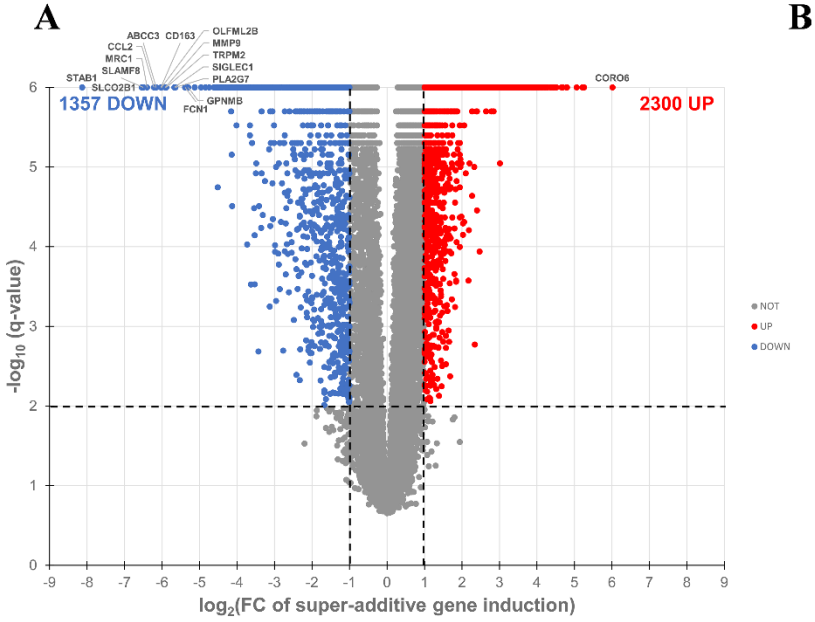

B

Gene	Fold change	Log_2 (FC)	Log_{10} (q-value)	Change trend
STAB1	0.004	-8.1286	1.00E-06	DOWN
SLCO2B1	0.011	-6.5429	1.00E-06	DOWN
SLAMF8	0.011	-6.5000	1.00E-06	DOWN
MRC1	0.012	-6.4000	1.00E-06	DOWN
CCL2	0.013	-6.2143	1.00E-06	DOWN
ABCC3	0.014	-6.1571	1.00E-06	DOWN
CD163	0.015	-6.0286	1.00E-06	DOWN
CORO6	64.638	6.0143	1.00E-06	UP
OLFML2B	0.015	-6.0143	1.00E-06	DOWN
MMP9	0.017	-5.9143	1.00E-06	DOWN
TRPM2	0.017	-5.8857	1.00E-06	DOWN
SIGLEC1	0.02	-5.6714	1.00E-06	DOWN
PLA2G7	0.02	-5.6429	1.00E-06	DOWN
FCN1	0.024	-5.3857	1.00E-06	DOWN
GPNMB	0.025	-5.3000	1.00E-06	DOWN

Figure 4-5. Differentially expressed genes induced by SUW133 plus panobinostat in PBMCs. RNA-seq was performed on PBMCs cultured for 24 hours untreated (DMSO only), with 1nM SUW133 alone, with 10nM panobinostat alone, or the combination of SUW133 plus panobinostat. **A)** Volcano plot of the distribution of all differentially expressed genes. The red and blue dots represent the upregulated and downregulated genes (q-value < 0.01 and $|\log_2(\text{FC super-additive gene induction})| > 2$), respectively. B) Table listing the 15 most differentially expressed genes.

A

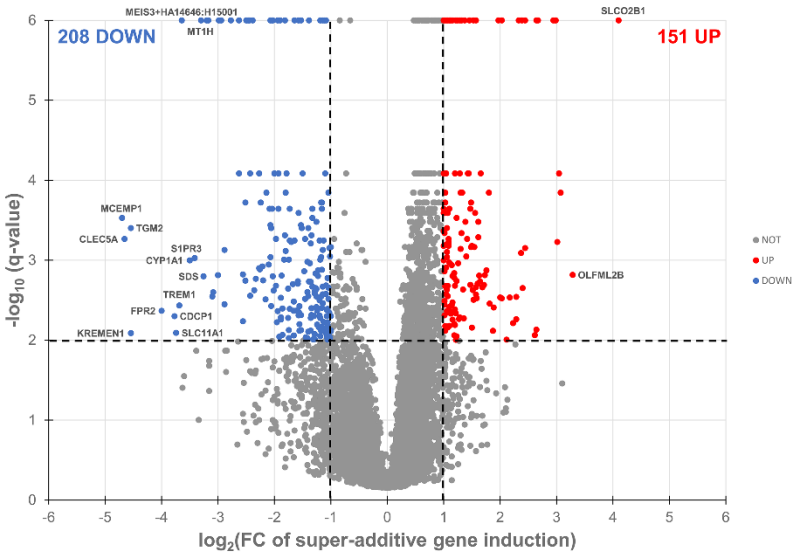

B

Gene	Fold change	Log_2 (FC)	Log_{10} (q-value)	Change trend
MCEMP1	0.038	-4.7000	6.00E-06	DOWN
CLEC5A	0.04	-4.6571	1.40E-05	DOWN
KREMEN1	0.043	-4.5429	7.36E-04	DOWN
TGM2	0.043	-4.5429	9.00E-06	DOWN
SLCO2B1	17.148	4.1000	1.00E-06	UP
FPR2	0.062	-4.0000	2.92E-04	DOWN
CDCP1	0.073	-3.7714	3.72E-04	DOWN
SLC11A1	0.075	-3.7429	7.29E-04	DOWN
TREM1	0.078	-3.6857	2.32E-04	DOWN
MEIS3+ HA14646: H15001	0.08	-3.6429	1.00E-06	DOWN
CYP1A1	0.088	-3.5000	3.50E-05	DOWN
S1PR3	0.094	-3.4143	3.20E-05	DOWN
MT1H	0.102	-3.3000	1.00E-06	DOWN
OLFML2B	9.752	3.2857	6.10E-05	UP
SDS	0.105	-3.2571	6.50E-05	DOWN

Figure 4-6. Differentially expressed genes induced by SUW133 plus entinostat in PBMCs. RNA-seq was performed on PBMCs cultured for 24 hours untreated (DMSO only), with 1nM SUW133 alone, with 300nM entinostat alone, or the combination of SUW133 plus entinostat. **A)** Volcano plot of the distribution of all differentially expressed genes. The red and blue dots represent the upregulated and downregulated genes (q-value < 0.01 and $|\log_2(\text{FC super-additive gene induction})| > 2$), respectively. B) Table listing the 15 most differentially expressed genes.

REFERENCES

Albert, B. J., Niu, A., Ramani, R., Marshall, G. R., Wender, P. A., Williams, R. M., Ratner, L., Barnes, A. B., & Kyei, G. B. (2017). Combinations of isoform-targeted histone deacetylase inhibitors and bryostatin analogues display remarkable potency to activate latent HIV without global T-cell activation. *Scientific Reports*, *7*(1). https://doi.org/10.1038/s41598-017-07814-4

Archin, N. M., Bateson, R., Tripathy, M. K., Crooks, A. M., Yang, K. H., Dahl, N. P., Kearney, M. F., Anderson, E. M., Coffin, J. M., Strain, M. C., Richman, D. D., Robertson, K. R., Kashuba, A. D., Bosch, R. J., Hazuda, D. J., Kuruc, J. D., Eron, J. J., & Margolis, D. M. (2014). HIV-1 expression within resting CD4+ T cells after multiple doses of vorinostat. *J Infect Dis*, *210*(5), 728-735. https://doi.org/10.1093/infdis/jiu155

Archin, N. M., Kirchherr, J. L., Sung, J. A., Clutton, G., Sholtis, K., Xu, Y., Allard, B., Stuelke, E., Kashuba, A. D., Kuruc, J. D., Eron, J., Gay, C. L., Goonetilleke, N., & Margolis, D. M. (2017). Interval dosing with the HDAC inhibitor vorinostat effectively reverses HIV latency. *J Clin Invest*, *127*(8), 3126-3135. https://doi.org/10.1172/JCI92684

Archin, N. M., Liberty, A. L., Kashuba, A. D., Choudhary, S. K., Kuruc, J. D., Crooks, A. M., Parker, D. C., Anderson, E. M., Kearney, M. F., Strain, M. C., Richman, D. D., Hudgens, M. G., Bosch, R. J., Coffin, J. M., Eron, J. J., Hazuda, D. J., & Margolis, D. M. (2012). Administration of vorinostat disrupts HIV-1 latency in patients on antiretroviral therapy. *Nature*, *487*(7408), 482-485. https://doi.org/10.1038/nature11286

Battivelli, E., Dahabieh, M. S., Abdel-Mohsen, M., Svensson, J. P., Tojal Da Silva, I., Cohn, L. B., Gramatica, A., Deeks, S., Greene, W. C., Pillai, S. K., & Verdin, E. (2018). Distinct chromatin functional states correlate with HIV latency reactivation in infected primary CD4(+) T cells. *Elife*, *7*. https://doi.org/10.7554/eLife.34655

Bauby, H., Ward, C. C., Hugh-White, R., Swanson, C. M., Schulz, R., Goujon, C., & Malim, M. H. (2021). HIV-1 Vpr Induces Widespread Transcriptomic Changes in CD4(+) T Cells Early Postinfection. *mBio*, *12*(3), e0136921. https://doi.org/10.1128/mBio.01369-21

Bliss, C. I. (1956). The calculation of microbial assays. *Bacteriol Rev*, *20*(4), 243-258. https://doi.org/10.1128/br.20.4.243-258.1956

Burnett, J. C., Lim, K. I., Calafi, A., Rossi, J. J., Schaffer, D. V., & Arkin, A. P. (2010). Combinatorial latency reactivation for HIV-1 subtypes and variants. *J Virol*, *84*(12), 5958-5974. https://doi.org/10.1128/JVI.00161-10

Desimio, M. G., Giuliani, E., Ferraro, A. S., Adorno, G., & Doria, M. (2018). In Vitro Exposure to Prostratin but Not Bryostatin-1 Improves Natural Killer Cell Functions Including Killing of CD4(+) T Cells Harboring Reactivated Human Immunodeficiency Virus. *Front Immunol*, *9*, 1514. https://doi.org/10.3389/fimmu.2018.01514

Emerman, M. (1996). HIV-1, Vpr and the cell cycle. *Curr Biol*, *6*(9), 1096-1103. https://doi.org/10.1016/s0960-9822(02)00676-0

Kauder, S. E., Bosque, A., Lindqvist, A., Planelles, V., & Verdin, E. (2009). Epigenetic regulation of HIV-1 latency by cytosine methylation. *PLoS Pathog*, *5*(6), e1000495. https://doi.org/10.1371/journal.ppat.1000495

Laird, G. M., Bullen, C. K., Rosenbloom, D. I., Martin, A. R., Hill, A. L., Durand, C. M., Siliciano, J. D., & Siliciano, R. F. (2015). Ex vivo analysis identifies effective HIV-1 latency-reversing drug combinations. *J Clin Invest*, *125*(5), 1901-1912. https://doi.org/10.1172/JCI80142

Maldarelli, F., Wu, X., Su, L., Simonetti, F. R., Shao, W., Hill, S., Spindler, J., Ferris, A. L., Mellors, J. W., Kearney, M. F., Coffin, J. M., & Hughes, S. H. (2014). Specific HIV integration sites are linked to clonal expansion and persistence of infected cells. *Science*, *345*(6193), 179-183. https://doi.org/10.1126/science.1254194

Marsden, M. D., Wu, X., Navab, S. M., Loy, B. A., Schrier, A. J., DeChristopher, B. A., Shimizu, A. J., Hardman, C. T., Ho, S., Ramirez, C. M., Wender, P. A., & Zack, J. A. (2018). Characterization of designed, synthetically accessible bryostatin analog HIV latency reversing agents. *Virology*, *520*, 83-93. https://doi.org/10.1016/j.virol.2018.05.006

Marsden, M. D., Zhang, T. H., Du, Y., Dimapasoc, M., Soliman, M. S. A., Wu, X., Kim, J. T., Shimizu, A., Schrier, A., Wender, P. A., Sun, R., & Zack, J. A. (2020). Tracking HIV Rebound following Latency Reversal Using Barcoded HIV. *Cell Rep Med*, *1*(9), 100162. https://doi.org/10.1016/j.xcrm.2020.100162

Mbonye, U., & Karn, J. (2014). Transcriptional control of HIV latency: cellular signaling pathways, epigenetics, happenstance and the hope for a cure. *Virology*, *454-455*, 328-339. https://doi.org/10.1016/j.virol.2014.02.008

Mirani, M., Elenkov, I., Volpi, S., Hiroi, N., Chrousos, G. P., & Kino, T. (2002). HIV-1 protein Vpr suppresses IL-12 production from human monocytes by enhancing glucocorticoid action: potential implications of Vpr coactivator activity for the innate and cellular immunity deficits observed in HIV-1 infection. *J Immunol*, *169*(11), 6361-6368. https://doi.org/10.4049/jimmunol.169.11.6361

Muthumani, K., Kudchodkar, S., Papasavvas, E., Montaner, L. J., Weiner, D. B., & Ayyavoo, V. (2000). HIV-1 Vpr regulates expression of beta chemokines in human primary lymphocytes and macrophages. *J Leukoc Biol.*, *68*(3), 366-372.

Pérez, M., de Vinuesa, A. G., Sanchez-Duffhues, G., Marquez, N., Bellido, M. L., Muñoz-Fernandez, M. A., Moreno, S., Castor, T. P., Calzado, M. A., & Muñoz, E. (2010). Bryostatin-1 Synergizes with Histone Deacetylase Inhibitors to Reactivate HIV-1 from Latency. *Curr HIV Res*, *8*(6), 418-419. https://doi.org/10.2174/157016210793499312

Prins, J. M., Jurriaans, S., van Praag, R. M., Blaak, H., van Rij, R., Schellekens, P. T., ten Berge, I. J., Yong, S. L., Fox, C. H., Roos, M. T., de Wolf, F., Goudsmit, J., Schuitemaker, H., & Lange, J. M. (1999). Immuno-activation with anti-CD3 and recombinant human IL-2 in HIV-1-infected patients on potent antiretroviral therapy. . *AIDS*, *13*(17), 2405-2410. https://doi.org/10.1097/00002030-199912030-00012

Radtke, S., Chan, Y. Y., Sippel, T. R., Kiem, H. P., & Rongvaux, A. (2019). MISTRG mice support engraftment and assessment of nonhuman primate hematopoietic stem and progenitor cells. *Exp Hematol*, *70*, 31-41 e31. https://doi.org/10.1016/j.exphem.2018.12.003

Rasmussen, T. A., Tolstrup, M., Brinkmann, C. R., Olesen, R., Erikstrup, C., Solomon, A., Winckelmann, A., Palmer, S., Dinarello, C., Buzon, M., Lichterfeld, M., Lewin, S. R., Østergaard, L., & Søgaard, O. S. (2014). Panobinostat, a histone deacetylase inhibitor, for latent-virus reactivation in HIV-infected patients on suppressive antiretroviral therapy: a phase 1/2, single group, clinical trial. *Lancet*, *1*(1), e13–e21. https://doi.org/10.1016/S2352-3018(14)70014-1

Reuse, S., Calao, M., Kabeya, K., Guiguen, A., Gatot, J. S., Quivy, V., Vanhulle, C., Lamine, A., Vaira, D., Demonte, D., Martinelli, V., Veithen, E., Cherrier, T., Avettand, V., Poutrel, S., Piette, J., de Launoit, Y., Moutschen, M., Burny, A., . . . Van Lint, C. (2009). Synergistic activation of HIV-1 expression by deacetylase inhibitors and prostratin: implications for treatment of latent infection. *PLoS One*, *4*(6), e6093. https://doi.org/10.1371/journal.pone.0006093

Richard, J., Sindhu, S., Pham, T. N., Belzile, J. P., & Cohen, E. A. (2010). HIV-1 Vpr up-regulates expression of ligands for the activating NKG2D receptor and promotes NK cell-mediated killing. *Blood*, *115*(7), 1354-1363. https://doi.org/10.1182/blood-2009-08-237370

Roesch, F., Richard, L., Rua, R., Porrot, F., Casartelli, N., & Schwartz, O. (2015). Vpr Enhances Tumor Necrosis Factor Production by HIV-1-Infected T Cells. *J Virol*, *89*(23), 12118-12130. https://doi.org/10.1128/JVI.02098-15

Rongvaux, A., Willinger, T., Martinek, J., Strowig, T., Gearty, S. V., Teichmann, L. L., Saito, Y., Marches, F., Halene, S., Palucka, A. K., Manz, M. G., & Flavell, R. A. (2014). Development and function of human innate immune cells in a humanized mouse model. *Nat Biotechnol*, *32*(4), 364-372. https://doi.org/10.1038/nbt.2858

Sloane, J. L., Benner, N. L., Keenan, K. N., Zang, X., Soliman, M. S. A., Wu, X., Dimapasoc, M., Chun, T. W., Marsden, M. D., Zack, J. A., & Wender, P. A. (2020). Prodrugs of PKC modulators show enhanced HIV latency reversal and an expanded therapeutic window. *Proc Natl Acad Sci U S A*, *117*(20), 10688-10698. https://doi.org/10.1073/pnas.1919408117

van Praag, R. M., Prins, J. M., Roos, M. T., Schellekens, P. T., Ten Berge, I. J., Yong, S. L., Schuitemaker, H., Eerenberg, A. J., Jurriaans, S., de Wolf, F., Fox, C. H., Goudsmit, J., Miedema, F., & Lange, J. M. (2001). OKT3 and IL-2 treatment for purging of the latent HIV-1 reservoir in vivo results in selective long-lasting CD4+ T cell depletion. . *J Clin Immunol*, *21*(3). https://doi.org/10.1023/a:1011091300321

Wang, Z., Gurule, E. E., Brennan, T. P., Gerold, J. M., Kwon, K. J., Hosmane, N. N., Kumar, M. R., Beg, S. A., Capoferri, A. A., Ray, S. C., Ho, Y. C., Hill, A. L., Siliciano, J. D., & Siliciano, R. F. (2018). Expanded cellular clones carrying replication-competent HIV-1 persist, wax, and wane. *Proc Natl Acad Sci U S A*, *115*(11), E2575-E2584. https://doi.org/10.1073/pnas.1720665115

Ward, J., Davis, Z., DeHart, J., Zimmerman, E., Bosque, A., Brunetta, E., Mavilio, D., Planelles, V., & Barker, E. (2009). HIV-1 Vpr triggers natural killer cell-mediated lysis of infected cells through activation of the ATR-mediated DNA damage response. *PLoS Pathog*, *5*(10), e1000613. https://doi.org/10.1371/journal.ppat.1000613

Williams, S. A., Chen, L. F., Kwon, H., Ruiz-Jarabo, C. M., Verdin, E., & Greene, W. C. (2006). NF-kappaB p50 promotes HIV latency through HDAC recruitment and repression of transcriptional initiation. *EMBO J*, *25*(1), 139-149. https://doi.org/10.1038/sj.emboj.7600900

Zahoor, M. A., Xue, G., Sato, H., & Aida, Y. (2015). Genome-wide transcriptional profiling reveals that HIV-1 Vpr differentially regulates interferon-stimulated genes in human monocyte-derived dendritic cells. *Virus Res*, *208*, 156-163. https://doi.org/10.1016/j.virusres.2015.06.017

Zaikos, T. D., Painter, M. M., Sebastian Kettinger, N. T., Terry, V. H., Collins, K. L., & Kirchhoff, F. (2018). Class 1-Selective Histone Deacetylase (HDAC) Inhibitors Enhance HIV Latency Reversal while Preserving the Activity of HDAC Isoforms Necessary for Maximal HIV Gene Expression. *Journal of Virology*, *92*(6). https://doi.org/10.1128/jvi.02110-17